In the Name of God

Journal of
Information Systems & Telecommunication
Vol. 1, No. 3, July-September 2013

Research Institute for Information and Communication Technology
Iranian Association of Information and Communication Technology

Affiliated to: Academic Center for Education, Culture and Research (ACECR)

Publisher: Iran University Press
Print ISSN: 2322-1437
Online ISSN: 2345-2773
Publication License: 91/13216

Editorial office Address: No.5, Saeedi Alley, Kalej Intersection., Enghelab Ave., Tehran, Iran,
P.O.Box: 13145-799 Tel: (+9821) 88930150 Fax: (+9821) 88930157
Email: info@jist.ir
URL: www.jist.ir

Indexed in:

- Research Institute for Information and Communication Technology www.ictrc.ir
- Islamic World Science Citation Center (ISC) www.isc.gov.ir
- Scientific Information Database (SID) www.sid.ir
- Regional Information Center for Sciences and Technology (RICeST) www.srlst.com
- Magiran www.magiran.com

This Journal is published with scientific supported by the Advanced Information systems Research Group (AIS) and Information Technology Business Model Research Group (ITBM) in Research Institute for Information and Communication Technology.

Acknowledgement

JIST Editorial-Board would like to gratefully appreciate the following distinguished referees for spending their invaluable time and expertise in reviewing the manuscripts and their constructive suggestions, which had a great impact on the enhancement of this issue of the JIST Journal.

(A-Z)

- Maghsood Abbaspour, Shahid Beheshti University, Tehran, Iran
- Hossein Charmchi, Sharif University of Technology, Tehran, Iran
- Mohammad Javad Emadi, Sharif University of Technology, Tehran, Iran
- Marzieh Eskandari, Alzahra University, Tehran, Iran
- Mir Mohammad Ettefagh, Tabriz University, Tabriz, Iran
- Abolfazl Falahati, Iran University Science and Technology, Tehran, Iran
- Abdolrasool Ghasemi, Khaje Nasir-edin Toosi University of Technology, Tehran, Iran
- Mehdi Ghatee, Amirkabir University of Technology, Tehran, Iran
- Amir Jafar Gholi, Amir Kabir University of Technology, Tehran, Iran
- Azizollah Jamshidi, Shiraz University, Shiraz, Iran
- Mohammad Hossein Kahaei, Iran University Science and Technology, Tehran, Iran
- Hossein Kamrani, Shiraz University, Shiraz, Iran
- Ali Mohammad Latif, Yazd University, Yazd, Iran
- Saeid Mashhadi, Shaif University, Tehran, Iran
- Seyed Hasan Mirian Hossein Abadi, Sharif University of Technology, Tehran, Iran
- Zahra Nilforooshan, Amirkabir University of Technology, Tehran, Iran
- Hamid Nooralizadeh, Islamic Azad University of Eslamshahr, Tehran, Iran
- Saber Pahlevan, Khaje Nasir-edin Toosi University of Technology, Tehran, Iran
- Behrooz Safari Nejadian, Shiraz University, Shiraz, Iran
- Mostafa Shabani, Shahid Rajaee Training Teacher, Tehran, Iran
- Mojtaba Shirazi, Amirkabir University of Technology, University Central of Florida
- Amin Torabi, Nanyang Technological University, Singapor
- Jafar Zarei, Shiraz University of Technology, Shiraz, Iran

Table of Content

Pose-Invariant Eye Gaze Estimation Using Geometrical Features of Iris and Pupil Images

Mohammad Reza Mohammadi*
Electrical Engineering, M.Sc. Student, Amirkabir University of Technology
mrmohammado@aut.ac.ir
Abolghasem A. Raie
Electrical Engineering, Associate Professor, Amirkabir University of Technology
raie@aut.ac.ir

Received: 03/Mar/2013 Accepted: 31/Aug/2013

Abstract
In the cases of severe paralysis in which the ability to control the body movements of a person is limited to the muscles around the eyes, eye movements or blinks are the only way for the person to communicate. Interfaces that assist in such communications often require special hardware or reliance on active infrared illumination. In this paper, we propose a non-intrusive algorithm for eye gaze estimation that works with video input from an inexpensive camera and without special lighting. The main contribution of this paper is proposing a new geometrical model for eye region that only requires the image of one iris for gaze estimation. Essential parameters for this system are the best fitted ellipse of the iris and the pupil center. The algorithms used for both iris ellipse fitting and pupil center localization pose no pre-assumptions on the head pose. All in all, the achievement of this paper is the robustness of the proposed system to the head pose variations. The performance of the method has been evaluated on both synthetic and real images leading to errors of 2.12 and 3.48 degrees, respectively.

Keywords: Gaze Estimation, Projective Geometry, Video-Based Human–Computer Interface, Pupil Center Localization, Iris Ellipse Fitting.

1. Introduction

Eye gaze estimation is utilized in many applications such as driver alertness systems [1,2], psychological researches and determining comprehension while reading texts or watching TV programs [3-5], handicapped rehabilitation and human–computer interaction (HCI) [6,7] which has received attention in the research community in more recent years.

All proposed algorithms of gaze estimation may be classified in two groups. Algorithms in the first group require special devices such as electrodes, special glasses or hats [8-10]. In contrast, algorithms in the second group use one (or much) non-contact camera and computer vision techniques to estimate the gaze direction [7, 11-18]. In most cases, algorithms of the first group result in higher accuracy, but for two reasons they cannot become universal. The first reason is their high cost due to using especial devices. The second one is the contact of their devices to the user body. So, the user cannot be comfortable when using them. Because of this contact, the first group is called “intrusive” and the second one “non-intrusive”. Fig. 1 shows two examples of intrusive and non-intrusive systems.

Fig. 1: Two samples of systems used in intrusive (top row) and non-intrusive (bottom row) methods [7, 17].

Many of the current camera-based interfaces that estimate eye gaze direction make use of active infrared illumination [11-14]. In many approaches, the infrared light reflects off the back of the eye to create a distinct “bright pupil effect” in the image. The light is synchronized with the camera to illuminate the eyes in alternate frames. The eyes are then located by comparing a frame with this bright pupil effect with a subsequent frame without the illuminated

* Corresponding Author

pupils. Typically, the relative gaze direction of an eye is found by analyzing the difference between the center of the bright eye pixel area and the reflection off the surface of the eye from the light source. There is a concern that infrared camera-based interfaces require a complicated calibration procedure which is difficult for small children to follow [7]. However, conventional (non-infrared) cameras are more available and the algorithms that work with them are more applicable.

In recent years, some systems have been proposed that do not require special lighting [7, 15-19]. These systems can be very practical. The principles of such systems are similar. First, the face of the user detects and then determines the location of his/her eyes. The last and the most important step of these algorithms is the estimation of the gaze direction from the eyes and other face landmarks.

Authors in [7] used symmetry between two eyes to classify gaze direction to 3 sides (center, left and right). In the proposed algorithm of [15], a circle is fitted to the iris boundary using Hough transform. Then, current gaze direction is determined by calculating the distance of the iris center from the iris position when it is looking forward. In this algorithm, the gaze direction is divided to 9 directions. In [16] coordinates of the center of mass of the eye region is computed and used to train an MLP (Multilayer Perceptron) to classify any gaze in 4 directions.

In the above algorithms, direction of gaze is limited to some sides. In other algorithms such as [17] gaze direction is represented as a vector in 3D space. In [17], a camera is used to detect the face location and then a pan/tilt/zoom camera with high resolution is used to zoom on the right eye. Finally, the authors in [17] have used geometry of eye in 3D and its projection to 2D to obtain the gaze vector. Using 2 cameras with high resolution and zooming ability for them are the most drawbacks of that algorithm.

In [7, 15, 16], rotation and displacement of the head are limited severely. This problem (limited rotation and displacement for the head) is popular in most of the gaze estimation systems and is very important in a practical system. In [17], another accurate system is used to estimate the eye corners positions in 3D. By adding this system, the authors in [17] claim that their final system is robust to head rotation. Therefore, their system is very expensive. Because of this, we propose an algorithm for gaze estimation that is robust to rotation and displacement of head and does not require another system. The proposed system requires only an inexpensive camera; so, it can be practical for usage. An algorithm box of the approach is given in Fig. 2.

The first step in this algorithm is face and eyes detection and the Viola-Jones algorithm [20] is used to implement them. The focus of this paper is on the next steps. In this paper, a new geometrical model for eye region is proposed that only requires an image of one iris for gaze estimation. Parameters required for gaze estimation in this model are the iris ellipse and the pupil center that novel algorithms are used to compute them.

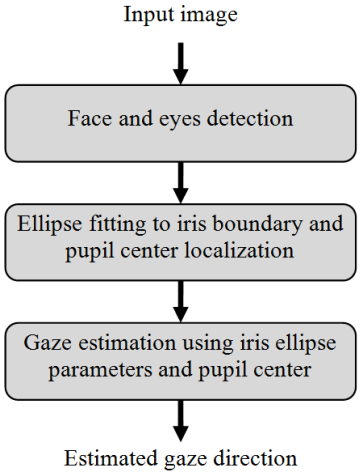

Fig. 2: Block diagram of the proposed gaze estimation approach.

The remainder of this paper is structured as follows. The proposed geometrical model for eye region and the approach to estimate the eye gaze from the iris image are discussed in Section 2 and Section 3, respectively. Experimental results are given on simulated data as well as on real images in section 4. The paper is concluded in Section 5.

2. Eye Model

Fig. 3 shows a physiological model of eye [21]. From this figure, it can be found that the eyeball is like a sphere and the iris boundary is a circle located on the surface of the eyeball. Also, the pupil is a hole on the iris surface with a circle boundary and its center coincides with the iris center. The gaze direction is approximated using a vector that passes through the eyeball center and the iris center [17].

The cornea is the transparent front part of the eye with refractive index of 1.376 that covers the iris, pupil, and anterior chamber [21] and may be regarded as a single spherical surface [22]. The anterior chamber is filled with transparent aqueous humour with refractive index of 1.336 [21], which is close to the refractive index of

cornea. This combination of cornea and aqueous humour acts similar to a plano-convex lens on the surface of the iris. From the camera stand point, considering the position of iris boundary and this plano-convex lens in Fig. 3, the image of the iris border is not affected, but the image of iris surface, including the pupil boundary is affected by refractive property of the lens. The image of pupil boundary from behind of the plano-convex lens, while being in focal distance, appears to the camera a bit larger circle and farther away with the center on the gaze vector [23]. Thus, in image space, the two boundaries of iris and pupil are no longer co-centered.

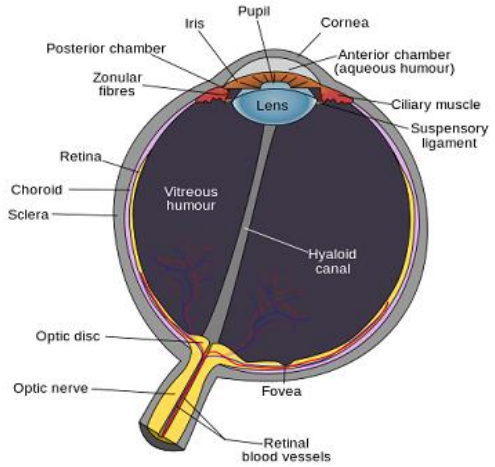

Fig. 3: A biological model of eye [21].

Hence, Fig. 4 is proposed as a simplified eye geometrical model in image space. In this model, the eyeball is a sphere with radius R. The iris boundary is a circle located on the eyeball surface and the distance between the eyeball center and the iris center is denoted by d_i. The pupil boundary is also a circle and the distance between the eyeball center and the pupil center is d_p while $d_p < d_i$. In addition, the gaze direction in the image space is a vector that passes from the eyeball center, the pupil center and the iris center. The eye geometrical model in [17] is similar to Fig. 4; however, the pupil position being a key element in unique solution selection procedure is not defined in it. This concept is discussed later.

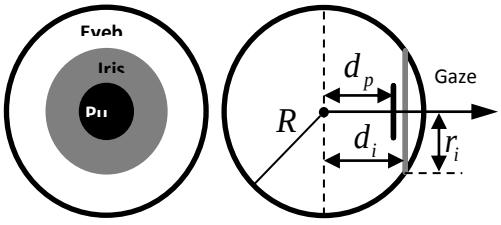

Fig. 4: Proposed geometrical model for eye region and gaze direction.

When changing the eye gaze, the eyeball rotates around its center and the 2D image of eye region may change. Fig. 5 shows three examples of different gaze directions. As can be observed in Fig. 5 and can be proved with projective geometry, the boundary of the iris and the pupil convert to ellipses. So, if an ellipse can fit to the iris boundary, gaze direction may be computed by its parameters. However, for gaze directions that are symmetric about the perpendicular vector to the camera plane (like the first and the third parts in Fig. 5), the iris ellipses are identical. In other words, the iris ellipse parameters return two solutions for gaze direction, but, only one of them is valid. As can be seen in Fig. 5, the position of the pupil in the iris region can separate two symmetric cases. Consideration of this feature for unique solution selection is the main contribution of this model.

Fig. 5: Three different gaze directions and their effects on the 2D images of the iris boundary and the pupil position.

3. Approach of Gaze Estimation

3.1 Gaze direction formulas using the iris boundary

As presented in previous part, it is assumed that the iris contour is a circle and the gaze vector is the normal vector to this circle passing through the eyeball center. From projective geometry, it is proved that the shape of the rotated circle when projected to 2D is an ellipse. But, when we have an ellipse, it can be created from 2 different circles in 3D. Fig. 6 shows an example of this issue. Part (a) of this figure is an ellipse in 2D space and part (b) shows 2 circles in 3D that can be converted to that ellipse by projection. In this figure, darker colors are related to closer sides of circle to the camera. So, if an ellipse can fit to the iris boundary, the gaze vector may be computed from its parameters (two solutions). In this part, the equations of these two ellipses are derived and in the next part, a novel method to select the true solution is proposed.

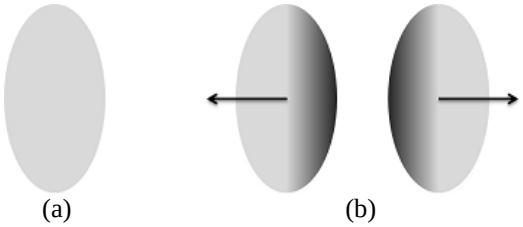

Fig. 6: An ellipse in 2D can be created from projection of two different circles in 3D, (a) an ellipse in 2D, and (b) two corresponding circles in 3D.

Fig. 7 shows an ellipse in 2D space. Parametric equations of such ellipse are as (1) and (2):

$$x(t) = h + a\cos(t)\cos(\varphi) - b\sin(t)\sin(\varphi), \quad (1)$$

$$y(t) = k + a\cos(t)\sin(\varphi) + b\sin(t)\cos(\varphi), \quad (2)$$

where t is a parameter that changes from 0 to 360 degrees; a and b are the major and minor radii, respectively; h and k are the ellipse center coordinate in x and y directions, respectively; φ is the angle between major radius of the ellipse and x direction.

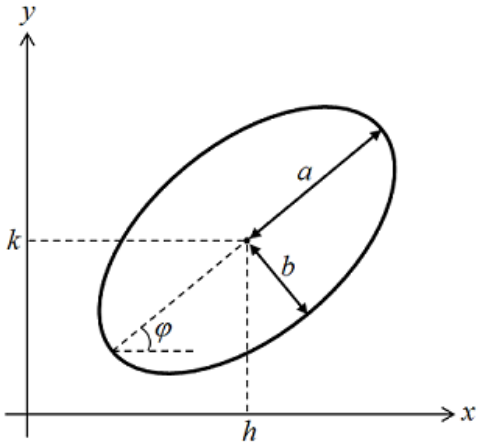

Fig. 7: An ellipse in 2D space.

If a circle with radius r_i rotates about z-axis by θ and about x-axis by ϕ (Fig. 8), equations (3) to (7) are its ellipse parameters:

$$a_i = r_i, \quad (3)$$

$$b_i = r_i \cos(\theta), \quad (4)$$

$$h_i = d_i \sin(\theta)\cos(\phi), \quad (5)$$

$$k_i = d_i \sin(\theta)\sin(\phi), \quad (6)$$

$$\varphi_i = \phi + \pi/2 + k\pi, \quad k = 0,1, \quad (7)$$

where in (5) and (6) d_i is the distance between the eyeball and the iris centers and can be computed from (8):

$$d_i = \sqrt{R^2 - r_i^2}. \quad (8)$$

Now, it is required to compute the invert equations to obtain gaze parameters (θ and ϕ) from ellipse parameters. Using (3), (4) and (7), (9) to (11) can be derived:

$$r_i = a_i, \quad (9)$$

$$\theta = \cos^{-1}(b_i / a_i), \quad (10)$$

$$\phi = \varphi_i - \pi/2 - k\pi, \quad k = 0,1. \quad (11)$$

Also, if (5) and (6) are used, (12) may be obtained as another solution for ϕ:

$$\phi = \text{atan2}(k_i, h_i), \quad (12)$$

where atan2 is the arctangent function with two arguments. However, values of k_i and h_i should be related to the eyeball center and this parameter is unknown. So, we cannot use (12) directly.

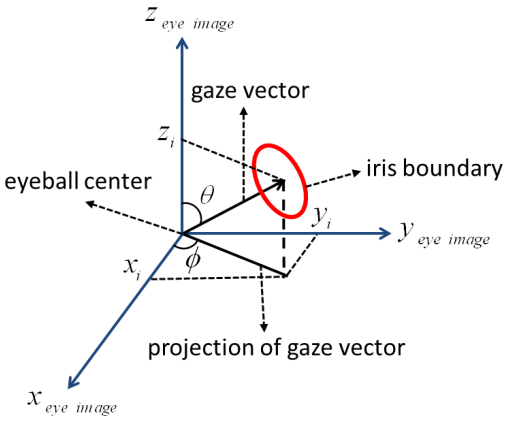

Fig. 8: Coordinate system of the proposed approach.

3.2 Unique solution selection using the pupil center

In [17], it is assumed that eye corners are located on the eyeball sphere. In addition, in [17], it is assumed that he ratio of the eyeball radius to the iris radius is a generic constant. So, their technique is as follows:

1. The eyeball radius estimated by multiplying the iris radius and the generic constant.
2. Two eyeball centers computed with respect to gaze directions and the eyeball radius.
3. Distances of two eyeball centers from two eye corners computed.
4. True solution is one that distances of two eye corners from the related eyeball center are approximately equal.

The main problem in this technique is the requirement to eye corners coordinates in 3D. Accurately localization of eye corners in 3D images is a very hard problem which requires another expensive system. To avoid this requirement, a novel technique obtained from the eye model and projective geometry is proposed. This technique is further discussed.

In previous part, Fig. 4 was proposed for eye model. From this figure, if eye rotates about the eyeball center, new coordinates of the pupil center in 2D image can be obtained from (13) and (14):

$$h_p = d_p \sin(\theta)\cos(\phi), \quad (13)$$

$$k_p = d_p \sin(\theta)\sin(\phi). \quad (14)$$

In (13) and (14) d_p is the distance between the eyeball and the pupil centers. From these equations, the gaze parameter ϕ may be computed as in (15):

$$\phi = \text{atan2}(k_p, h_p). \quad (15)$$

Because the eyeball center coordinate is unknown, we cannot use (15) directly, like (12). To use (12) and (15), a relative equation between the iris and the pupil centers by ϕ is obtained. In previous part, it is shown that in the image space the pupil center is observed to be closer to the eyeball center than the iris center. On the other hand, from (12) and (15) it can be found that coordinate of the pupil and the iris centers are on a line with angle ϕ. Fig. 9 shows this issue that the iris and the pupil centers are located on a line with angle ϕ as well as the reality that the pupil center is closer to the eyeball center. So, if a line connects the pupil center to the iris center, the direction of that line may be equal to ϕ. Therefore, (16) is obtained for ϕ without requiring to know the eyeball center coordinates:

$$\phi = \text{atan2}(k_i - k_p, h_i - h_p). \quad (16)$$

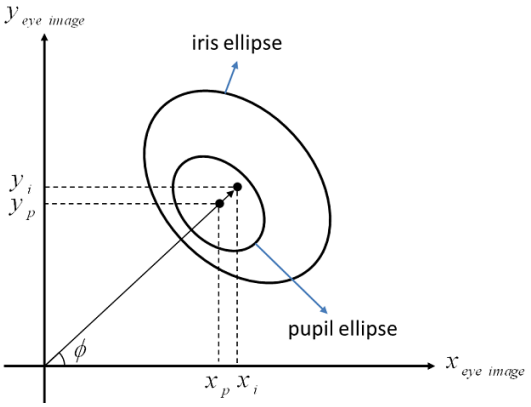

Fig. 9: Positions of the pupil and the iris centers to the eyeball center.

The centers of the pupil and the iris are close together in a conventional image. Thus, the result of (16) may be less accurate than the true result of (11). Thus, it is proposed to use (16) to select the true solution of (11). In other words, one solution of (11) is selected as the true solution that is closer to the result of (16). Fig. 10 shows the proposed technique for unique solution selection. Moreover, Fig. 11 shows two real images of eye region with the connecting vectors from the pupil centers to the iris centers. It can be seen from these images that our assumption about the pupil and the iris relation is valid.

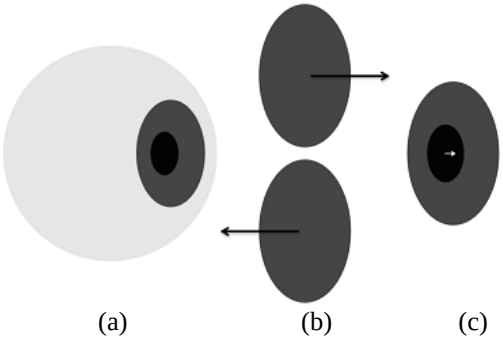

Fig. 10: Unique solution selection based on the position of the pupil center, (a) original image of the eye region, (b) two computed gaze directions with respect to the iris ellipse, and (c) connecting a vector from the pupil center to the iris center and selecting one solution from part (b) which is closer to this vector.

Fig. 11: Connecting the pupil centers to the iris centers for two real images of the eye region.

Table 1 shows the pseudo code of the gaze estimation approach proposed in this paper. In this pseudo code, ϕ_1 is the result of (11) with k = 0 and ϕ_2 is the result of (16). In the 6th command, the closeness of ϕ_2 to the solutions of (11) is investigated. If the absolute distance of ϕ_2 from ϕ_1 is lower than 90°, k must be 0 and ϕ_1 is the true solution. Otherwise, the absolute distance of ϕ_2 from ϕ_1-π will be lower than 90° and k should be 1.

Table 1: Pseudo code of the proposed approach for gaze estimation

Input: an image of one iris

1) Iris ellipse fitting
2) Pupil center localization
3) Compute θ using iris ellipse radii:
   $\theta = \cos^{-1}(b_i / a_i)$
4) Compute ϕ_1 using iris ellipse angle:
   $\phi_1 = \varphi_i - \pi/2$
5) Compute ϕ_2 using iris end pupil centers:
   $\phi_2 = \text{atan2}(k_i - k_p, h_i - h_p)$
6) If $\cos(\phi_2 - \phi_1) > 0$:
   $\phi = \phi_1$
   Otherwise
   $\phi = \phi_1 - \pi$

Output: θ and ϕ

3.3 Sensitivity of the proposed model to the requiring parameters

In this part, the sensitivity of rotation angles in the proposed model w.r.t. requiring parameters is calculated. Angle θ has dependency only upon the ratio of the iris and pupil ellipse radii. So, its sensitivity can be calculated as (17):

$$\frac{d\theta}{d\left(b/a\right)}=\frac{-1}{\sqrt{1-\left(b/a\right)^2}}. \quad (17)$$

Equation (17) expresses that maximum sensitivity of the proposed algorithm is when two radii of ellipse are equal and its minimum is when the minor radius is zero. In other words, when user looks straight to the camera, the sensitivity of the algorithm is max.

Angle ϕ in (11) has a direct relationship to φ; so its sensitivity to φ is 1. On the other hand, for unique solution selection ϕ depends on the pupil center coordinates. Dependency of ϕ upon the pupil center coordinates is discrete since it specifies that k is 0 or 1 in (11). Thus, sensitivity of ϕ to the pupil center coordinates is infinite.

Because of the high sensitivity of θ to diameters of the iris ellipse and ϕ to the pupil center coordinates, algorithms which compute these parameters with high accuracy are required. So, two recently accurate algorithms for iris ellipse fitting [24] and pupil center localization [25] by the authors are used.

4. Experimental Results

The proposed algorithms will be tested first with synthetic and then with real images.

4.1 Experimental results on synthetic images

In this section, to evaluate the performance of the proposed algorithm, we create some sets of synthetic images and apply the algorithm on them.

4.1.1 Synthetic images creation

The proposed geometrical model of eye is used to create the synthetic images. Four samples of these images with the fitted iris ellipse and the estimated gaze direction are shown in Fig. 12. In these images, it is assumed that the eyeball center is located at the origin of the coordinate system. The eyeball, the iris and the pupil radii and ratio of d_p to d_i are assumed to be 1.5, 0.6, 0.15 and 0.9, respectively. Also, it is assumed that eye corners are at (-1.4 , 0) and (1.4 , 0). Upper and lower eyelids pass from (0 , 0.6) and (0 , -0.4), respectively. These assumptions are based on anatomical features of the eye region for human beings.

The algorithm was tested on some sets of synthetic images with different sizes (150×100, 300×200 and 600×400) and the effect of eyelid occlusion was checked.

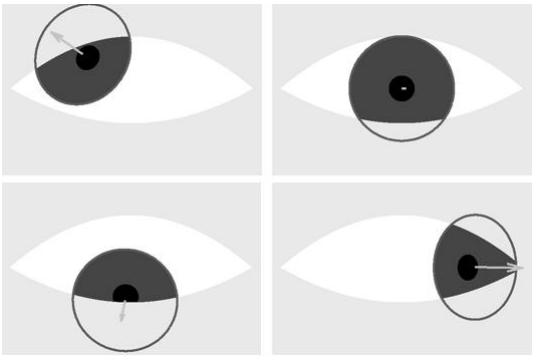

Fig. 12: Fitted ellipse to the iris boundary and estimated gaze direction for 4 samples of the synthetic images.

4.1.2 Accuracy of the proposed algorithm

To evaluate the performance of the proposed algorithm, 5111 images are created for $0 \le \theta \le 35$ and $0 \le \phi \le 360$. However, only 3739 of them, in which less than half of their pupils are occluded by eyelids, are used. The average errors of the proposed algorithm in different sizes (with and without considering eyelid occlusion) are listed in Table 2. As can be seen, the average error of the proposed algorithm is increased when the size of the images decreases. Moreover, by considering eyelid occlusion, pixels on the iris boundary reduced, so, the error of the ellipse fitting algorithm and thereby, the error of the proposed gaze estimation approach increase.

Table 2: The average error of the proposed algorithm on the synthetic images by different sizes (in degrees)

Size of images	150×100	300×200	600×400
With eyelid occlusion	2.1160	0.8462	0.3855
Without eyelid occlusion	0.5880	0.2163	0.0825

It is notable that for the synthetic images by the proposed model, any error for the unique solution selection cannot be occurred. In other words, all of the reported errors in Table 2 are related to the error of the ellipse fitting algorithm. The ellipse fitting algorithm is not under scope of this paper; however, analyzing of the errors can be very interesting.

To analyze the error of the proposed algorithm in more details, the average error for different values of θ (changing ϕ) is plotted in Fig. 13. As can be observed, the maximum error

of the proposed algorithm occurs in $\theta = 0$, whose reason is the high sensitivity of the proposed model for this case. As θ increased, sensitivity of the model reduced, but, more pixels of the iris boundary covered by eyelids and error of the fitted ellipse increased. So, the overall behavior of the average error is descending versus θ, but, in some points, the average error shows a small increasing behavior.

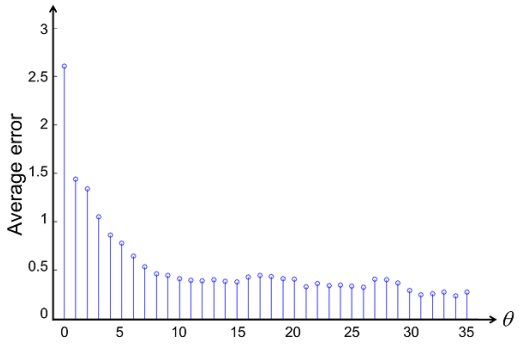

Fig. 13: The average error of the proposed algorithm for different values of θ (changing ϕ).

The average error for different values of ϕ (changing θ) is shown in Fig. 14. We find some important notes in this figure:

1. The average error has two maximum values at angles about 90 and 270 degrees. In these angles, only one part of the iris boundary is observable and the error of their ellipse fitting is high.
2. Values of the maxima are different. Existing difference on concavity for upper and lower eyelids is the reason of this phenomenon.
3. The average error has two minimum values at angles about 0 and 180 degrees. In these angles, two different parts of the iris boundary are observable and the error of their ellipse fitting is low.
4. Locations of the minimum values are not exactly on the 0 and 180 degrees. They have leanings toward the 90 degrees (about 10 and 170 degrees). Its reason is that the concavity of the upper eyelid is higher than the lower one.

Thus, it can be concluded that horizontal error of the proposed algorithm is lower than the vertical one. In addition, eyelid occlusion affects the average error directly.

4.2 Experimental results on real images

One of the problems to evaluate the performance of the proposed algorithm is the lack of a proper database. So, we first prepare a database and then apply our algorithms on it.

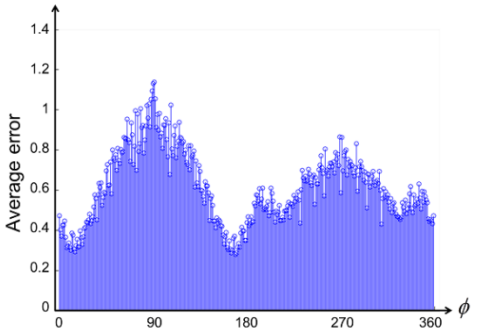

Fig. 14: The average error of the proposed algorithm for different values of ϕ (changing θ).

4.2.1 Database preparation

To evaluate the performance of a gaze estimation algorithm, some images whose gaze directions were known are needed. So, a device that its model can be observed in Fig. 15 is made. In this device a board with sizes of 50cm×50cm and 30 points plotted on it is used. With 40cm distance from the board, there is a location for user's chin that fixes the distance of the user eyes by the floor of the device to approximately 25cm.

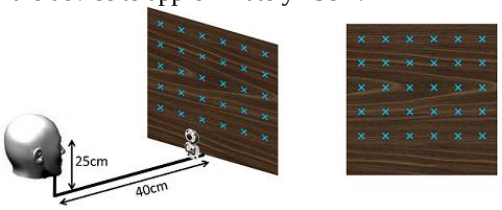

Fig. 15: Two views of the designed device to prepare the gaze estimation database.

The implemented device is shown in Fig. 16. Camera is located at the bottom of the device. This location has two main reasons. First, in real applications, camera cannot be located on the center of the plane which is usually a monitor. So, camera should be located at the top or the bottom of the plane. Second, when the user looks at the bottom of the plane, his upper eyelid covers much of his iris region. In this case, if the image is captured from the bottom of the plane, the iris region is larger in the image. Therefore, the accuracy of the system may be higher than that of a camera located at the top of the plane.

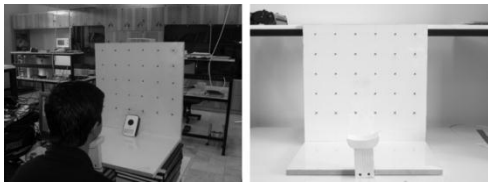

Fig. 16: Two views of the made device to prepare the gaze estimation database.

We got the images from 10 persons. So, the created database has 300 images one of them is shown in Fig. 17.

Fig. 17: A sample image of the created database.

4.2.2 Accuracy of the proposed algorithm

Four samples of the estimated gaze direction, for the images on the database, are shown in Fig. 18. In this figure, the fitted ellipse for two eyes and the estimated gaze direction for them are shown.

Table 2: The average error of the proposed algorithm in estimation of the gaze direction for 10 subjects

Subject	Error (degrees)
1	4.3512
2	3.6551
3	3.1206
4	3.9568
5	3.6545
6	2.9061
7	2.6699
8	4.6781
9	1.7701
10	4.0473
Average	3.4810

Fig. 18: Four samples of the images in the prepared database and their estimated gaze directions.

The average errors of the proposed algorithm for subjects in the database are listed in Table 3. For the 300 images in the database, the average error 3.48 degrees is obtained.

4.3 Sensitivity of the proposed model to head rotation

An important property of the proposed algorithm is its robustness to head rotation. In the proposed model for gaze estimation, only geometrical properties of the iris and the pupil are used. So, if we fit a proper ellipse to the iris boundary and localize the pupil center, the direction of gaze may be estimated without requiring the information of head rotation. Proposed algorithms for iris ellipse fitting [24] and pupil center localization [25] does not use any pre-assumption for head pose; therefore, the proposed system may be robust to head rotation.

There are two different types of the head rotation which are rotation-in-plane (RIP) and rotation-off-plane (ROP) [26] (Fig. 19). RIP is considered to be a rotation about Yaw and Pitch axes and ROP about Roll axis. Fig. 20 shows four images which support all possible head rotations. The eye regions for these images are cropped manually. As can be observed, a proper ellipse is fitted to the iris boundary, and the gaze direction is properly estimated. Therefore, it may be found that the proposed algorithm is robust to head rotations.

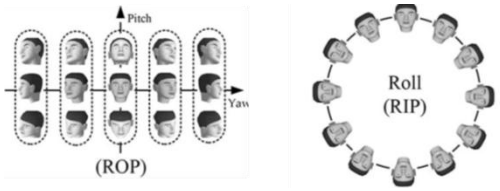

Fig. 19: Different possible head rotations [25].

Fig. 20: Four real images which support different head rotations and estimated gaze directions for them.

4.4 Comparing the proposed system with previous works

Generally speaking, with respect to the experimental results, the average error of the proposed algorithm is about 3.48 degrees. A comparison of the results of this paper with the previous works is listed in Table 4. As can be seen in this table, the average error of the proposed algorithm is lower than the algorithms of [27, 28], but it is higher than algorithms of [17, 29-33]. The main reason for higher accuracy of the algorithms of [17, 29-32] is their equipment. In [29-33], some IR cameras with high zooming capabilities are used which have increased the cost of the system. In addition, algorithm of [17] has employed pan/tilt/zoom cameras as well as a pose estimation system. In contrast, our proposed algorithm and the algorithm of [27] use only an inexpensive webcam. Therefore, the cost of these systems is very lower than the systems of [17, 29-33].

5. Conclusion

In this paper, a non-intrusive method working with video input from an inexpensive camera and without special lighting is presented. As the structures based on desktop cameras are preferred over the head mounted ones according to their ease of use, we used the same structure in our setup. The main contribution of this paper was proposing a new geometrical model for eye region and gaze direction.

To evaluate the performance of the proposed algorithm, we made two sets of synthetic and real images. For real images, the average error of estimated gaze direction was 3.48 degrees.

The sensitivity of the system increases in directions that the subject looks directly toward the camera. To reduce this sensitivity, we can add another camera to the proposed system. In this case, there is always at least one camera which is not in the path of gaze and has low sensitivity. In addition, a hierarchical keyboard can be designed to prepare this system for eye typing.

Table3: Comparing the proposed system by the previous ones

system	Requiring devices	Price	User mode	Horizontal accuracy (degrees)	Vertical accuracy (degrees)
Commercial systems in [28-32]	IR cameras with high zooming ability	Averagely, tens of thousands dollar	Desktop - Head mounted	0.5-1	0.5-1
Proposed system in [17]	Precise pose detection system and two cameras with pan/tilt/zoom ability	-	Desktop	1	1
Proposed system in [26]	IR camera with high zooming ability	-	Desktop	5	8
Proposed system in [27]	Webcam	A few hundred dollars	Desktop	8	8.5
Proposed system in this paper	webcam	A few hundred dollars	Desktop	2.23	3.03

References

[1] P. Smith, M. Shah, and N. da Vitoria Lobo, "Monitoring head/eye motion for driver alertness with one camera," 15th International Conference on Pattern Recognition, pp. 636-642, vol.4, 2000.

[2] B. Bhowmick, and K. S. Chidanand Kumar, "Detection and classification of eye state in IR camera for driver drowsiness identification," IEEE International Conference on Signal and Image Processing Applications, pp. 340-345, 2009.

[3] N. Franck, E. Daprati, F. Michel, M. Saoud, J. Daléry, M. Marie-Cardine, and N. Georgieff, "Gaze discrimination is unimpaired in schizophrenia," Psychiatry Research, vol. 81, no. 1, pp. 67-75, 1998.

[4] D. D. Salvucci, "Inferring intent in eye-based interfaces: tracing eye movements with process models," SIGCHI conference on Human factors in computing systems, Pittsburgh, Pennsylvania, United States, 1999.

[5] Y. Sawahata, R. Khosla, K. Komine, N. Hiruma, T. Itou, S. Watanabe, Y. Suzuki, Y. Hara, and N. Issiki, "Determining comprehension and quality of TV programs using eye-gaze tracking," Pattern Recognition, vol. 41, no. 5, pp. 1610-1626, 2008.

[6] O. Spakov, and P. i. Majaranta, "Scrollable Keyboards for Casual Eye Typing," Psychnology Journal, vol. 7, no. 2, pp. 159-173, 2009.

[7] J. J. Magee, M. Betke, J. Gips, M. R. Scott, and B. N. Waber, "A Human-Computer Interface Using Symmetry Between Eyes to Detect Gaze Direction," IEEE Transactions on Systems, Man and Cybernetics, Part A: Systems and Humans, vol. 38, no. 6, pp. 1248-1261, 2008.

[8] D. G. Evans, R. Drew, and P. Blenkhorn, "Controlling mouse pointer position using an infrared head-operated joystick," IEEE Transactions on Rehabilitation Engineering, vol. 8, no. 1, pp. 107-117, 2000.

[9] R. Vaidyanathan, C. Beomsu, L. Gupta, K. Hyunseok, S. Kota, and J. D. West, "Tongue-Movement Communication and Control Concept for Hands-Free Human-Machine Interfaces," IEEE Transactions on Systems, Man and Cybernetics, Part A: Systems and Humans, vol. 37, no. 4, pp. 533-546, 2007.

[10] R. Barea, L. Boquete, M. Mazo, and E. Lopez, "System for assisted mobility using eye movements based on electrooculography," IEEE Transactions on Neural Systems and Rehabilitation Engineering, vol. 10, no. 4, pp. 209-218, 2002.

[11] C. H. Morimoto, D. Koons, A. Amir, and M. Flickner, "Pupil detection and tracking using multiple light sources," Image and Vision Computing, vol. 18, no. 4, pp. 331-335, 2000.

[12] Z. Zhu, and Q. Ji, "Eye and gaze tracking for interactive graphic display," Machine Vision and Applications, vol. 15, no. 3, pp. 139-148, 2004.

[13] P. Kang Ryoung, "A Real-Time Gaze Position Estimation Method Based on a 3-D Eye Model," IEEE Transactions on Systems, Man, and Cybernetics, Part B: Cybernetics, vol. 37, no. 1, pp. 199-212, 2007.

[14] Y. Dong Hyun, and C. Myung Jin, "Non-intrusive eye gaze estimation without knowledge of eye pose," Sixth IEEE International Conference on Automatic Face and Gesture Recognition, pp. 785-790, 2004.

[15] D. B. B. Liang, and H. Lim Kok, "Non-intrusive eye gaze direction tracking using color segmentation and Hough Transform," International Symposium on Communications and Information Technologies, pp. 602-607, 2007.

[16] H. M. Peixoto, A. M. G. Guerreiro, and A. D. D. Neto, "Image processing for eye detection and classification of the gaze direction," International Joint Conference on Neural Networks, pp. 2475-2480, 2009.

[17] J. G. Wang, E. Sung, and R. Venkateswarlu, "Estimating the eye gaze from one eye," Computer Vision and Image Understanding, vol. 98, pp. 83-103, 2005.

[18] M. R. Mohammadi, and A. Raie, "Robust pose-invariant eye gaze estimation using geometrical features of iris and pupil image," 20th Iranian Conference on Electrical Engineering, pp. 593-598, 2012.

[19] M. R. Mohammadi, and A. Raie, "Selection of Unique Gaze Direction Based on Pupil Position," IET Computer Vision, vol. 7, 2013.

[20] P. A. Viola, and M. J. Jones, "Robust Real-Time Face Detection," International Journal of Computer Vision, vol. 57, no. 2, pp. 137-154, 2004.

[21] http://en.wikipedia.org/wiki/Eye.

[22] A. Villanueva, and R. Cabeza, "Evaluation of Corneal Refraction in a Model of a Gaze Tracking System," IEEE Transactions on Biomedical Engineering, 2008, vol. 55, no. 12, pp. 2812-2822.

[23] http://en.wikipedia.org/wiki/Lens_(optics)

[24] M. R. Mohammadi, and A. Raie, "A Novel Accurate Algorithm to Ellipse Fitting for Iris Boundary Using Most Iris Edges," Journal of American Science, vol. 8, 2012.

[25] M. R. Mohammadi and A. Raie, "A Novel Technique for Pupil Center Localization Based on Projective Geometry," 7th Iranian Conference on Machine Vision and Image Processing, pp. 1-5, 2011.

[26] H. Chang, A. Haizhou, L. Yuan, and L. Shihong, "High-Performance Rotation Invariant Multiview Face Detection," IEEE Transactions on Pattern Analysis and Machine Intelligence, vol. 29, no. 4, pp. 671-686, 2007.

[27] Z. Zhu, K. Fujimura, and Q. Ji, "Real-time eye detection and tracking under various light conditions," Symposium on Eye tracking research & applications, New Orleans, Louisiana, 2002.

[28] P. Majaranta and K.-J. Räihä, "Text entry by gaze: Utilizing eye-tracking," Text entry systems: Mobility, accessibility, universality, pp. 175-187, 2007.

[29] http://www.eyecan.ca, 2012.

[30] http://www.eyegaze.com, 2012.

[31] http://www.eyetechds.com, 2012.

[32] http://www.sr-research.com, 2012.

[33] http://www.tobii.com, 2012.

Mohammad Reza Mohammadi was born in Qom in Iran, on July 25, 1987. He received BSc and MSc degrees both in electrical engineering with rank one from Amirkabir University of Technology (Tehran Polytechnic). He is currently PhD candidate of electrical engineering in Sharif University of Technology. His interests and researches include Machine Vision and Machine Learning.

Abolghasem Asadollah Raie received the B.Sc. degree in Electrical Engineering from Sharif University of Technology, Iran, in 1973 and the M.Sc. and Ph.D. degrees in Electrical Engineering from University of Minnesota, USA, in 1979 and 1982, respectively. Currently, he is an Associate Professor with the Electrical Engineering Department of AmirKabir University of Technology, Iran. His research interests are algorithm design and performance analysis, machine vision, sensor fusion, and mobile robots navigation.

Cyclic Correlation-Based Cooperative Detection for OFDM-Based Primary Users

Hamed Sadeghi*
Electrical and Computer Engineering Department, Ph.D Candidate Tarbiat Modares University, Tehran, Iran
hamed.sadeghi@modares.ac.ir
Paiez Azmi
Electrical and Computer Engineering Department, Professor Tarbiat Modares University, Tehran, Iran
pazmi@modares.ac.ir

Received: 15/Jul/2013 Accepted: 31/Aug/2013

Abstract
This paper develops a new robust cyclostationary detection technique for spectrum sensing of OFDM-based primary users (PUs). To do so, an asymptotically constant false alarm rate (CFAR) multi-cycle detector is proposed and its statistical behavior under null hypothesis is investigated. Furthermore, to achieve higher detection capability, a soft decision fusion rule for performing cooperative spectrum sensing (CSS) in secondary networks is established. The proposed CSS scheme aims to maximize the deflection criterion at the fusion center (FC), while the reporting channels are under Rayleigh fading. In order to be able to evaluate the performance of the cooperative detector, some analytic threshold approximation methods are provided for the cases where the FC has direct sensing capability or not. Through numerical simulations, the proposed local and CSS schemes are shown to significantly enhance CR network performance in terms of detection probability metric.

Keywords: Cooperative Spectrum Sensing, Cyclostationary, Cognitive Radio, Primary User Detection.

1. Introduction

Cooperative spectrum sensing (CSS) methods were proposed in literature to improve the detection performance of secondary networks [1, 2]. However, most existing scenarios assume that all the cooperating users use the commonly adopted energy detection (ED) technique for their local sensing. But, despite the simplicity, quickness and no requirements of pre-knowledge about the PU's signal, the ED method has some challenging issues. For example, it cannot differentiate primary users (PUs) from secondary users (SUs), and requires knowing the noise variance to ensure proper detection performance [3]. Therefore, ED-based CSS methods are prone to false detections [2, 4].

In addition, ED-based soft decision fusion rules that has been recently introduced in literature, such as [5-7], assume that the perfect knowledge about the noise variances of sensing channels are available at fusion center (FC). However, in practice, this assumption may be unrealistic. Therefore, the cooperative sensing methods based on local ED may be very susceptible to noise uncertainties of sensing channels and therefore their performance can be dictated by the accuracy of the noise power estimations at SUs.

Cyclostationary detection (CD)-based sensing methods are proposed in literature to address the above issues [2,4,8-11]. These detectors exploit inherent cyclostationary properties of digitally-modulated signals and have acceptable performance in very low SNRs [2,12]. However, despite the advantages of CD over ED-based spectrum sensing, there are rather limited researches on CD-based CSS, mostly because of its complicated analytic expressions and also complexities that may arise in implementation of the CD algorithms.

Some recent works were addressed the complexity issue of CD methods. For example, a new CD-based CSS method is proposed in [13]. But, there are two drawbacks with this method. Firstly, its performance can be dictated by the uncertainties in estimating the noise variances of sensing channels at the SUs since the thresholds for the single-cycle and multi-cycle detectors are functions of the noise variance. Secondly, because the proposed detectors are constructed based on the cyclic autocorrelation function (CAF) estimates at zero time-lags, the performance for detecting OFDM-based primary or secondary users may be very poor. It is well-known that the strong cyclic frequencies of OFDM-based transmissions are located at time-lags equal to $\tau = T_u$, where T_u is the useful symbol length of the OFDM symbol [11].

In this paper, we propose a simplified cyclic correlation-based detection algorithm for the

* Corresponding Author

local spectrum sensing which does not require any specific assumption about the distribution of PU signals. In other words, to combat the above-mentioned spectrum sensing problems (that exist in conventional ED and some CD methods), we propose a CD detector that does not:

- require any specific assumption about the statistical distribution of PU signal,
- need any prior knowledge about the noise variance of the sensing channel,
- know the statistics of fading channel.

In this context, we derive a Generalized Likelihood Ratio Test (GLRT) based on asymptotic distribution of second-order cyclic correlation vector. Then, we analytically characterize the asymptotic distributions of the test statistic under null and alternative hypotheses. In order to evaluate the performance of the test, we derive closed-form expressions for the false alarm and detection probabilities, and verify them through numerical simulations.

It is widely-known that using multiple cycle frequencies at cyclostationary detectors does improve the detection performance. Thus, we also propose a new multi-cycle detector.

Based on the proposed local sensing method, we then develop a weighted soft combination method for the CSS. This method is based on the deflection criterion maximization at the FC and achieves better detection performance compared to the conventional cooperative detectors. Furthermore, it provides reliable detection performance when both the reporting and sensing channels are under fading impairments.

In this paper, a threshold estimation method for CSS is provided in order to perform decision making at the fusion center. Simulation results confirm that the proposed analytical threshold setting procedures have adequate accuracy for performance analysis purposes. It should be noted that our proposed method does not need any prior knowledge about the noise variances of sensing channels or their fading statistics.

The remainder of this paper is organized as follows. System model is presented in Section 2. The local sensing strategy is described in Section 3. The cooperative detection algorithm is developed in Section 4. Performances of proposed schemes are investigated in Section 5. Finally, the conclusions are drawn in Section 6.

2. System Model

It is assumed that the base-band discrete-time received signal for ith SU, $x_i(n)$, $i = 1,2,\cdots,L$, at a time instance n is given by:

$$x_i(n) = \eta\, g_i\, \tilde{x}(n) + w_i(n), \qquad n = 1,\cdots,M, \qquad (1)$$

where L refers to the number of secondary users existing in the network, g_i denotes the channel fading coefficient between PU to ith SU, and $w(n) \sim \mathcal{CN}(0, \delta_i^2)$ with δ_i^2 as the variance of the complex additive Gaussian noise. Note that δ_i^2 and g_i are generally unknown.

Moreover, $\eta = 0$ and $\eta = 1$ correspond to null (inactive PU) and alternative (active PU) hypotheses, respectively. We assume that the PU is either active or inactive during the sensing duration. The signal transmitted by PU is denoted by $\tilde{x}(n)$. Without loss of generality, $\tilde{x}(n)$, g_i and $w_i(n)$ are assumed to be independent of each other. Furthermore, conditional independence of spatially distributed SUs is assumed [2].

After the decision statistic $\mathcal{T}_i$ at the ith SU is computed, it is transmitted to the FC through an independent reporting channel that experiences fading. Hence,

$$\tilde{\mathcal{T}}_i = h_i \mathcal{T}_i + z_i, \qquad i = 1,\cdots,L, \qquad (2)$$

where $z_i \sim \mathcal{N}(0, \sigma_i^2)$ and h_i is a real-valued fading envelope with $h_i > 0$. We assume that $\{h_i\}_{i=1}^{L}$ are constant during the detection interval. Without loss of generality, we assume that the Rayleigh fading channels have unit powers (i.e. $E(h_i^2) = 1$). In addition, the above model assumes the well-known phase-coherent reception at FC. Note that $\tilde{\mathcal{T}}_i$ represents the received signal from ith SU.

Since in many cognitive radio scenarios the envelope of the fading channel and the noise variance can be estimated in advance, we assume that the quantities $\{h_i\}_{i=1}^{L}$ and $\{\sigma_i^2\}_{i=1}^{L}$ are perfectly known to the FC [5-7, 14, 15].

3. Proposed Cyclostationarity-based Detection Method

Assume that we want to test for the presence of the cyclostationarity at a candidate cycle frequency α (known prior or can be estimated [12]) in the received signal x(n).

For a given time lag τ and a cycle frequency α, the estimated cyclic autocorrelation function (CAF) is defined to be [12]:

$$\widehat{\mathcal{M}}_{2x}(\alpha;\tau) \triangleq \hat{E}_M\{x(n)x^*(n+\tau)e^{-j2\pi n\alpha}\}, \qquad (3)$$

where $\hat{E}_M\{f(n)\} \triangleq (\frac{1}{M}).\sum_{n=1}^{M} f(n)$ denotes the M-sample average. It has been proven in [16] that subject to certain mixing conditions, $\widehat{\mathcal{M}}_{2x}(\alpha;\tau)$ is a consistent and asymptotically (i.e. as $M \to \infty$) normal estimator of the cyclic moment $\mathcal{M}_{2x}(\alpha;\tau)$. In essence, the expression $\sqrt{M}[\widehat{\mathcal{M}}_{2x}(\alpha;\tau) - \mathcal{M}_{2x}(\alpha;\tau)]$ asymptotically converges in distribution to a complex normal

variable [16]. Therefore, the real and imaginary parts of $\widehat{\mathcal{M}}_{2x}(\alpha;\tau)$ are jointly Gaussian.

In this paper, we propose to only consider the real part of $\widehat{\mathcal{M}}_{2x}(\alpha;\tau)$. This causes the resulting test statistic to have a reduced complexity, as compared to the case where the whole structure is considered for deriving the decision statistic. Let,

$$\widehat{\mathcal{M}}_{2x}(\alpha;\tau) \triangleq \Re\{\widehat{\mathcal{M}}_{2x}(\alpha;\tau)\} + j\Im\{\widehat{\mathcal{M}}_{2x}(\alpha;\tau)\} \quad (4)$$

where $\Re$ and $\Im$ denote the real and imaginary parts, respectively. Consequently, the following convergence holds true for the asymptotic case:

$$\sqrt{M}[\Re\{\widehat{\mathcal{M}}_{2x}(\alpha;\tau)\} - \Re\{\mathcal{M}_{2x}(\alpha;\tau)\}] \xrightarrow{\mathcal{L}} \mathcal{N}(0,\varrho^2) \quad (5)$$

Our aim is to devise a cyclic feature detector based on the above property. To this end, let us define

$$\mathcal{U} \triangleq \sqrt{M}\,\Re\{\mathcal{M}_{2x}(\alpha;\tau)\}, \quad (6)$$

and its estimation:

$$\hat{\mathcal{U}} \triangleq \sqrt{M}\,\Re\{\widehat{\mathcal{M}}_{2x}(\alpha;\tau)\}. \quad (7)$$

Following the discussions in [16], it can be shown that:

$$\hat{\mathcal{U}} \xrightarrow{\mathcal{L}} \begin{cases} \mathcal{N}(0,\varrho^2), & \text{under } \mathcal{H}_0 \\ \mathcal{N}(\mu_1,\varrho^2), & \text{under } \mathcal{H}_1 \end{cases}, \quad (8)$$

where $\mu_1 = \mathcal{U}$, which is unknown but is non-random. Based on above discussions we can constitute the following generalized likelihood ratio test (GLRT):

$$\mathcal{L}_G = \frac{\Pr(\hat{\mathcal{U}};\hat{\mu}_1,\hat{\varrho}^2|\mathcal{H}_1)}{\Pr(\hat{\mathcal{U}};\hat{\varrho}^2|\mathcal{H}_0)} = \frac{\frac{1}{\sqrt{2\pi\hat{\varrho}^2}}\exp(-\frac{(\hat{\mathcal{U}}-\hat{\mathcal{U}})^2}{2\hat{\varrho}^2})}{\frac{1}{\sqrt{2\pi\hat{\varrho}^2}}\exp(-\frac{\hat{\mathcal{U}}^2}{2\hat{\varrho}^2})}. \quad (9)$$

In the above equation, the numerator is obtained by substituting μ_1 with its estimation. Thus, the decision statistic can be computed from the generalized log-likelihood ratio (GLLR) function:

$$\mathcal{T}_G = 2\ln\mathcal{L}_G = \frac{\hat{\mathcal{U}}^2}{\hat{\varrho}^2} \begin{cases} \le \eta: & \text{Decide } \mathcal{H}_0 \\ \ge \eta: & \text{Decide } \mathcal{H}_1 \end{cases} \quad (10)$$

where η is the threshold value. Since $\widehat{\mathcal{M}}_{2x}(\alpha;\tau)$ is mean-square sense consistent [16], we can obtain that

$$\lim_{M\to\infty} \hat{\mathcal{U}}_{2x}(\alpha;\tau) \xrightarrow{\text{m.s.s.}} \mathcal{U}_{2x}(\alpha;\tau) \quad (11)$$

where denotes the mean-square sense convergence. Therefore, under null hypothesis,

$$\lim_{M\to\infty} \hat{\mathcal{U}}_{2x}(\alpha;\tau) \xrightarrow{\mathcal{L}} \mathcal{Z} \sim \mathcal{N}(0;\varrho^2) \quad (12)$$

Furthermore, $\hat{\varrho}^2$ converges in the m.s.s. to ϱ^2 [12, 16]. Since convergence in m.s.s. implies convergence in probability [p. 234][17], we can conclude that $\lim_{M\to\infty}\hat{\varrho}^2 \xrightarrow{P} \varrho^2$. Therefore, based on Slutsky's theorem [Th.3.3][18], we deduce that

$$\lim_{M\to\infty} \frac{\hat{\mathcal{U}}^2}{\hat{\varrho}^2} \xrightarrow{\mathcal{L}} \frac{1}{\varrho^2}\mathcal{Z}^2. \quad (13)$$

Consequently, under $\mathcal{H}_0$ the following result can be obtained:

$$\lim_{M\to\infty} \mathcal{T}_G \xrightarrow{\mathcal{L}} \chi_1^2, \quad (14)$$

and under $\mathcal{H}_1$ we have

$$\lim_{M\to\infty} \mathcal{T}_G \xrightarrow{\mathcal{L}} \acute{\chi}_1^2\left(\frac{\mathcal{U}^2}{\varrho^2}\right). \quad (15)$$

Hence, once the threshold is fixed for a given P_{fa}, the obtained P_d will depend naturally on the unknown parameter $\hat{\varrho}^2$. Therefore, in practice, we propose to use the following approximate distribution for large values of M:

$$\mathcal{T}_G \sim \acute{\chi}_1^2\left(\frac{\hat{\mathcal{U}}^2}{\hat{\varrho}^2}\right). \quad (16)$$

The variance ϱ^2 can be computed by the following expression:

$$\begin{aligned} \varrho^2 &= \mathrm{Var}\{\mathcal{U}\} \\ &= \mathrm{Mcum}\left\{\Re\{\widehat{\mathcal{M}}_{2x}(\alpha;\tau)\}, \Re\{\widehat{\mathcal{M}}_{2x}(\alpha;\tau)\}\right\} \\ &= \frac{1}{2}\Re\left\{\mathrm{M}\mathbb{C}\mathrm{um}\{\widehat{\mathcal{M}}_{2x}(\alpha;\tau)\} + \mathrm{M}\mathbb{C}\mathrm{um}\{\widehat{\mathcal{M}}_{2x}^*(\alpha;\tau)\}\right\}. \end{aligned} \quad (17)$$

where $\mathbb{C}\mathrm{um}\{.,.\}$ denotes the cumulant operator. Therefore, if we define two asymptotic covariance:

$$\mathcal{Q} \triangleq \mathrm{M}\mathbb{C}\mathrm{um}\{\widehat{\mathcal{M}}_{2x}(\alpha;\tau), \widehat{\mathcal{M}}_{2x}(\alpha;\tau)\}, \quad (18)$$

and

$$\mathcal{S} \triangleq \mathrm{M}\mathbb{C}\mathrm{um}\{\widehat{\mathcal{M}}_{2x}(\alpha;\tau), \widehat{\mathcal{M}}_{2x}^*(\alpha;\tau)\}, \quad (19)$$

then, the asymptotic variance of $\hat{\mathcal{U}}$ can be expressed as:

$$\varrho^2 = \frac{1}{2}\Re\{\mathcal{S}+\mathcal{Q}\}. \quad (20)$$

In practice, these elements can be estimated respectively by:

$$\hat{\mathcal{Q}} \triangleq \frac{M}{P}\sum_{s=-\frac{P-1}{2}}^{\frac{P-1}{2}} W_P(s)\widehat{\mathcal{M}}_{2x}\left(\alpha-\frac{s}{M};\tau\right)\widehat{\mathcal{M}}_{2x}\left(\alpha+\frac{s}{M};\tau\right), \quad (21)$$

and

$$\hat{\mathcal{S}} \triangleq \frac{M}{P}\sum_{s=-\frac{P-1}{2}}^{\frac{P-1}{2}} W_P(s)\left|\widehat{\mathcal{M}}_{2x}\left(\alpha+\frac{s}{M};\tau\right)\right|^2. \quad (22)$$

In the above equation, W_P is a normalized smoothing window with an odd length P,

$$W_P(s) \triangleq \begin{cases} I_0\left(\beta\sqrt{1-\frac{4s^2}{P^2}}\right), & -\frac{P-1}{2} \le s \le \frac{P+1}{2} \\ 0, & \text{o.w.} \end{cases}, \quad (23)$$

where $I_0(.)$ is the modified Bessel function of first-kind and zero-order. It should be noted that the values of P and β should be pre-set in the detection algorithm.

Using the above results, the estimated variance can be expressed as $\hat{\varrho}^2 = \frac{1}{2}[\Re\{\hat{\mathcal{Q}}\}+\hat{\mathcal{S}}]$. However, in the low-SNR regimes, which is of interest in spectrum sensing scenarios as well as cyclostationarity-based detection applications, we have $\hat{\mathcal{S}} \gg \Re\{\hat{\mathcal{Q}}\}$. Thus, in practice, we propose the following expression for the variance estimation:

$$\hat{\varrho}^2 \approx \frac{M}{2P}\sum_{s=-\frac{P-1}{2}}^{\frac{P-1}{2}} W_P(s)\left|\widehat{\mathcal{M}}_{2x}\left(\alpha+\frac{s}{M};\tau\right)\right|^2. \quad (24)$$

Since this expression is derived for low-SNR conditions, it may not provide enough accuracy for moderate- and high-SNR regimes. However, we will show in Section II through simulation results that (24) results in an acceptable performance for all SNR values.

3.1 Threshold Selection and Analytic Performance Expression

Using (14) we can obtain the false alarm probability as below:

$$P_{fa} = \Pr\{\mathcal{T}_G > \eta|\mathcal{H}_0\} = 1-\mathcal{F}_{\chi_1^2}(\eta) = 1-\frac{\gamma\left(\frac{1}{2},\frac{\eta}{2}\right)}{\Gamma\left(\frac{1}{2}\right)}, \quad (25)$$

where $\mathcal{F}_{\chi_1^2}$ is cumulative distribution function (CDF) of chi-square variable with one degrees of freedom. In addition, $\gamma(.,.)$ and $\Gamma(.)$ denote the lower incomplete Gamma function and Gamma function, respectively [19]. It can be shown that

$$\gamma\left(\frac{1}{2},\frac{\eta}{2}\right) = \sqrt{\pi}.\,\mathrm{erf}\left(\sqrt{\eta/2}\right) = 1-2Q\left(\sqrt{\eta}\right), \quad (26)$$

where

$$\mathrm{erf}(x) = \frac{2}{\sqrt{\pi}}\int_0^x \exp(-t^2)\,dt, \quad (27)$$

and Q denotes the right-tail probability of standard Gaussian distribution [19]. Therefore, the threshold value can be determined by

$$P_{fa} = 2Q\left(\sqrt{\eta}\right). \quad (28)$$

Since the threshold value does not depend on the sensing channel parameters (e.g. SNR value, noise variance, fading gain, etc.), it can be computed directly from the P_{fa} value, and therefore the proposed detection algorithm can be introduced as a constant false alarm rate (CFAR) test.

Using the same line as above, the detection probability can be derived as follows:

$$P_d = \Pr\{\mathcal{T}_G > \eta|\mathcal{H}_1\} = 1-\mathcal{F}_{\acute{\chi}_1^2(\lambda)}(\eta) = 1-\mathcal{F}_{\acute{\chi}_1^2(\lambda)}((Q^{-1}(0.5P_{fa}))^2), \quad (29)$$

where

$$\lambda \triangleq \frac{\hat{\mathcal{U}}^2}{\hat{\varrho}^2}, \quad (30)$$

Validity of the above asymptotic distributions is confirmed in our subsequent discussions in Section 5.

3.2 Extension to the Multi-Cycle Detectors

It is well-known that detecting multiple cyclic frequencies at the same time would enhance the detection performance [2, 13, 20]. Most of the current researches have simply proposed the summation of test statistics of different cyclic frequencies for multi-cycle detection purposes [2, 8, 13]. However, using the same procedure as in [20], we alternatively propose the following multi-cycle (MC) detector:

$$\mathcal{T}_{MC} = \frac{1}{\sqrt{\sum_{i=1}^{N_\alpha} w_i^2}}\sum_{i=1}^{N_\alpha} w_i^2 \mathcal{T}_G^{\alpha_i}, \quad (31)$$

where

$$w_i \triangleq \left\{\frac{\mathcal{U}^2}{\varrho^2}\right\}\Big|_{\alpha_i}, \quad (32)$$

and $\mathcal{T}_G^{\alpha_i}$ denote the noncentrality parameter and the test statistic corresponding to a cyclic frequency α_i, respectively. In the same equation, N_α denotes the number of intended cyclic frequencies. It is noteworthy that the above detector combines different cyclic frequencies in a way that the deflection coefficient is maximized [20].

To perform hypothesis testing, the null distribution of (31) is required to be computed. Since CAFs of different cyclic frequencies are statistically independent under the null hypothesis [8], we can approximate the CDF by inversion of corresponding characteristic function (CF) of $\mathcal{T}_{MC}$. Fist, assume that the CF of $\mathcal{T}_{MC}$ is defined as:

$$\Phi_i(t) \triangleq E\left[\exp(jt\mathcal{T}_G^{\alpha_i})\right]. \quad (33)$$

In this case, we can write

$$\Phi_{\mathcal{T}_{MC}}(t) = \prod_{i=1}^{N_\alpha}\Phi_i(w_i t). \quad (34)$$

Since $\mathcal{T}_G^{\alpha_i} \sim \chi_1^2$, the following equation holds true:

$$\Phi_i(t) = (1-2jt)^{-1/2}. \quad (35)$$

Using the above expression, we can conclude that:

$$\Phi_{\mathcal{T}_{MC}}(t) = \prod_{i=1}^{N_\alpha}(1-2jw_i t)^{-1/2}. \quad (36)$$

Now, employing the well-known Gil-Palaez theorem [21], we can compute the corresponding CDF of $\Phi_{\mathcal{T}_{MC}}$ under $\mathcal{H}_0$ as follows:

$$\mathcal{F}_{\mathcal{T}_{MC}}(x) = \frac{1}{2}-\frac{1}{\pi}\int_0^\infty \frac{\Im\{\Phi_{\mathcal{T}_{MC}}(t)e^{-jtx}\}}{t}dt. \quad (37)$$

Consequently, substitution of (36) into (37) yields the resultant CDF expression:

$$\mathcal{F}_{\mathcal{T}_{MC}|\mathcal{H}_0}(x) = \frac{1}{2}-\frac{1}{\pi}\int_0^\infty \frac{\Im\left\{\prod_{i=1}^{N_\alpha}(1-2jw_i t)^{-\frac{1}{2}}e^{-jtx}\right\}}{t}dt, \quad (38)$$

which can be simply computed using the numerical integration techniques. Finally, since

$$P_{fa} = \Pr\{\mathcal{T}_{MC} > \check{\eta}|\mathcal{H}_0\} = 1-\mathcal{F}_{\mathcal{T}_{MC}}(\check{\eta}), \quad (39)$$

we can calculate the threshold value as below:

$$\check{\eta} = \mathcal{F}_{\mathcal{T}_{MC}}^{-1}(1 - P_{fa}). \quad (40)$$

Accuracy of the proposed method is investigated in Fig. 1. We have simulated the distribution function of sum of five central chi-square variables as $0.4927\chi_1^2 + 0.5478\chi_2^2 + 0.0768\chi_4^2 + 0.5523\chi_6^2 + 0.3824\chi_2^2$. The weights are generated in a random manner. The simulation curve presents the real accurate distribution. As we can see, the estimated CDF, which is computed from (38), follows very closely the simulated distribution. Thus, the proposed threshold determination method can be reliably implemented at SUs.

Fig. 2 provides another example. The sum of ten random variables is simulated. The sum distribution is selected to be $0.4507\chi_2^2 + 0.2453\chi_3^2 + 0.3899\chi_7^2 + 0.1190\chi_1^2 + 0.4874\chi_5^2 + 0.0337\chi_4^2 + 0.4693\chi_6^2 + 0.2782\chi_2^2 + 0.0779\chi_7^2 + 0.1676\chi_1^2$. The results of numerical simulations confirms the superior performance of the proposed method.

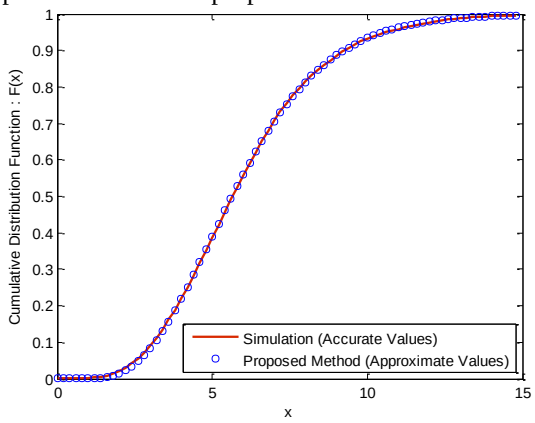

Fig. 1 Accuracy of the proposed threshold selection method. The simulated distribution is $0.4927\chi_1^2 + 0.5478\chi_2^2 + 0.0768\chi_4^2 + 0.5523\chi_6^2 + 0.3824\chi_2^2$ (random-generated weights).

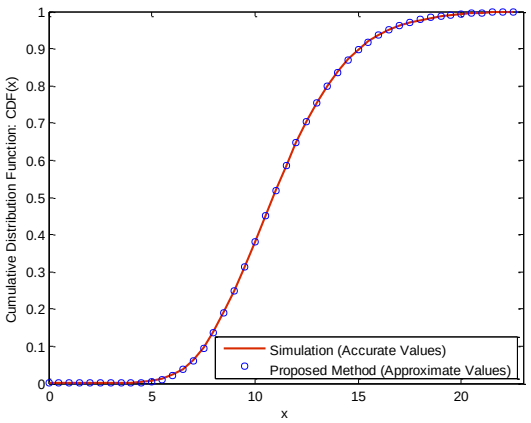

Fig. 2 Accuracy of the proposed threshold selection method. The simulated distribution is $0.4507\chi_2^2 + 0.2453\chi_3^2 + 0.3899\chi_7^2 + 0.1190\chi_1^2 + 0.4874\chi_5^2 + 0.0337\chi_4^2 + 0.4693\chi_6^2 + 0.2782\chi_2^2 + 0.0779\chi_7^2 + 0.1676\chi_1^2$. (random-generated weights).

4. Proposed Cooperative Spectrum Sensing Method

In this paper, we only consider the soft combination-based cooperative spectrum sensing method. We propose that the fusion center has the capability to directly sense the radio frequency spectrum. As we will confirm by simulation results, this improves the reliability of the final decision. Furthermore, we propose to employ a weighted combination fusion rule for fusing the soft decisions transmitted by SUs. Therefore, the proposed global decision rule at the FC can be expressed as:

$$\tilde{y} = w_0 \mathcal{T}_{G,0} + \sum_{i=1}^{L} w_i \tilde{\mathcal{T}}_{G,i} = w\Gamma \underset{\mathcal{H}_0}{\overset{\mathcal{H}_1}{\gtrless}} \tilde{\eta}, \quad (41)$$

where

$$w = [w_0, w_1, w_2, \cdots, w_L]^T, \qquad w_i \geq 0 \quad (42)$$

is the weight vector used to build the weighted fusion rule, and

$$\Gamma = \left[\mathcal{T}_{G,0}, \tilde{\mathcal{T}}_{G,1}, \tilde{\mathcal{T}}_{G,2}, \cdots, \tilde{\mathcal{T}}_{G,L}\right]^T \quad (43)$$

denotes the vector of observations. Note that w_0 corresponds to the weight that is assigned to the FC and the others are the corresponding weights of SUs.

4.1 Weight Vector Computation

The problem that we are encountering is how we should calculate the weight vector w, thereby the resultant detector achieves the best performance. To this end, we choose the deflection coefficient [22] as the performance metric.

In order to compute the deflection coefficient, we require the first and second-order moments of the test statistic (41). After some manipulation, we obtain the following expressions:

$$\begin{aligned}
E_0[\tilde{y}] &= w_0 + \sum_{i=1}^{L} w_i h_i = w^T h \\
Var_0[\tilde{y}] &= 2w_0^2 + \sum_{i=1}^{L} w_i^2 (2h_i^2 + \sigma_i^2) = w^T m_0 w \\
E_1[\tilde{y}] &= w_0(1 + \lambda_0) + \sum_{i=1}^{L} w_i h_i (1 + \lambda_i) \\
&= w^T (h + H\lambda) \\
Var_1[\tilde{y}] &= 2w_0^2(1 + 2\lambda_0) + \sum_{i=1}^{L} w_i^2 (2h_i^2(1 + 2\lambda_i) + \sigma_i^2) \\
&= w^T m_1 w
\end{aligned} \quad (44)$$

where $E_0[.]$ ($Var_0[.]$) and $E_1[.]$ ($Var_1[.]$) denote the statistical expectation (variance) under null and alternative hypotheses, respectively. In the above equations,

$$\lambda = [\lambda_0, \lambda_1, \lambda_2, \cdots, \lambda_L]^T \quad (45)$$

denotes the vector of estimated noncentrality parameters at different SUs, where $\lambda_i = \hat{\mathcal{U}}_i^2 / \hat{\varrho}_i^2$.

Furthermore, the following definitions are supposed:

$$\begin{aligned} &h = [1, h_1, h_2, \cdots, h_L]^T, \\ &m_0 = 2H^2 + \mathrm{diag}(\sigma), \\ &\sigma = [0, \sigma_1^2, \sigma_2^2, \cdots, \sigma_L^2]^T \\ &H = \mathrm{diag}(1, h_1, h_2, \cdots, h_L), \\ &m_1 = 2H^2[I_{L+1} + 2\mathrm{diag}(\lambda)] + \mathrm{diag}(\sigma). \end{aligned} \tag{46}$$

After some manipulation, we can obtain the deflection of cooperative detector as:

$$\mathcal{D}(w) \triangleq \frac{(E_1[\tilde{y}] - E_0[\tilde{y}])^2}{\mathrm{Var}_0[\tilde{y}]} = \frac{(w^T H\lambda)^2}{w^T m_0 w}. \tag{47}$$

We rewrite (45) and define the optimal weighting vector w_{DC} as the one that meets the following optimization problem:

$$w_{DC} = \underset{w \geq 0, \|w\|_2 = 1}{\mathrm{argmax}} \frac{w^T \tilde{m} w}{w^T m_0 w}, \tag{48}$$

where

$$\tilde{m} \triangleq H\lambda\lambda^T h^T, \tag{49}$$

and $\|.\|_2$ denotes the Euclidian norm (i.e. $\|w\|_2 = \left(\sum_{i=0}^{L} w_i^2\right)^{1/2}$). In order to achieve a unique solution for the optimization problem, we have confined the weight vector to have a unit norm.

If $m_0^{-1/2}$ be the square root obtained from the Cholesky decomposition of m_0, substituting $w = m_0^{-T/2} v$, we can get

$$\mathcal{D}(v) = \frac{v^T\left(m_0^{-1/2} H\lambda\lambda^T H^T m_0^{-T/2}\right)v}{v^T v}, \tag{50}$$

which is in the Rayleigh's quotient form [23]. Hence, $v = m_0^{-1/2} H\lambda$ and normalizing the result gives the optimal weight vector as:

$$w_{DC} = \frac{m_0^{-T/2} m_0^{-1/2} H\lambda}{\left\| m_0^{-T/2} m_0^{-1/2} H\lambda \right\|_2}. \tag{51}$$

It should be note that the suboptimal linear sum-detector is obtained by substituting $w_{EGC} = [1,1,\cdots,1]^T/\sqrt{L}$ into (41).

4.2 Threshold Selection at Fusion Center

4.2.1 The case that FC does not have direct observation

According to the central limit theorem [24], if the number of SUs in network is large enough (in practice, greater than or equal to 10), we can write

$$\tilde{y} \sim \begin{cases} \mathcal{N}(E_0[\tilde{y}], \mathrm{Var}_0[\tilde{y}]), & \text{under } \mathcal{H}_0 \\ \mathcal{N}(E_1[\tilde{y}], \mathrm{Var}_1[\tilde{y}]), & \text{under } \mathcal{H}_1 \end{cases} \tag{52}$$

Based on above distributions, we can find the decision threshold in (41), or equivalently, the false alarm probability:

$$\tilde{\eta} \simeq \sqrt{w^T m_0 w} Q^{-1}(P_{fa}) + w^T h \tag{53}$$

The accuracy of the above distribution is subsequently examined by Monte-Carlo simulations.

4.2.2 The case that FC has direct observation

In this section, we introduce a method to estimate the decision threshold in (41) for a given probability of false alarm. Since an analytical closed-form expression for the null distribution of the test statistic does not exist, we propose to approximate the distribution function by the numerical inversion of corresponding characteristic function (CF).

Under null hypothesis, the CF of a random variable X is $\Phi_{X|\mathcal{H}_0}(t) \triangleq E[\exp(jtX)|\mathcal{H}_0]$. From (2), the CF of received statistic can be obtained as ($i = 1, \cdots, L$)

$$\Phi_{\tilde{\mathcal{T}}_{G,i}|\mathcal{H}_0}(t) = (1 - 2jh_i t)^{-\frac{1}{2}} \exp\left(-\frac{\sigma_i^2 t^2}{2}\right). \tag{54}$$

Applying the fact that

$$\Phi_{\tilde{y}|\mathcal{H}_0}(t) = \Phi_{\mathcal{T}_{G,0|\mathcal{H}_0}}(w_0 t) \times \prod_{k=1}^{L} \Phi_{\tilde{\mathcal{T}}_{G,k}|\mathcal{H}_0}(w_k t), \tag{55}$$

we can write:

$$\begin{aligned} &\Phi_{\tilde{y}|\mathcal{H}_0}(t) \\ &= \left[\prod_{k=1}^{L}(1 - 2jw_k h_k t)\right]^{-\frac{1}{2}} \exp\left(\frac{-t^2}{2}\sum_{k=1}^{L} w_k^2 \sigma_k^2\right) \\ &\times (1 - 2jw_0 t)^{-\frac{1}{2}}. \end{aligned} \tag{56}$$

Since $P_{fa} = \Pr\{\tilde{y} > \tilde{\eta}|\mathcal{H}_0\} = 1 - \mathcal{F}_{\tilde{y}|\mathcal{H}_0}(\tilde{\eta})$, we numerically invert the CF of $\tilde{y}$ under $\mathcal{H}_0$ using the method introduced in [25]. This technique approximately calculates the distribution function of a standardized random variable, when its characteristic function is known. Following the strategy discussed in [25], we first define the standardized test statistic

$$Z \triangleq \frac{\tilde{y} - E_0[\tilde{y}]}{\sqrt{\mathrm{Var}_0[\tilde{y}]}}, \tag{57}$$

so the approximate distribution function of Z can be obtained as:

$$\hat{\mathcal{F}}_{Z|\mathcal{H}_0}(z) \simeq \frac{1}{2} + \frac{\xi z}{2\pi} - \sum_{\substack{\upsilon=1-H \\ \upsilon \neq 0}}^{H-1} \frac{\Phi_{Z|\mathcal{H}_0}(\xi\upsilon)}{2\pi j\upsilon} e^{-j\xi\upsilon z}, \tag{58}$$

where ξ is a constant variable which ensures that the full range of $\hat{\mathcal{F}}_{Z|\mathcal{H}_0}(z)$ is considered (i.e. it includes 0 and 1) and H defines the number of points used in the approximation of CDF. The values for z may be chosen as the Fourier frequencies, that is, $z_k = (2\pi(k - H)/2\xi(H - 1))$ for $k = 1, 2, \cdots, 2H - 1$. The summation in the approximation formula (58) can be computed using the fast Fourier transform, if the $\upsilon \neq 0$

term is subtracted from the FFT result. Furthermore, the characteristic function $\Phi_{Z|\mathcal{H}_0}(.)$ in (58) can be calculated as follows:

$$\Phi_{Z|\mathcal{H}_0}(t) = e^{\frac{-j(w_0+\sum_{i=1}^{L} w_i h_i)}{(w^T m_0 w)^{1/2}}} \times \Phi_{\tilde{y}|\mathcal{H}_0}\left((w^T m_0 w)^{-1/2} t\right), \quad (59)$$

Finally, the intended distribution function can be obtained as

$$\hat{\mathcal{F}}_{\tilde{y}|\mathcal{H}_0}(\tilde{\eta}) \simeq \hat{\mathcal{F}}_{Z|\mathcal{H}_0}\left((w^T m_0 w)^{-\frac{1}{2}}(\tilde{\eta} - w_0 - \sum_{i=1}^{L} w_i h_i)\right), \quad (60)$$

Therefore, the global decision threshold in (41) can be analytically determined as

$$\tilde{\eta} \simeq \hat{\mathcal{F}}^{-1}_{\tilde{y}|\mathcal{H}_0}(1 - P_{fa}). \quad (61)$$

5. Simulation Results and Discussions

In this section, we evaluate the performance of the proposed CSS method. The simulated primary signal is a DVB-T ((Digital video broadcasting, Terrestrial television) signal with 64-QAM subcarrier modulation. Following the settings in DVB standard, we set the values of FFT length, number of occupied channels, and the length of guard interval as $N_{FFT} = 8192$, $N_{occ} = 6817$, and $N_g = 1024$, respectively. The transmission mode is selected to be 8K mode and carrier frequency is set to 750 MHz. It is assumed that Pfa=0.01, L=10 and the sensing duration is 3 OFDM symbols.

It is well-known that the peaks of the cyclic autocorrelation function of an OFDM signal occurs at $\tau = \pm N_{FFT}$ and $\alpha = k/(N_{FFT} + N_g)$ for integer k.

In all single-cycle simulations, the SU employs $\alpha = 1/(N_{FFT} + N_g)$ and $\tau = N_{FFT}$. Furthermore, the cyclostationary detectors use a Kaiser window with length $P = 2048$ and $\beta = 10$. The average signal-to-noise ratio (SNR) in the i th observation channel is defined as $SNR_i = 10\log_{10}(\tilde{\delta}_x^2/\delta_i^2)$, where $\tilde{\delta}_x^2$ denotes the variance of the PU's signal.

5.1 Local Sensing

Fig. 3 presents the receiver operating characteristics (ROC) curves for the non-cooperative spectrum sensing over frequency-flat Rayleigh fading channel. Analytical curves are obtained from (29). It is evident that, for a sufficiently large sample size, the numerical results follow very closely the theoretical curves.

The accuracy of the analytical null distribution (28) is examined in Fig. 4. As it can be seen, the simulated CDF under null hypothesis matched well with the asymptotic analytical distribution. Therefore, analytically-computed

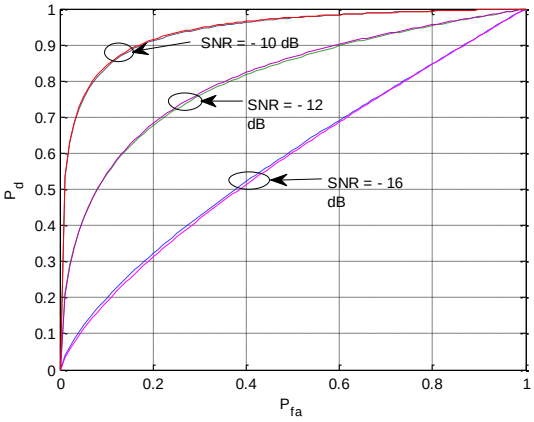

Fig. 3 ROC curves over frequency-flat Rayleigh fading channels (dashed lines: simulation, solid lines: analysis).

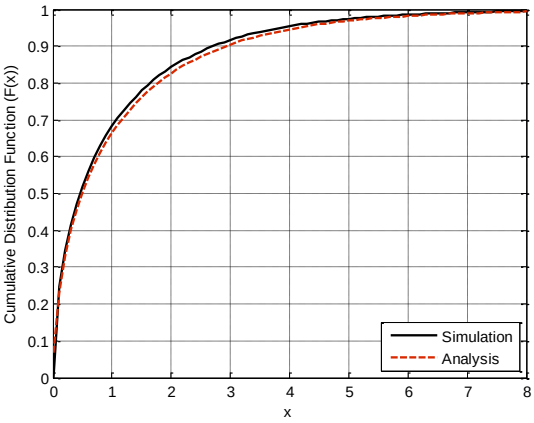

Fig. 4 Null distribution function of the proposed cyclic detector.

threshold values for a pre-defined false alarm rates are almost accurate.

In addition, performance comparisons between the proposed multi-cycle sensing method and some state-of-the-art competing methods are provided in Figs. 5 and 6. The simulated sensing methods are the conventional energy detector [3], well-known Lunden-Koivunen's (LK) cyclostationary detector [2], Chaudhari-Koivunen's autocorrelation-based detector [26], and Derakhshani-Le-Ngoc's cyclostationary detector [13].

As we can see, the proposed method has close detection performance to the LK detector which employs the full correlation structure of the second-order cyclic moment. Since the proposed test statistic has lower computation complexity compared to the LK algorithm, it can be considered as a potential substitute.

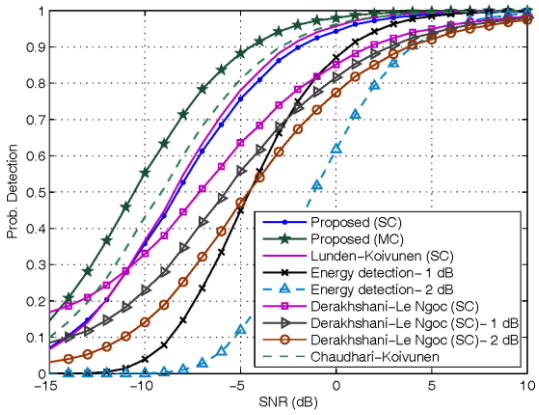

Fig. 5 Detection performance of proposed multi-cycle detector over frequency-flat Rayleigh fading channel (fd=150 Hz and Pfa=0.01).

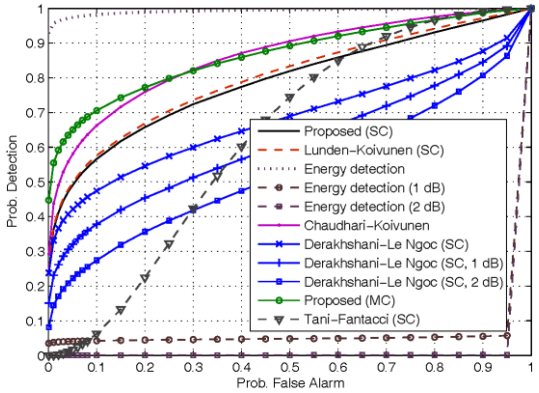

Fig. 6 ROC curves over Rayleigh fading channels with average SNR = -10 dB and fd=150 Hz.

Furthermore, the single-cycle cyclostationary detector of [13] uses the following hypothesis test:

$$\mathbb{T}_{\mathrm{DL}} = \left|\widehat{\mathcal{M}}_{2\mathrm{x}}(\alpha;\tau=0)\right|^2 \underset{\mathcal{H}_0}{\overset{\mathcal{H}_1}{\gtrless}} \eta_{\mathrm{DL}}. \tag{62}$$

where the associated threshold, which is set so the target Pfa is met, can be obtained as

$$\eta_{\mathrm{DL}} = -\frac{2\delta^4}{\mathrm{M}^2}\log \mathrm{P_{fa}}. \tag{63}$$

In the above equation, δ^2 denotes the variance of complex AWGN channel. To illustrate the impact of noise uncertainty, assume $\delta^2 = \zeta\delta_{\mathrm{n}}^2$, where δ_{n}^2 is the nominal noise power and $\zeta > 1$ is a parameter that specifies the size of the uncertainty [27]. Then, for a target Pfa, the threshold is $\eta_{\mathrm{DL}} = \zeta^2\eta_{\mathrm{DL,n}}$, where $\eta_{\mathrm{DL,n}}$ is the true nominal threshold value. This problem causes a loss in detection performance. As it is evident in Figs. 5 and 6, the performance of $\mathbb{T}_{\mathrm{DL}}$ is significantly degraded in the presence of an uncertainty in the noise power estimation. Consequently, in realistic applications, our proposed method provides much better detection performance for OFDM signals as compared to the cyclostationary detector of [13].

We also study the performance of low complexity cyclostationary detection method of [4]. The decision statistic of this method is

$$\mathbb{T}_{\mathrm{TF}} = \left|\frac{\widehat{\mathcal{M}}_{2\mathrm{x}}(\alpha;\tau)}{\widehat{\mathcal{M}}_{2\mathrm{x}}(\alpha+\mathrm{S};\tau)}\right| \underset{\mathcal{H}_0}{\overset{\mathcal{H}_1}{\gtrless}} \eta_{\mathrm{TF}}, \tag{64}$$

where

$$\eta_{\mathrm{TF}} = \tan\left\{\frac{\pi(1-\mathrm{P_{fa}})}{2}\right\}. \tag{63}$$

The detection performance of $\mathbb{T}_{\mathrm{TF}}$ is assessed in Fig. 6 through numerical simulation. The result reveals that our proposed multi-cycle sensing method outperforms this detector, as well as the other competing methods.

5.2 Cooperative Sensing Without Direct Observation at FC

In this subsection, it is assumed that there are 14 SUs in secondary network, and the vector of reporting channel variances is set to σ = [0.9, 1.2, 0.6, 2.2, 0.7, 1.5, 1.0, 0.7, 1.8, 0.8, 0.9, 1.5, 1, 2]T. In each simulation run, the fading coefficients of reporting channels are estimated for use in weight vector computation.

The accuracy of the proposed null distribution (i.e. (53)) is investigated in Fig. 7. As we can see, the analytical CDF follows very carefully the empirical accurate CDF. Furthermore, ROC curves for the proposed method as well as the conventional equal-gain combining (EGC) method are shown in Fig. 8. As it is evident, the proposed method outperforms the well-known EGC method of [2].

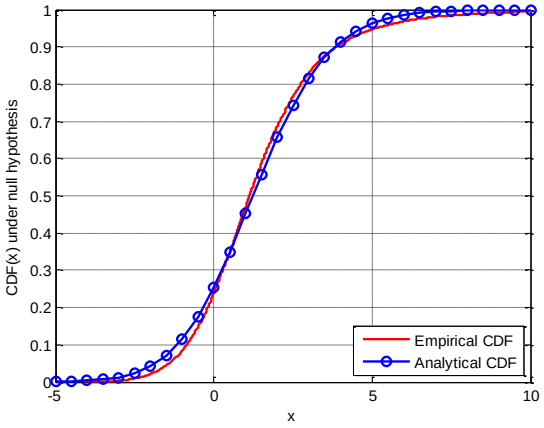

Fig. 7 Analytical versus simulated CDF for the null distribution in (53).

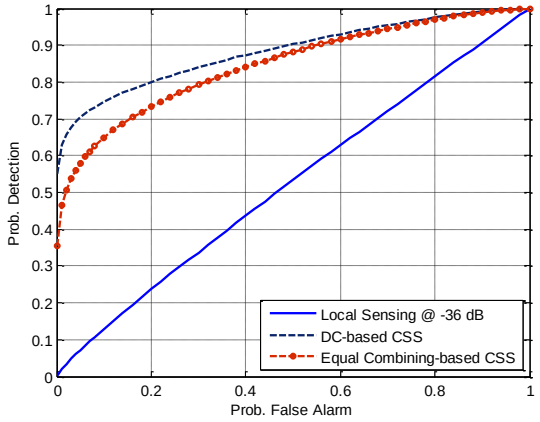

Fig. 8 ROC curves over frequency-flat Rayleigh fading channel (fd=150 Hz).

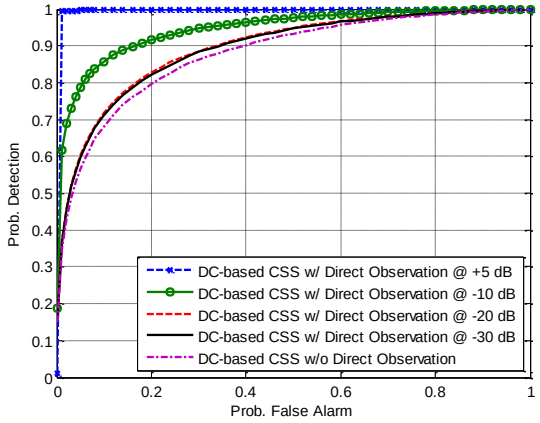

Fig. 9 ROC curves for the cases where the FC has direct sensing capability, as compared to the conventional case. The sensing channels are assumed to be under frequency-flat Rayleigh fading channel (fd=150 Hz).

5.3 Cooperative Sensing With Direct Observation at FC

Performance of proposed CSS with FC's direct sensing capability assumption is evaluated in Fig. 9. It is assumed that there are 10 SUs in the secondary network, and the vector of reporting channel variances is set to σ = [0.9, 1.2, 0.6, 2.2, 0.7, 1.5, 1.0, 0.7, 1.8, 2.8]T. As it is evident, if the FC has the ability to perform direct spectrum sensing, the global probability of detection can be improved. This capability can greatly increase the reliability of secondary network, even if the sensing channel of FC has very low SNR.

6. Conclusions

We proposed a spectrum sensing method based on properties of the second-order cyclic moment, and showed that this local sensing method significantly outperforms the conventional energy detector. In order to be able to perform statistical test, the null and alternative distributions of the proposed method are derived and verified through extensive numerical simulations.

Based on the proposed primary user detection method, we then developed a cooperative spectrum sensing (CSS) scheme. Numerical simulations show the advantageous of the proposed CSS over the widely-accepted equal-gain combining method of [2]. In addition, we proposed some local and global analytic threshold setting methods. Illustrative results confirm that the proposed methods provide enough accuracy.

Acknowledgments

This work was supported in part by the Iran Telecommunication Research Center (ITRC) under grant T-8755-500.

References

[1] Z. Quan, S. Cui, V. H. Poor, and A. H. Sayed, "Collaborative wideband sensing for cognitive radios," *IEEE Signal Process. Mag*., vol. 25, pp. 60-73, 2008.

[2] J. Lunden, V. Koivunen, A. Huttunen, and H. V. Poor, "Collaborative cyclostationary spectrum sensing for cognitive radio systems," *IEEE Trans. Signal Process*., vol. 57, pp. 4182-4195, Sep. 2009.

[3] R. Tandra and A. Sahai, "Fundamental limits on detection in low SNR under noise uncertainty," in *Int. Conf. Wireless Networks, Commun. and Mobile Computing*, Maui, HI, 2005, pp. 464-469.

[4] A. Tani and R. Fantacci, "A low-complexity cyclostationary-based spectrum sensing for UWB and WiMAX coexistence with noise uncertainty," *IEEE Trans. Vehic. Tech*., vol. 59, pp. 2940-2950, Jun. 2010.

[5] Z. Quan, S. Cui, and A. H. Sayed, "Optimal linear cooperation for spectrum sensing in cognitive radio networks," *IEEE J. Sel. Topics Signal Process*., vol. 2, pp. 28-40, Feb. 2008.

[6] G. Taricco, "Optimization of linear cooperative spectrum sensing for cognitive radio networks," *IEEE J. Sel. Topics in Signal Process*., vol. 5, pp. 77-86, 2011.

[7] G. Taricco, "Robust detection analysis of linear cooperative spectrum sensing for cognitive radio networks," *Physical Communications*, vol. 4, pp. 244-250, Sep. 2011.

[8] A. Al-Habashna, O. A. Dobre, R. Venkatesan, and D. C. Popescu, "Second-order cyclostationarity of mobile WiMAX and LTE OFDM signals and application to spectrum awareness in cognitive radio systems," *IEEE J.*

Sel. Topics in Signal Process., vol. 6, pp. 26-42, Feb. 2012.

[9] C. R. C. M. da Silva, B. Choi, and K. Kim, "Distributed spectrum sensing for cognitive radio systems," in *Proc. Information Theory Applications Workshop 2007*, La Jolla, CA, 2007, pp. 120–123.

[10] A. B. MacKenzie, J. H. Reed, P. Athanas, C. W. Bostian, R. M. Buehrer, L. A. DaSilva, *et al*., "Cognitive radio and networking research at Virginia Tech," *Proc. IEEE*, vol. 97, pp. 660-688, 2009.

[11] M. Oner and F. Jondral, "Air interface identification for Software Radio systems," *Elsevier Int. J. Electron. Commun. (AEÜ)*, vol. 61, pp. 104-117, Feb. 2007.

[12] A. V. Dandawate and G. B. Giannakis, "Statistical tests for presence of cyclostationarity," *IEEE Trans. Signal Process*., vol. 42, pp. 2355-2369, Sep. 1994.

[13] M. Derakhshani, T. Le-Ngoc, and M. Nasiri-Kenari, "Efficient cooperative cyclostationary spectrum sensing in cognitive radios at low SNR regimes," *IEEE Trans. Wireless Commun*., vol. 10, pp. 3754-3764, 2011.

[14] Z. Quan, W. Ma, S. Cui, and A. H. Sayed, "Optimal linear fusion for distributed detection via semidefinite programming," *IEEE Trans. Signal Process*., vol. 58, pp. 2431-2436, Apr. 2010.

[15] G. Taricco, "On the accuracy of the Gaussian approximation with linear cooperative spectrum sensing over Rician fading channels," *IEEE Signal Process. Letter*, vol. 17, pp. 651-654, Jul. 2010.

[16] A. V. Dandawate and G. B. Giannakis, "Asymptotic theory of mixed time averages and kth-order cyclic-moment and cumulant statistics," *IEEE Trans. Inf. Theory*, vol. 41, pp. 216-232, 1995.

[17] G. R. Terrell, *Mathematical Statistics: A Unified Introduction*. New York: Springer-Verlag, 1999.

[18] K. Knight, *Mathematical Statistics*. Florida: Chapman & Hall/CRC Press, 2000.

[19] M. Abramowitz and I. A. Stegun, *Handbook of Mathematical Functions with Formulas, Graphs, and Mathematical Tables*, 9th ed. New York: Dover Publications, 1972.

[20] H. Sadeghi, P. Azmi, and H. Arezumand, "Optimal multi-cycle cyclostationarity-based spectrum sensing for cognitive radio networks," in *19th Iranian Conf. Elect. Eng. (ICEE)*, Tehran, 2011.

[21] J. Gil-Pelaez, "Note on the inversion theorem," *Biometrika*, vol. 38, pp. 481-2, 1951.

[22] S. M. Kay, *Fundamentals of Statistical Signal Processing: Detection Theory* vol. 2: Prentice Hall, 1998.

[23] G. A. F. Seber, A *Matrix Handbook for Statisticians*. New Jersey: John Wiley and Sons, 2008.

[24] A. DasGupta, *Asymptotic Theory of Statistics and Probability*. New York: Springer, 2008.

[25] L. A. Waller, B. W. Turnbull, and J. M. Hardin, "Obtaining distribution functions by numerical inversion of characteristic functions with applications," *The American Statistician*, vol. 49, pp. 346-350, 1995.

[26] S. Chaudhari, V. Koivunen, and H. V. Poor, "Autocorrelation-based decentralized sequential detection of OFDM signals in cognitive radios," *IEEE Trans. Signal Process*., vol. 57, pp. 2690-2700, 2009.

[27] R. Tandra and A. Sahai, "SNR walls for signal detection," *IEEE J. Sel. Topics Signal Process*., vol. 2, pp. 4–17, Feb. 2008.

Hamed Sadeghi is a Ph.D. candidate with the Communication Systems Division of the Department of Electrical and Computer Engineering, Tarbiat Modares University, Tehran, Iran. He was born in Tehran on March 21, 1983. He received his B.S. degree in electronic engineering from Shahed University, Tehran, Iran, and the M.Sc. degree with distinction in communication systems engineering from Tarbiat Modares University (TMU), Tehran, Iran, in 2005 and 2008, respectively. His main research interests are within the areas of statistical signal processing and its applications, including detection, estimation, data fusion, and spectrum sensing for cognitive radio and acoustic sensor networks.

Paeiz Azmi was born in Tehran-Iran, on April 17, 1974. He received the B.Sc., M.Sc., and Ph.D. degrees in electrical engineering from Sharif University of Technology (SUT), Tehran-Iran, in 1996, 1998, and 2002, respectively. Since September 2002, he has been with the Electrical and Computer Engineering Department of Tarbiat Modares University, Tehran-Iran, where he became an associate professor on January 2006 and he is a full professor now. Prof. Azmi is a senior mebmer of IEEE.

From 1999 to 2001, Prof. Azmi was with the Advanced Communication Science Research Laboratory, Iran Telecommunication Research Center (ITRC), Tehran, Iran. From 2002 to 2005, he was with the Signal Processing Research Group at ITRC.

A New Cooperative Approach for Cognitive Radio Networks with Correlated Wireless Channels

Mehdi Ghamari Adian*
Electrical Engineering Department, Ph.D Student, Amirkabir University of Technology (Tehran Polytechnic), Tehran, Iran
mehdi.ghamari@aut.ac.ir
Hassan Aghaeinia
Electrical Engineering Department, Associate Professor, Amirkabir University of Technology (Tehran Polytechnic), Tehran, Iran
aghaeini@aut.ac.ir

Received: 16/Jul/2013 Accepted: 31/Aug/2013

Abstract
An effective cooperative cognitive radio system is proposed, when the wireless channels are highly correlated. The system model consists of two multi-antenna secondary users (SU TX and SU RX), constituting the desired link and some single-antenna primary and secondary users. The objective is the maximization of the data rates of the desired SU link subject to the interference constraints on the primary users. An effective system, exploiting Transmit Beamforming (TB) at SU TX, cooperation of some single-antenna SUs and Cooperative Beamforming (CB) at them and the antenna selection at SU RX to reduce the costs associated with RF-chains at the radio front end at SU RX, is proposed. Due to the issue of MIMO channels with correlated fading, some problems arise such as inapplicability of the well-known Grassmanian Beamforming as TB scheme at SU TX. We then propose a method to overcome this problem. After formulating the problem, a novel iterative scheme is proposed to find the best TB weight vector in SU TX and best subset of antennas at SU RX, considering the correlated channel.

Keywords: Cognitive Radio Networks, Cooperative Communications, MIMO Systems, Correlated Channels.

1. Introduction

Cognitive radio (CR) and multi-input multi-output (MIMO) communications are among the most promising solutions to improve spectrum utilization and efficiency. Dynamic and opportunistic spectrum access allows secondary users (SUs) to communicate on temporarily idle or underutilized frequencies. MIMO systems boost spectral efficiency by having a multi-antenna node simultaneously transmit multiple data streams. Newly emerging systems and standards (e.g., WiMAX, 4G Advanced-LTE, IEEE 802.16e) adopt MIMO communications as a core feature. TV white bands have also been approved by the FCC for opportunistic, secondary use [1]. A timely issue is to embrace recent innovations of the two technologies into a single system.

Transmit beamforming with receive combining is one of the simplest approaches to achieving full diversity. Compared with traditional space-time codes, beamforming and combining systems provide the same diversity order as well as significantly more array gain [2] at the expense of requiring channel state information (CSI) at the transmitter. The issue of transmit beamfroming in cognitive radio networks (CRN) has been investigated from various points of view in [3-6]. In [3], transmit beamforming (TB) is designed for MIMO cognitive radio networks with a single primary user-single secondary user network, to minimize the transmit power of the SU, while limiting the interference temperature to PU. The joint problems of TB and power control in CRN were considered in [4], [5], where the objective was to optimize the sum rate of SUs. The joint problems of TB in transmitter and antenna sub-set selection at receiver of a secondary network was considered in [6], where TB was recruited at multi-antenna secondary transmitter to maximize the data rates in SU link, meanwhile the interference on PUs was minimized.

The cooperative beamforming (CB) issue in Cooperative Cognitive Radio Networks (CCRN) was discussed in a few papers such as [7-9]. In [7], with the objective of maximizing the worst SINR of the destinations, a number of relays in a dual-hop amplify-and-forward cooperative scheme in CCRN were recruited. The bursty traffic case in CRN was considered in [8], where CB was exploited to access busy time slots or spatial spectrum holes. A cooperative beamforming aided incremental relaying scheme in CRN was presented in [9], in which, the

* Corresponding Author

source and relays can exploit CB to activate packet retransmission in busy time slots without inducing interference to primary users.

To the best knowledge of authors, the application of joint TB and CB in CCRN has not been investigated, yet. In addition to the complexity of the CCRN with joint TB and CB, another reason of not taking advantage of joint TB and CB can be attributed to the unavailability of CSI at the transmitter and relay side. In [10], based on Grassmannian Line Packing technic (GLP), a method was presented which does not need CSI at transmitter for TB and works when a limited feedback is available from receiver to transmitter. The beamforming codebook is generated using GLP technic. The transmitter and the receiver preserve the same codebook, which contains, for example, M weight vectors for the Grassmannian beamforming (GB). In the GB, the index for the optimal beamforming weight vector, not the vector itself, is fed back from the receiver to the transmitter. Thus, the amount of feedback information can be reduced to $[\log_2 M]$ bits.

A promising way of capturing a large portion of the capacity in MIMO systems at reduced hardware costs and computational complexity is to select a small number of the best antennas from the larger set of antennas available. The performance of systems with antenna selection was shown to be significantly higher than that of the systems using the same number of antennas without any sub-set selection [11]. However, the number of computations required for such optimal selection grows exponentially with the total number of the antennas available. In [6], an alternative approach for receive antenna selection was presented that offers near optimal performance at a complexity significantly lower than the schemes in [12]. In this paper a similar method is employed.

As shown in [13], realistic channel models show a temporal correlation as opposed to the conventional Rayleigh fading channel model. Whereas, the solution introduced in [10], is not able to exploit these correlations to further improve the accuracy of the feedback. To address this issue, new methodologies were proposed [14] [15]; however, their codebooks are fixed codebooks in the sense that once they are designed for a specific transmitter, they cannot adaptively change as the channel changes. In [16], the successive beamforming was proposed which uses an adaptive codebook that was designed for a specific channel model, and does not address more geneic spatio-temporally correlated channel models.

The motivation of this work is to determine the optimum TB weight vector at the transmitter side, the optimum CB weight vector at relay side and antenna sub-set selection in the receiver side of a CCRN. Moreover, we introduce a novel adaptive algorithm that utilizes the temporal correlation of the channel to change the TB codebook in a real-time fashion. Initially, the codebook is set to one of the conventional beamforming codebooks in [10], [14], [15]. The codebook is then updated with new feedback information that the transmitter receives. The simulation results show that this adaptive updating technique significantly improves the BER performance compared to the case where the codebook remains fixed.

The contributions of this work can be summarized as

- Proposing a low complexity method to determine the optimum TB and CB weight vectors and the best set of antennas in CCRN.
- Determining the optimal CB weight vector in the virtual array comprised of cooperating relays to remove the interference on PUs.
- Proposing an algorithm to adapt the TB fixed codebook to the correlation of the channels.

The remainder of the paper is organized as follows: in section 2, the system model is described and the problem is formulated. Section 3 proposes a solution for the problem. In section 4, simulation results are presented and section 5 concludes the paper.

Notation: Boldface uppercase is used for matrices and boldface lowercase for vectors. $\det(.)$, $\mathrm{Tr}(.)$ and $(.)^H$ denote the determinant, trace and the conjugate transpose operators respectively. I_M denotes an $M \times M$ identity matrix. $CN(0, I)$ represents the distribution of a zero mean circularly symmetric complex Gaussian (ZMCSCG) vector with covariance matrix I.

2. System Model and Problem Formulation

2.1 System Description

The system model is depicted in Fig. 1. It is assumed that there are $N_{SU} + 2$ SUs, two multi-antenna and N_{SU} single-antenna SUs and N_{PU} single-antenna PUs in the system. All users use the same frequency band. Two multi-antenna secondary users (SU TX and SU RX) constitute the desired SU link. The core aim of this work is to maximize the data rates of the desired SU link, using TB at SU TX and CB at cooperating SUs. The strategy of cooperation of single-antenna SUs with the desired multi-antenna SU link is

decode-and-forward. Other cooperation strategies can be analyzed in a similar fashion. It is assumed that the CSI is not available at SU TX.

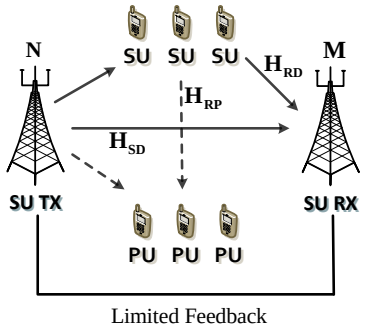

Fig. 1 System Model

Thus, we assume that a kind of quantized beamfroming, i.e., Grassmannian beamforming is utilized as transmit beamforming scheme at SU TX. As previously stated, the SU TX and the SU RX preserve the same codebook, which contains a number of beamforming weight vectors for the Grassmannian beamforming (GB). The beamforming codebook is generated using Grassmannian Line Packing techniqc (GLP) [10]. The GB method works when a limited feedback is available from SU RX to SU TX. Therefore, the optimum TB weight vector is determined at SU RX. Then the index for the optimal TB weight vector is fed back, using a few bits of limited feedback, from SU RX to SU TX. SU RX is equipped with M antennas. At SU RX m out of M antennas are selected. Also, the optimum TB weight vector is the one which maximizes the achievable rates, on condition that interference on PUs does not exceed the threshold. Moreover, zero-forcing beamforming is utilized in the virtual MIMO of cooperating SUs, in order not to disturb the existing PUs as a result of cooperation. The channels between all nodes are assumed to experience frequency at Rayleigh fading.The array manifold, defined as the set of steering vectors is known.

2.2 Problem Formulation

The received signal at SU RX can be written as

$$y = H_{SD}w_{TB}x + H_{RD}w_{ZFBF}\hat{x} + i + z \quad (1)$$

where w_{ZFBF} denotes the zero-forcing beamforming (ZFBF) weight vector at the cooperating SUs; $H_{SD} \in \mathbb{C}^{M\times N}$ and $H_{RD} \in \mathbb{C}^{M\times N_{SU}}$ represent the channel coefficients matrix with ZMCSCG entries from SU TX to SU RX and from single-antenna SUs (virtual MIMO) to SU RX, respectively; i is interference due to primary users and z represents the white noise (where $z\sim CN(0, I_M)$). Note that all channel matrices must be considered for each subcarrier, to be more accurate. However, as we aim to find the optimal set of antennas at SU RX, the optimum transmit and cooperative beamformer weight vectors are applied to all of the subcarriers regardless of different channel characteristics of different subcarriers, the dependence of all system parameters on the subcarrier index can be dropped. For simplicity we also assume that the detection process at cooperating SUs is error-free and as a result (1) can be rewritten as

$$y = (H_{SD}w_{TB} + H_{RD}w_{ZFBF})x + i + z \quad (2)$$

The transmit covariance matrix at the SU TX and at the cooperating SUs are denoted by Q and Q′, respectively. We assume that the total transmit power of the SU TX is limited to $P_{T,1}$, i.e.,

$$Q = E\{w_{TB}w_{TB}^H xx^*\} = w_{TB}w_{TB}^H P_x \le P_{T,1} \quad (3)$$

We further assume that the transmit power of the cooperating SUs is constrained to $P_{T,2}$:

$$Q' = E\{w_{ZFBF}w_{ZFBF}^H xx^*\} = w_{ZFBF}w_{ZFBF}^H P_x \le P_{T,1} \quad (4)$$

The covariance matrix of the noise and interference at SU RX is given by

$$U = E\{ii^H + zz^H\} = \sigma_0^2 I_M + H_{PS}H_{PS}^H \quad (5)$$

where H_{PS} denotes the channel matrix from PUs to SU RX and σ_0^2 is the noise level at the SU RX. For satisfactory operation of the incumbent PUs in the presence of the SU TX, interference seen at the PU RX should not exceed a particular threshold, P_j ($j = 1, \dots, N_{PU}$):

$$h_{SP,j}Qh_{SP,j}^H \le P_j, \quad j = 1, \dots, N_{PU} \quad (6)$$

where $h_{SP,j}$ denotes the channel vector from the SU TX to PU j. The achievable rates of the desired SU link at the output of the maximum ratio combiner at SU RX, using the cooperation of single-antenna SUs and also all available antennas at SU RX can be written as [17]

$$R = \frac{1}{2}\log_2 det(I_M + H_{SD}QH_{SD}^H U^{-1} + H_{RD}Q'H_{RD}^H U^{-1}) \quad (7)$$

The coefficient $1/2$ is due to the fact that cooperative transmission only uses half of resources (e.g., time slots, frequency bands, etc.). Similar to the method presented in [6], we define a diagonal matrix S (where $S \in \mathbb{R}^{M\times M}$):

$$(S)_{ii} = \begin{cases} 1 & i-\text{th receive antenna selected} \\ 0 & \text{otherwise} \end{cases} \quad (8)$$

In the SU RX, the antennas that maximize the achievable data rates are selected. The diagonal matrix provides us with the index of selected antennas in the SU RX. Hence, if m antennas are chosen ($m \le M$), new channel matrices, $\hat{H}_{SD}$ and $\hat{H}_{RD}$, with the same dimension as H_{SD} and H_{RD}, will have $M - m$ all-zero rows. Thus, the rate expression at SU RX can be expressed as

$$R = \frac{1}{2}\log_2 det(I_M + \hat{H}_{SD}Q\hat{H}_{SD}^H + \hat{H}_{RD}Q'\hat{H}_{RD}^H) \quad (9)$$

where $\hat{H}_{SD} = \hat{U}^{-1/2}SH_{SD}$, $\hat{H}_{RD} = \hat{U}^{-1/2}SH_{RD}$ and $\hat{U}$ is defined as follows. With the selected receive antennas we have reduced $m \times 1$ interference and noise vectors which give a new

interference and noise covariance matrix, $U_{reduced}$, of dimension $m \times m$. This matrix is inflated to form $\widehat{U}$, an $M \times M$ matrix, by adding rows and columns of zeros corresponding to the receive antennas not selected.

The distributed zero-forcing (ZF) beamforming can be realized by a virtual antenna array, which can be created by a set of relays in cooperative relaying networks [18]. With this notation, the problem of joint transmit beamforming, cooperative beamforming and antenna selection can be mathematically explained by

$$\begin{aligned} P: \max_{Q,Q',S} & \frac{1}{2}\log_2 det\left(I_M + \widehat{H}_{SD} Q \widehat{H}_{SD}^H + \widehat{H}_{RD} Q' \widehat{H}_{RD}^H\right) \\ s.t.\quad & (C1): (S)_{ii} \in \{0,1\},\ i = 1, \dots, M \\ & (C2): Tr(Q) \le P_{T,1} \\ & (C3): Tr(Q') \le P_{T,2} \\ & (C4): Tr(S) = m \\ & (C5): h_{SP,j} Q h_{SP,j}^H \le P_j,\ j = 1, \dots, N_{PU} \\ & (C6): \left|h_{RP,j} w_{ZFBF}\right| = 0,\ j = 1, \dots, N_{PU} \end{aligned} \quad (10)$$

where $h_{RP,j},\ j = 1, \dots, N_{PU}$, denotes the channel coefficients from cooperating SUs to single-antenna PUs.

2.3 Correlated Channels

It is time to consider the issue of correlated channels. It is noteworthy that the effect of correlated channels must only be considered in determining the TB weight vector, where the Grassmanian codebook matrix has to be adapted to the correlation of the channel. A correlated channel between SU TX and SU RX can be modeled as [19]

$$H_{SD,corr} = A_T^{1/2} H_{SD,iid} A_R^{1/2} \quad (11)$$

where A_T and A_R are the correlation matrices for the transmitter and receiver antennas, respectively. $H_{SD,iid}$, is a matrix with zero-mean circularly symmetric complex Gaussian entries (ZMCSCG). It is must be mentioned that for practical applications, the correlation matrices change at a rate much slower than $H_{SD,iid}$. At first, we consider the simple MISO case, i.e. $M = 1$ and propose an algorithm to adapt the codebook of GB to the correlated channel case. Then, the proposed method is extended to the general case of MIMO systems. If A_T is known in both the SU TX and the SU RX, a codebook adapted to the correlation of the channel can be computed in both the SU TX and the SU RX:

$$K_{corr} = A_T^{1/2} K_{iid} \quad (12)$$

where K_{iid} is the codebook matrix with its columns corresponding to the codewords of the codebook, e.g. taken from the Grassmanian codebook and only applicable to uncorrelated channels. Note that by performing (12), the modified codebook for the correlated channel, K_{corr}, would have code vectors more shaped in the directions close to the direction of the channel. Clearly, to compute (12), A_T must be estimated in both the SU TX and the SU RX. If both the SU TX and the SU RX knew the exact channel realization, they could both calculate A_T as [19]

$$A_T = E\left\{H_{SD,corr}^H H_{SD,corr}\right\} \quad (13)$$

It is also possible to estimate the expected value using the average of the last P channel realizations:

$$A_T \cong \frac{1}{P}\sum_{i=1}^{P} H_{SD,corr,i}^H H_{SD,corr,i} \quad (14)$$

where $H_{SD,corr,i}$ is the channel estimate at the receiver at time i. Based on (14), A_T can be estimated only if channel realizations are completely known in both the SU TX and SU RX, which is not a practical assumption for SU TX. In order to compute A_T only based on the feedback link, we assume that at time i, the SU RX and SU TX use the updated K_i as the codebook, which is known to both of them. Based on the channel estimate at the receiver, the index of the best codeword, $w_{i,j}$ (j-th column of K_i) is sent to the SU TX through the feedback link. After P iterations, the correlation matrix in both sides can be approximated by

$$A_T \cong \frac{1}{P}\sum_{i=1}^{P} w_{i,j} w_{i,j}^H \quad (15)$$

This approximation relies on the fact that for a sufficiently large number of feedback bits, the selected codeword, $w_{i,j}$ converges to $H_{SD,corr,i}^H$.

In order to extend the adaptive codebook design to MIMO case, it is enough to perform (15) for both SU TX and SU RX. We will postpone extending the results achieved for MISO desired SU link to after proposing an iterative solution for problem P. The target of the next section is to provide an applicable solution for problem P.

3. A Sub-optimal Method to Determine the Optimum TB and CB weight vectors and best antennas in Correlated Channels

In problem P, four unknown variables must be determined jointly. Due to excessive complexity, in this section we propose a suboptimum solution to solve P. In this way, the problem P is decomposed into two problems, P1 and P2, according to the following:

$$\begin{aligned} P1: \max_{w_{TB},S,P_x} & \frac{1}{2}\log_2 det\left(I_M + P_x \widehat{H}_{SD} w_{TB} w_{TB}^H \widehat{H}_{SD}^H\right) \\ s.t.\quad & (C1): (S)_{ii} \in \{0,1\},\ i = 1, \dots, M \\ & (C2): Tr(w_{TB} w_{TB}^H) \le \frac{P_{T,1}}{P_x} \\ & (C3): Tr(S) = m \end{aligned}$$

$$(C4): h_{SP,j} w_{TB} w_{TB}^H h_{SP,j}^H \le \frac{P_j}{P_x},\ j = 1, \dots, N_{PU} \quad (16)$$

and:

$$P2: \max_{w_{ZFBF}} \|H_{RD} w_{ZFBF}\|^2$$
$$s.t.\ (C1): \mathrm{Tr}(w_{ZFBF} w_{ZFBF}^H) \le \frac{P_{T,2}}{P_x}$$
$$(C2): \left|h_{RP,j} w_{ZFBF}\right| = 0, \quad j = 1, \dots, N_{PU} \quad (17)$$

Note that prior to solving the problem P2, the problem P1 has to be solved to determine the optimum value of P_x and S. Moreover, in problem P2, the received signal power at SU RX due to cooperation of single-antenna SUs is aimed to be maximized, instead of achievable data rates at SU RX. This facilitates the finding the optimal ZF beamforming weight vector, as will be discussed soon.

3.1 Solving P1

A straightforward way to solve P1 is to perform an exhaustive search (ES) over all possible combinations of antenna elements and TB weight vectors and optimize over P_x. Hence, ES amounts to optimizing P_x, $\binom{M}{m} \times \binom{K}{1}$ times subject to interference and power constraints, where K denotes the number of codewords in the TB codebook matrix. Each optimization of P_x can be considered as a convex problem. However, the need to iterate through all possible combinations gives a complexity which explodes for higher dimensional systems.

The problem P1 is highly non-convex and can be classified as an example of an integer programming problem, since matrix S has only binary elements [20]. The non-convexity of the problem arises due to the nature of the objective function, interference and binary constraints. Further, the binary variable renders the problem NP-hard problem. In order to obtain a more computationally efficient approach, we modify the problem in the following way. The binary structure of S can be relaxed so that the antenna selection variable takeson values in the interval 0 to 1. Finally we note that in this approach the effect of matrix U cannot be included. This limitation is discussed below. With these changes, P1 can be written as

$$P3: \max_{w_{TB},S,P_x} \log_2 \det(I_M + P_x S H_{SD} w_{TB} w_{TB}^H H_{SD}^H S^H)$$
$$s.t.\ (C1): 0 \le (S)_{ii} \le 1,\ i = 1, \dots, M$$
$$(C2), (C3) \text{ and } (C4) \text{ as in P1} \quad (18)$$

Note that the problem P3 is still non-convex, due to non-concavity of the objective function. Thus, we seek a convex aproximation (CA) to this problem.

Proposition 1: With two of the three variables known, the utility function in the problem P3 is concave in the third one and this renders the problem convex in this variable.

Proof: Three different cases must be investigated and for each case it is straightforward to prove concavity of the utility function in (20). Details are omitted for brevity.

Thus, to solve P3, we initialize P_x, w_{TB} and optimize over S. Then using the optimum S and the initial value for P_x, optimum TB weight vector is chosen and ultimately, with S and w_{TB} known, optimum value for P_x is obtained. Since elements of S are non-binary, the index of the chosen antennas are the K-largest diagonal elements of S. In Table 1, the proposed procedure is summarized.

A comment on the convergence of the proposed iterative algorithm is in order here. During the $(k+1)$ -th iteration $S^{(k+1)} = \mathrm{argmax}_S\, P3\left(S, w^{(k)}, P_x^{(k)}\right)$ is calculated and we obtain achievable data rate r_1. Then $w^{(k+1)} = \mathrm{argmax}_{w_{TB}}\, P3\left(w, P_x^{(k)}, S^{(k+1)}\right)$ is calculated, giving rate r_2. Finally $P_x^{(k+1)} = \mathrm{argmax}_{P_x}\, P3\left(P_x, S^{(k+1)}, w^{(k+1)}\right)$ is evaluated and the corresponding achievable data rate r_3. Since $r_1 \le r_2 \le r_3$ forms a monotonically increasing sequence which is bounded above, we conclude that the sequence of achievable data rates converges to a limit. It is time to incorporate the issue of correlated channels into the proposed iterative algorithm. As mentioned, for each channel realization, the codebook matrix needs to be updated and the best TB weight vector is utilized in estimating the correlation matrices in SU TX and SU RX. The details are described in Table I. Our simulations indicate that iterating 6 times is almost sufficient to attain an optimum value of problem P3.

3.2 Solving P2

The cooperating SUs are assumed cognitive in the sense that they can obtain the channel state information (CSI) on the channels from themselves to PUs. The objective function of P2 can be written as

$$\|H_{RD} w_{ZFBF}\|^2 = \sum_{i=1}^{m} \left|h_{RD,i} w_{ZFBF}\right|^2 \quad (19)$$

where $h_{RD,i}$ denotes the i-th row of H_{RD}.

Theorem 1: The optimal zero-forcing beamforming weight vector which maximizes $\|H_{RD} w_{ZFBF}\|^2$ and satisfies the constraints of the problem P2 is one of the orthogonal projection of rows of H_{RD} onto the orthogonal complementary $\gamma^{\perp}$ of the subspace $\gamma = \mathrm{span}\left\{h_{CP}^{(2)}, \dots, h_{CP}^{(N_{PU})}\right\}$ which maximizes $\sum_{i=1}^{m} \left|h_{RD,i} w_{ZFBF}\right|^2$. To satisfy the cooperative transmit power constraint, the elements of the optimum ZFBF weight vector must be multiplied to $\sqrt{\frac{P_{T,1}}{P_x \mathrm{Tr}(w_{ZFBF} w_{ZFBF}^H)}}$.

Proof: The channel vector $h_{RD,i}, i = 1, \dots, m$, can be written as $h_{RD,i} = a_1^{(i)} e_1 + \cdots + a_{N_{SU}}^{(i)} e_{N_{SU}}$, using the N_{SU} basis vectors $\{e_1, \dots, e_{N_{SU}}\}$ (where $a_k^{(i)} \sim CN(0,1)$, $k = 1, \dots, N_{SU}$, $i = 1, \dots, m$) [21]. Hence, the matrix $E = [e_1, \dots, e_{N_{SU}}] = I_{N_{SU}}$, is $N_{SU} \times N_{SU}$ identity matrix. Then, we consider the set of basis vectors $\{e'_1, \dots, e'_{N_{PU}}\}$, which is the orthogonal basis for the subspace $\gamma = \text{span}\{h_{RP,1}, \dots, h_{RP,N_{PU}}\}$. Actually, γ is a N_{PU} dimensional subspace, for the reason that the probability of the realizations of the independent and continuous random vectors $h_{RP,1}, \dots, h_{RP,N_{PU}}$ being interrelated is very much small and thus can be ignored. If $\{e'_{N_{PU}+1}, \dots, e'_{N_{SU}}\}$, is an orthogonal basis for $\gamma^{\perp}$, the orthogonal set $\{e'_1, \dots, e'_{N_{PU}}\} \cup \{e'_{N_{PU}+1}, \dots, e'_{N_{SU}}\}$, is another orthogonal basis for $\mathbb{C}^{1 \times N_{SU}}$. Similarly, $h_{RD,i}$ can be represented by $h_{RD,i} = b_1^{(i)} e'_1 + \cdots + b_{N_{SU}}^{(i)} e'_{N_{SU}}$. Clearly, $L = [e'_1, \dots, e'_{N_{SU}}]$ is also a unitary matrix. Moreover, by matrix manipulation we have

$$[b_1^{(i)}, \dots, b_{N_{SU}}^{(i)}]^T = L^H [a_1^{(i)}, \dots, a_{N_{SU}}^{(i)}]^T \quad (20)$$

Since the random matrix L^H is unitary and independent with $h_{RP,i}$, $[a_1^{(i)}, \dots, a_{N_{SU}}^{(i)}]$ has the same distribution as $[b_1^{(i)}, \dots, b_{N_{SU}}^{(i)}]$, from (A.22) in [22]. As a result, $b_k^{(i)} \sim CN(0,1)$, $k = 1, \dots, N_{SU}$, $i = 1, \dots, m$. The ZF beamforming weight vector w_{ZFBF} is orthogonal to each $h_{RP,i}$ $(i = 1, \dots, m)$. Hence, it is perpendicular to each vector in γ, and belongs to $\gamma^{\perp}$. In order to maximize $\sum_{i=1}^{m} |h_{RD,i} w_{ZFBF}|^2$, we need to find the vector $w_{ZFBF}^{(i)} \in \gamma^{\perp}$. which is closest to $h_{RP,i}$ $(i = 1, \dots, N_{PU})$. From the Closest Point Theorem, $w_{ZFBF}^{(i)}$ is the orthogonal projection of $h_{RP,i}$ onto the subspace $\gamma^{\perp}$. The optimum ZFBF weight vector is the one which maximizes $\sum_{i=1}^{m} |h_{RD,i} w_{ZFBF}|^2$:

$$w_{ZFBF,opt} = \max_{w_{ZFBF}^{(k)}} \sum_{i=1}^{m} |h_{RD,i} w_{ZFBF}|^2, \quad k = 1, \dots, m \quad (21)$$

Table 1. The proposed algorithm for solving P1 (joint TB and antenna selection in CCRN with correlated channels)

Step1-Initializations
- Select an initial value for P_x and $P_{T,1}$
- Set $K_{corr} = K_{iid}$.
- Set $\tilde{A}_T = I_M$ and $\tilde{A}_R = I_N$
- (Estimates of channel correlation matrices)
- Select an Initial value for w (one of columns of codebook matrix K_{iid} which satisfies $tr(w_{TB} w_{TB}^H) \le P_{T,1}/P_x$)

Step 2-Calculation: repeat the following for each new channel realization

In SU RX do the following
- Find correlated channel realization, H_{SD}.
- Solve the convex optimization problem and find S
- Change the codebook to $K_{corr} = \tilde{A}_R^{1/2} K_{iid}$.
- Find the optimum $w_{TB,i}$ from K_{corr} that maximizes achievable rates.
- Update $\tilde{A}_R = (1-\beta)\tilde{A}_R + \beta w_{TB,i} w_{TB,i}^H$.
- Send i, the index of the codeword, to SU TX using limited feedback bits.
- Solve the resultant convex optimization problem, knowing S and w_i, to calculate the optimum P_x.

In SU TX do the following
- Receive the codeword index, i.
- Look up w_i from the codebook.
- Change the codebook to $K_{corr} = \tilde{A}_T^{1/2} K_{iid}$.
- Update $\tilde{A}_T = (1-\beta)\tilde{A}_T + \beta w_i w_i^H$.
- Use w_i for transmit beamforming.

Step 3-Iteration
- Repeat steps 1 and 2 until convergence. The achievable rate will be the average of the results.
- Using the optimum value of P_x , find the SER.

The cooperative transmit power constraint in P2 makes such $w_{ZFBF,opt}$ unique and the Theorem 1 is proved.

4. Performance Evaluation

In this section we explain the simulation results based on the proposed solutions for the problem P . However, before elaborating the results, we introduce a new parameter, α, which controls the interference threshold at the PUs. α is chosen so that allowable interference at the PUs is a fraction of PU SNR, i.e. $P_i = \alpha SNR_{PU}$ at the PUs. To compare the different approaches, we use the measures of achievable rates and symbol error rates. These are the assumptions for the simulations:

- Achievable rates are determined by averaging over the results obtained from 1000 i.i.d. channels realizations.

- CVX package is used along with MATLAB for simulations [23].
- The SU TX and SU RX are equipped with 3 and 6 antennas, respectively. The codebook matrix is given by [10]

$$\boldsymbol{K} = \begin{bmatrix} \frac{1}{\sqrt{2}} & \frac{1}{\sqrt{2}} & 0 & \frac{1}{\sqrt{2}}e^{\frac{2\pi j}{3}} & \frac{1}{\sqrt{2}}e^{\frac{4\pi j}{3}} & \frac{1}{\sqrt{2}}e^{\frac{4\pi j}{3}} & \frac{1}{\sqrt{2}} & 0 \\ \frac{1}{\sqrt{2}} & 0 & \frac{1}{\sqrt{2}} & \frac{1}{\sqrt{2}}e^{\frac{4\pi j}{3}} & 0 & 0 & \frac{1}{\sqrt{2}}e^{\frac{2\pi j}{3}} & \frac{1}{\sqrt{2}}e^{\frac{4\pi j}{3}} \\ 0 & \frac{1}{\sqrt{2}} & \frac{1}{\sqrt{2}} & 0 & \frac{1}{\sqrt{2}}e^{\frac{4\pi j}{3}} & \frac{1}{\sqrt{2}}e^{\frac{2\pi j}{3}} & 0 & \frac{1}{\sqrt{2}}e^{\frac{2\pi j}{3}} \end{bmatrix}$$

Note that for highly correlated matrices, A_T and A_R have relatively high mean absolute values. The correlation matrices are the same as the correlation matrices proposed in [13], with mean absolute values of 0.96 and 0.37 for high and low correlation matrices, respectively. For the Rayleigh fading scenario, $A_T = I_M$ and $A_R = I_N$. The correlation matrices remain the same throughout the transmission and adaptation phases; whereas, $H_{SU,iid}$ changes for each new transmission.

In order to depict the BER performance, we assume that 4-QAM is used in the desired link as the modulation scheme. Fig. 2 shows the comparison between the BER performance of CCRN with high and low correlation channel. We assume that 10 cooperating SUs exist in the system and also 3 out of 6 antennas at SU RX have been selected. Note that using the proposed algorithm for a correlated channel scenario results in more than 2 dB performance improvement; while, for low correlation matrices, the BER performance remains the same for both of the TB with fixed codebook and the TB with adaptive codebook. This is because the adaptive codebook is designed to track the correlation matrix; for low correlation channels, the correlation matrices are close to the identity matrix, and thus, the TB with fixed codebook cannot be improved any further; whereas, for highly correlated channels, the correlation matrices have further deviated from the identity matrix and the proposed algorithm can improve the performance by approximating a reliable non-identity correlation matrix. The effect of cooperating SUs on the BER performance of joint TB (with adaptive codebook) and antenna selection in the CCRN with highly correlated channels is depicted in Fig. 3. 3 out of 6 antennas are selected at SU RX.

It can be implied from Fig. 4 that higher data rates can be attained by utilizing the cooperation of SUs. More specifically, by making use of only two cooperative users and for $\alpha = 0.1$, data rate is almost identical to the case with no cooperative users and $\alpha = 0.1$. Note that the case of highly correlated channel with adaptive codebook for TB have been considered. An impossible case, i.e. $\alpha = 1$, has also been considered to confirm the necessity of cooperation of single-antenna SUs in the proposed system.

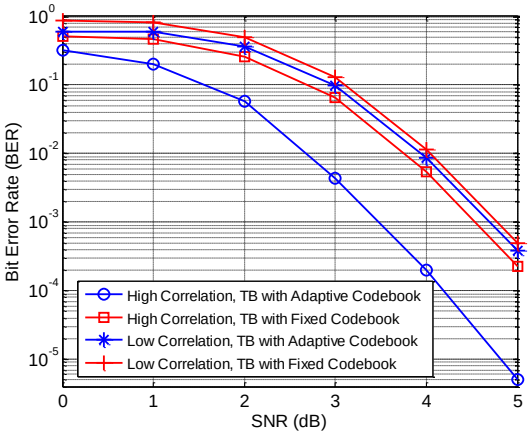

Fig. 2 BER versus SNR for CCRN with highly and lowly correlated channels ($N_{SU} = 10$ and 3 out of 6 antennas selected at SU RX)

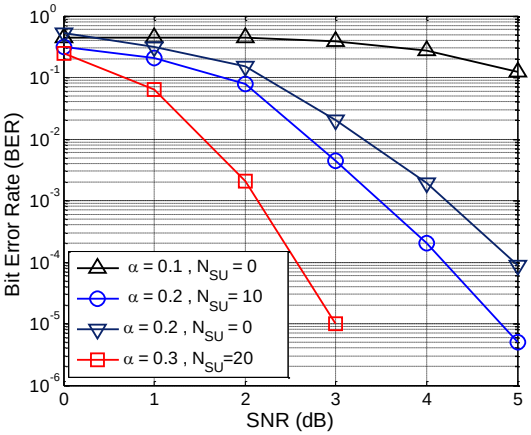

Fig. 3 Symbol Error Rates versus SNR for different values of α and N_{SU} (highly correlated channel)

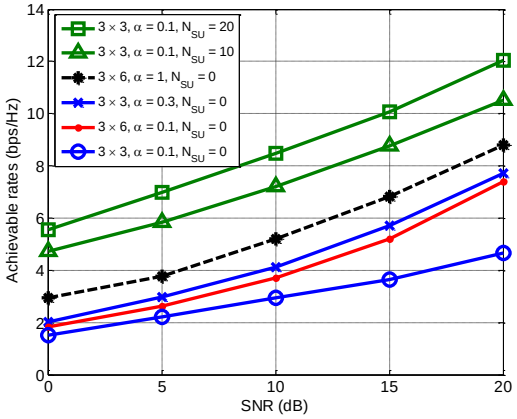

Fig. 4 Achievable data rates versus SNR for different number of N_{SU}, different value of α and different number of selected antennas at SU RX

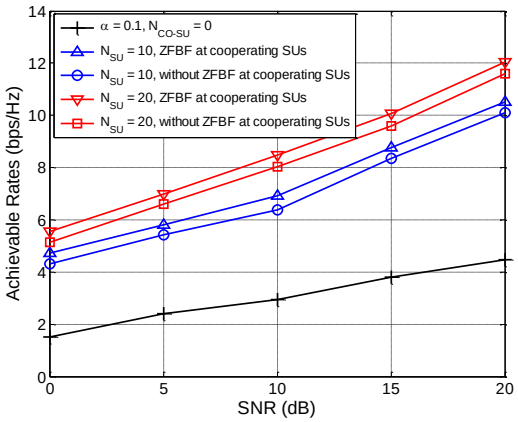

Fig. 5 The effect of ZF beamforming on the data rates of the system

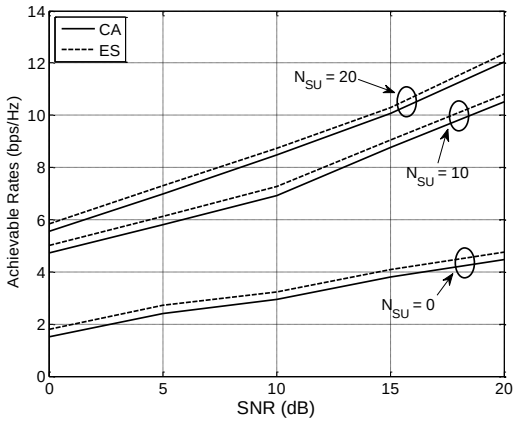

Fig. 6 Comparison between the performance of Convex Approximation and Exhaustive Search method

In Fig. 5, we demonstrate that CB not only removes the interference on PUs, due to cooperation of single-antenna SU with desired SU link, but also leads to an increase in the achievable rates of the desired link. Note that for all graphs in Fig. 5, $\alpha = 0.1$. Note the highly correlated channel case was considered. A comparison between the achievable rates of the multi-antenna SU link, using the CA and ES methods has been performed in Fig. 6. Evidently, the proposed CA method performs very close to ES method, which is very promising.

5. Conclusions

Jointly determining the optimum TB and CB weight vectors and antenna selection in the MIMO-CCRN was discussed, considered the correlation in the wireless channels. The scenario consists of 2 multi-antenna SUs and a number of single-antenna SUs and PUs. The problem was formulated and to achieve a computationally efficient solution with much less complexity, we utilized convex approximation method. It was shown through simulations that using the proposed method, a rather complex problem can be solved with reduced complexity. It was further proved, using simulations, that taking advantage of cooperation of single-antenna SUs and ZF beamforming, along with adapting the codebook of the TB to the correlated channel is an inevitable task in the proposed scenario.

Acknowledgments

This work was supported in part by CSRI (CyberSpace Research Institute) under contract number 17169/500.

References

[1] FCC, Spectrum policy task force report. ET Docket No. 02-380 and No. 04-186, Sep. 2010.

[2] H. Du and T. Ratnarajah, "Transmit Beamforming in MIMO Cognitive Radio Network via Semidefinite Programming", IEEE VTC (Spring), 2011, pp. 1-5.

[3] S. You, G. Noh, J. Lee, H. Wang, and D. Hong, "Joint Beamforming and Power Control Algorithm for Cognitive Radio Network with the Multi-Antenna Base Station," IEEE WCNC, 2010 , pp. 1-6.

[4] F. Wang and W. Wang, "Robust Beamforming and Power Control for Multiuser Cognitive Radio Network,"IEEE GLOBECOM, 2010, pp.1-5.

[5] M. G. Adian and H. Aghaeinia, "Joint transmit beamforming and antenna selection in cognitive radio networks", in Proc IEEE International Symposium on Telecommunications (IST), 2010, pp. 33 -37.

[6] K. Zarifi, S. Affes and A. Ghrayeb, "Joint Source Power Control and Relay Beamforming in Amplify-and-Forward Cognitive Networks with Multiple Source-Destination Pairs", in Proc. IEEE ICC, 2011, pp. 1-6.

[7] J. Liu, W. Chen and Z. Cao, "Delay Optimal Scheduling for Cognitive Radio Networks with Cooperative Beamforming", in Proc. IEEE ICC, 2011, pp. 1-5.

[8] J. Liu, W. Chen, Z. Cao and Y. J. Zhang, "Cooperative Beamforming Aided Incremental Relaying in Cognitive Radios", in Proc. IEEE ICC, 2011, pp. 1-5.
[9] D. Love, J. Heath, R.W., and T. Strohmer, "Grassmannian beamforming for multiple input multiple-output wireless systems", IEEE Trans. on Inform. Theory, vol. 49, no. 10, pp. 2735-2747, Oct. 2003.
[10] A. F. Molisch, M. Z. Win, and J. H. Winters, "Capacity of MIMO systems with antenna selection", in Proc. IEEE ICC, June 2001, pp. 570-574.
[11] A. Gorokhov, D. Gore and A. Paulraj, "Receive antenna selection for MIMO spatial multiplexing: theory and algorithms", IEEE Trans. On Signal Process., vol. 51, no. 11, pp. 2796-2807, Nov. 2003.
[12] J. P. Kermoal, L. Schumacher, K.I. Pedersen, P.E. Mogensen and F. Frederiksen, "A stochastic MIMO radio channel model with experimental validation," IEEE J. Sel. Areas in Commun., vol. 20, no. 6, pp. 1211–1226, Aug. 2002.
[13] V. Raghavan, A. M. Sayeed, and N. Boston, "Near-optimal codebook constructions for limited feedback beamforming in correlated mimo channels with few antennas," IEEE ISIT, 2006 pp. 2622–2626.
[14] D. Love and J. Heath, R.W., "Grassmannian beamforming on correlated mimo channels," IEEE GLOBECOM, 2004, pp. 106–110.
[15] L. Liu and H. Jafarkhani, "Novel transmit beamforming schemes for time-selective fading multiantenna systems," IEEE Trans. On Sig. Process., vol. 54, no. 12, pp. 4767–4781, Dec. 2006.
[16] T. M. Cover and J. A. Thomas, Elements of Information Theory. NewYork: Wiley, 1991.
[17] J. N. Laneman and G. W. Wornell, "Distributed space-time coded protocols for exploiting cooperative diversity in wireless networks", IEEE Trans. on Inform. Theory, vol. 49, no. 10, pp. 2415-2425, Oct. 2003.
[18] D.P. McNamara, M.A. Beach and P.N. Fletcher "Spatial correlation in indoor MIMO channels," IEEE PIMRC, 2002, vol. 1, pp. 290–294.
[19] S. Boyd and L. Vandenberghe, "Convex Optimization", Cambridge University Press, 2004.
[20] C. D. Meyer, "Matrix Analysis and Applied Linear Algebra", SIAM,2000.
[21] D. N. C. Tse and P. Viswanath, "Fundamentals of Wireless Communication", Cambridge, U.K.: Cambridge Univ. Press, 2005.
[22] M. Grant and S. Boyd, CVX: Matlab software for disciplined convex programming, 2009.[Online]. Available: http://stanford.edu/~boyd/cvx

Mehdi Ghamari Adian received his B.Sc. degree from Amirkabir University of Technology (Tehran Polytechnic) Tehran, Iran in 2004 and his M.Sc. degree from Sharif University of Technology, Tehran, Iran in 2006, both in Electrical Engineering (Communication Systems). He is currently pursuing his Ph.D. degree in the field of Electrical Engineering (Communication Systems) in Amirkabir University of Technology (Tehran Polytechnic) Tehran, Iran. His current research focus is in the areas of cognitive radio networks, cooperative communications and the applications of game theory and benefits of incorporating the MIMO systems in the cooperative cognitive radio networks.

Hassan Aghaeinia received his B.Sc. degree from Amirkabir University of Technology (Tehran Polytechnic) in electronic engineering, in 1987. In 1989 he finished his M.Sc. in Amirkabir University of Technology. Then, in 1992 he received the M.Sc. from Valenciennes University (UVHC), Valenciennes, France. Then he continued his studies towards Ph.D. in UVHC in electronic engineering. He finished his Ph.D. in 1996. From 1996 till present, he is a faculty member in Amirkabir University of Technology, where he is an associate professor in the Communication Engineering Group. His research includes work in digital communications, spread spectrum and advanced communication systems and digital image processing.

Optimal Sensor Scheduling Algorithms for Distributed Sensor Networks

Behrooz Safarinejadian*
Electrical and Electronics Engineering Department, Shiraz University of Technology, Shiraz, Iran
safarinejad@sutech.ac.ir
Abdolah Rahimi
Electrical and Electronics Engineering Department, Shiraz University of Technology, Shiraz, Iran
ab.rahimi@sutech.ac.ir

Received: 25/Jul/2013 Accepted: 31/Aug/2013

Abstract
In this paper, a sensor network is used to estimate the dynamic states of a system. At each time step, one (or multiple) sensors are available that can send its measured data to a central node, in which all of processing is done. We want to provide an optimal algorithm for scheduling sensor selection at every time step. Our goal is to select the appropriate sensor to reduce computations, optimize the energy consumption and enhance the network lifetime. To achieve this goal, we must reduce the error covariance. Three algorithms are used in this work: sliding window, thresholding and randomly chosen algorithms. Moreover, we will offer a new algorithm based on circular selection. Finally, a novel algorithm for selecting multiple sensors is proposed. Performance of the proposed algorithms is illustrated with numerical examples.

Keywords: Sensor scheduling, Sub-optimal algorithm, Offline optimization, Error covariance.

1. Introduction

In recent decades there has been much interest in using sensor networks to improve estimation process [1]. Nowadays; many projects have been defined based on sensor networks. Works such as the EYES project [2], WINS [3] and Smart Dust [4] are examples of systems implementing such networks. Such networks have a complex implementation. Wireless sensor networks have the potential to improve the estimation process. It is obvious that estimates obtained using several sensors will be better than estimates obtained from a single sensor. Furthermore, many systems are constructed based on using these networks. In some sensor networks, there are some problems in order to use data from multiple sensors at the same time. The main issue is selecting a sensor from multi sensors. The sensor management issues will be raised when we have problems in communication protocols or hardware sensor networks. Selection of the most appropriate sensor for optimal performance based on sensor capabilities and network characteristics is an important aspect of the problem. The choice of sensors is calculated off line, and then will be used by the system.

Sensor scheduling problems are used when one (or more) sensors have to be selected in N given sensors at every time step. This might be the case if there are echo-based sensors like sonars [5,6]. If the sensors observe a schedule and thus minimize simultaneous measurements, the total sensor power consumption can be reduced. Another situation where sensor scheduling is useful is in tracking problems, where radar can make different types of measurements by transmitting a suitable waveform each of which has a different power requirement. There might be shared communication resources (e.g., broadcast channels or a shared communication bus) that constrain the usage of many sensors at the same time. Such a situation arises in telemetry-data aerospace systems.

The systems that use Bluetooth technology can communicate with a single system at any moment [7]. In such cases, the main issue is scheduling of sensors to minimize the error covariance, or cost function. In this paper, we consider the optimal scheduling of sensors. In such a way that at each time step, one (or multiple) sensors are allowed to send their data. That can be caused by several problems such as communication problems, system hardware limitations and energy problems in the system.

There are several techniques for optimal scheduling of sensors in the literature. If we want to probe all options to choose the best arrangement of the sensors, we will be faced with a lot of computation. In order to avoid such a huge computation, sub-optimal algorithms can

* Corresponding Author

be used. For example, sliding window and thresholding algorithms with tree structure are proposed. Another method that can be used is choosing the sensors randomly according to some optimal probability distribution. In this paper, we will present a new algorithm which has less computational burden than other algorithms. The algorithm is based on ring selection and can be used as a sub-optimal method. In this algorithm we move on a circular path on which all off the sensor are located, and considering the covariance of the error, the sub-optimal sensor will be chosen.

In more cases, by selecting one sensor at each time step, the system accuracy will not be as good as expected; therefore, multiple sensors should be selected. When the number of sensors increases, high accuracy will be achieved, but more complex hardware and energy will be necessary too. In this paper, an algorithm will also be proposed in order to select multiple sensors at each time step.

The rest of the paper is organized as follows. In section 2, the problem formulation will be presented. In section 3, the question of choosing the optimal sensor schedule is considered and new algorithms will be proposed. In section 3, we will compare the performance of these algorithms using some examples. Finally, Section 4 concludes the paper.

2. MODELING AND PROBLEM FORMULATION

Suppose we have a linear discrete-time system given as follows [8,9,10]:

$$x[k+1] = Ax[k] + Bw[k] \quad (1)$$

$$y_i[k] = C_i x[k] + v_i[k] \quad (2)$$

Where $x[k] \in R^n$ represents the state and $y[k] \in R^m$ is the measurement vector. We have N sensors for state estimation so that $y_i[k]$ is output of i-th sensor in step k. It is assumed that $w[k]$, $v_i[k]$, and $x[0]$ are independent Gaussian random vectors and $w[k] \square N(0,Q)$, $v[k] \square N(0,R)$ and $x[0] \square N(0,\Pi)$, are positive definite matrices where $Q,R,\Pi > 0$. It is assumed that only one sensor can be used at any time. Note that each sensor can communicate with the fusion center in an error-free manner. We use the one-step Kaman filter to estimate the process states. Kalman filter equations are as follows:

$$\hat{x}[k+1] = A\hat{x}[k] + K[k](y_i[k] - C_i\hat{x}[k]) \quad (3)$$

$$k[k] = AP[k]C_i^T (C_i P[k] C_i^T + R_i)^{-1} \quad (4)$$

$$P[k+1] = (A - K[k]C_i)P[k](A - K[k]C_i)^T + BQB^T + K[k]R_i[k]K[k]^T \quad (5)$$

The optimal estimation is given by a Kalman filter assuming a time-varying measurement equation. Assuming that the i-th sensor takes the measurement at time step k, the covariance of the estimation error P[k] evolves according to the Riccati recursion:

$$p[k+1] = Ap[k]A^T + BQB^T - Ap[k]C_i^T (C_i p[k] C_i^T + R_i)^{-1} C_i p[k] A^T \quad (6)$$

In the above relations, $p[k]$ is the error covariance and $x[k]$ is the estimated state at time step k. In the next section, $p[k]$ will be considered as the cost function.

Now, we assume that we want to select m sensors throughout n sensors in a sensor network at each time step $(n \geq m)$ [11,12]. The following relations can be used for data fusion in a central node:

$part\,1(time\,update)$:

$$p^-[k+1] = A\,p^+[k]\,A^T + B\,Q\,B^T \quad (7)$$
$$x^-[k+1] = A\,x^+[k]$$

$part\,2(measurment\,update)$

$$K_i[k] = p^-[k+1]C_i^T (C_i\, p^-[k+1]C_i^T + R_i)^{-1}$$
$$x_i^+[k+1] = x^-[k+1] + k_i[k](y_i[k] - C_i\, x^-[k+1]) \quad (8)$$
$$P_i^+[k+1] = (I - k_i[k]C_i)\, p^-[k+1](I - k_i[k]C_i)^T + k_i[k]R_i\, k_i^T[k]$$

Each iteration of the Kalman filter consists of one iteration of time update equations and m iterations of measurement update equations, where m is number of selected sensors.

2.1 Optimization of Sensor Scheduling

In the analysis presented so far, it is assumed that scheduling of the sensors is available.

It is natural that the minimum error covariance that can be achieved is a function of the sensor schedule. We will try to find a sensor schedule in order to minimize the covariance matrix P[k], over a special time horizon.

In order to simplify the problem, we assume that we have only three sensors and the cost function is defined to be the sum of the error covariance matrices for the three sensors as follows [5, 6]:

$$J = \sum_{k=0}^{N} trace(p_1[k] + p_2[k] + p_3[k]) \quad (9)$$

At any time step, only one sensor is allowed to send its data to the central node. It is assumed that the system begins at time $k=0$ and goes on until $k=N$.

Generally, the covariance can be variously weighed in cost function, because there are some sensors which are more important than others. All possible schedules for the sensors can be seen in Figure 1 for the case of three sensors.

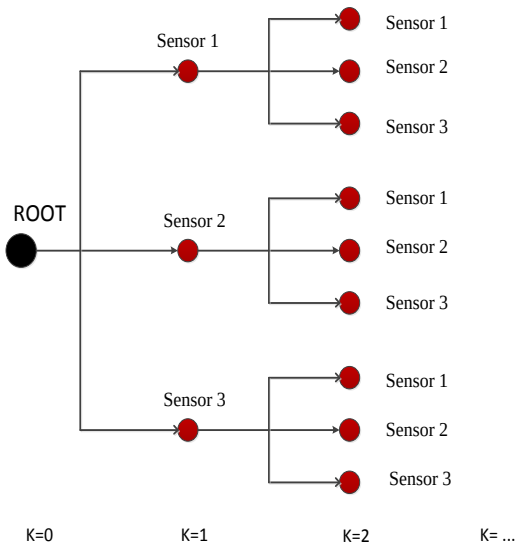

Figure 1. The tree structure defined by the various possible choices of sensor schedules illustrated for the case of 3 sensors.

At each time step, a branch of the tree will be selected according to the previous selected branch. If we want to check all possible options in order to find an optimal scheduling, we may face problems such as large computational burden and lack of memory. For example, in a schedule with only three sensors for N time step, we have 3^N selections. It should be noted that if x is the number of available sensors, to obtain an optimal scheduling, x^N different choices are available. So heavy computations are required to find the optimal sensor scheduling; therefore, we may use a sub-optimal method. In the following, four sub-optimal methods will be proposed for sensor selection.

If we want to use multiple sensors at each time step by using equation 8, the cost function will be as follows:

$$J = \sum_{k=1}^{N} trace(p_1^+[k] + p_2^+[k] + p_3^+[k]) \quad (10)$$

The above cost function can also be used in cases that one sensor is selected at each time step.

2.2 Sliding Window Algorithm

This algorithm is similar to a pseudo real time version of the Viterbi algorithm [13]. A window size d is defined where $d<N$. The algorithm proceeds as follows:

1) Initialization: Start from root node at $k = 0$
2) Traversal:
   a) Traverse all the possible paths in the tree for the next d levels from the current node.
   b) Find the sensor sequence $S_k, S_{k+1}, ..., S_{k+d+1}$ that gives the minimum cost at the end of this window of size d.
   c) Choose the first sensor S_k from the sequence.
3) Sliding the Window:
   a) If $k=N$ then quit, else go to the next step.
   b) Designate the sensor S_k as the root.
   c) Update time $k=k+1$.
   d) Repeat the traversal step.

It should be noted that the choice of the parameter d is arbitrary.

2.3 Thresholding

This algorithm is similar to the algorithm presented in [14], in the context of choosing the optimal controller from a set of many possible choices. We describe a factor f where $f \geq 1$. The algorithm steps are as follows:

1) Initialization: Start from root node with cost $J=0$.
2) Pruning:
   a) Extend the tree by one level (i.e. time step) through all possible paths from the current node.
   b) Calculate the minimum cost up to that time step.
   c) Remove the branches that have a cost greater than f times the minimum.
   d) For the remaining branches, denote the cost of the nodes as the cost achieved by moving down the tree till the node.

2.4 Randomly Chosen Sensors

In this algorithm, at each time step, the sensors will be chosen randomly based on some probability distribution. Then the probability distribution is chosen so as to minimize the expected steady state error covariance. Note that we can't compute the accurate value of the error covariance since it will depend on the specific sensor schedule chosen.

2.5 Circular selection algorithm

This algorithm is based on a circular selection; all sensors are placed on a ring. The computational burden of algorithm is less than

other algorithms because in each time step, it is possible to select more than one sensor.

Sensor selection order of the proposed algorithm is shown in Figure 2.

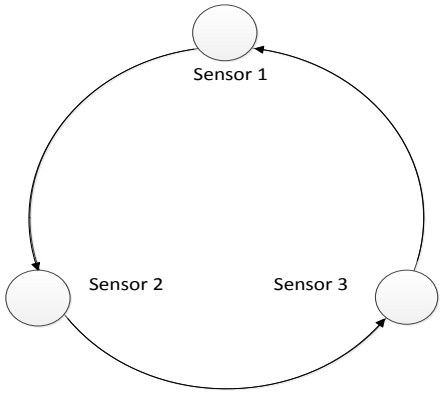

Figure 2. Sensor selection in the circular selection algorithm.

Proposed algorithm

1) Initialization: Start with the cost function $J > 0$ and a time step $k = 0$.
2) Calculation :
   a) Calculate the cost function of the first sensor. If the obtained cost function is less than J then it will be substituted by the new cost function, and the first sensor is chosen as the optimal sensor k. Then, $k = k + 1$ and number of the optimal sensor is stored in a vector z.
   b) Repeat the previous step for the next sensors.
3) If in above steps the optimal sensor isn't selected then the sensor with the smallest cost function is selected as optimal sensor between the sensors. J is substituted by cost function of the optimal sensor, and number of the optimal sensor is stored in z, and $k=k+1$.
4) if k ≥ N stop the iteration, else go to 2.

2.6 A new sensor scheduling algorithm for selecting multiple sensors at each time step

The main purpose of this sub-section is presenting a new algorithm that is able to select one or more than one sensor at each time step. Thus, the following algorithm is suggested. There are n sensors in the network which we want to select m sensors at each time step. The algorithm steps are as follows:

1) Initialization: Start from root node at $k=0$.
2) Traversal:
   a) Traverse all the possible paths in the tree for the next d levels from the current node.
   b) Find m string of sensors which have the least cost function and select them as optimal sensors at k'th time step.
3)
   a) a) If k=N then the algorithm is finished, otherwise go to the next .
   b) b) k = k+1
   c) c) go to the step 2.

3. Simulation Results

3.1 Simulation 1

In this part, we apply our algorithm to an application presented in [5] in which we have a system that track motion of an automobile in two dimensions x and y. Several sensors are located on the car that send information about position of automobile to the central node. In the central node, automobile velocity will be estimated. Equations of system are

$$x[k+1] = Ax[k] + Bw[k]$$

$$y_i[k] = C_i x[k] + v_i[k]$$

where

$$A=\begin{bmatrix} 1 & 0 & h & 0 \\ 0 & 1 & 0 & h \\ 0 & 0 & 1 & 0 \\ 0 & 0 & 0 & 1 \end{bmatrix}, B=\begin{bmatrix} \frac{h^2}{2} & 0 \\ 0 & \frac{h^2}{2} \\ h & 0 \\ 0 & h \end{bmatrix}, X=\begin{bmatrix} p_x \\ p_y \\ v_x \\ v_y \end{bmatrix}$$

where h=0.2 and $w[k]$ in equation (1) is a zero mean white Gaussian noise. The process noise is assumed to have covariance matrix Q given by:

$$Q=\begin{bmatrix} 1 & 0.25 \\ 0.25 & 1 \end{bmatrix}$$

We assume measurements taken by the three sensors being described by:

$$y_i[k] = C_i X[k] + v_i[k]$$

In this simulation, the matrix C_i will be constant as below

$$C_i=\begin{bmatrix} 1 & 0 & 0 & 0 \\ 0 & 1 & 0 & 0 \end{bmatrix}$$

The terms $v_i[k]$ model the measurement noise, again assumed white, zero mean and Gaussian and also independent from each other and from w[k].We consider values of the sensor noise covariance's as:

$$R_1=\begin{bmatrix} 1.62 & 0 \\ 0 & 0.57 \end{bmatrix}, R_2=\begin{bmatrix} 0.59 & 0 \\ 0 & 1.65 \end{bmatrix}, R_3=\begin{bmatrix} 1.21 & 0 \\ 0 & 0.64 \end{bmatrix}$$

In the following figures, performance of the proposed algorithm and other algorithms can be observed:

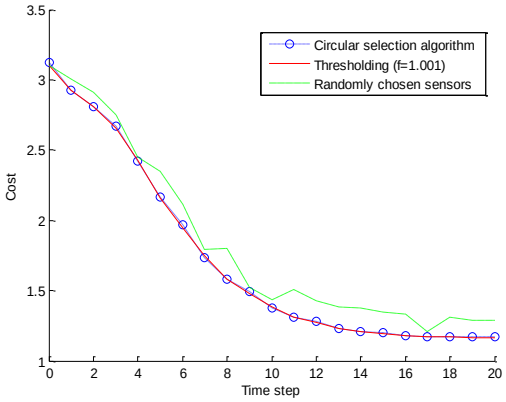

Figure 3: Comparison between circular selection, thresholding, and randomly chosen algorithms.

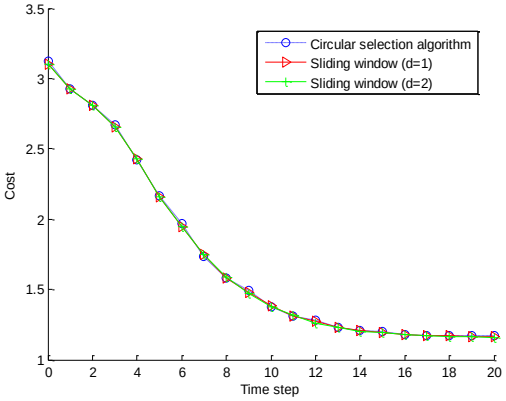

Figure 4: Comparison between circular selection, sliding window (d=1), and sliding window (d=2) algorithms.

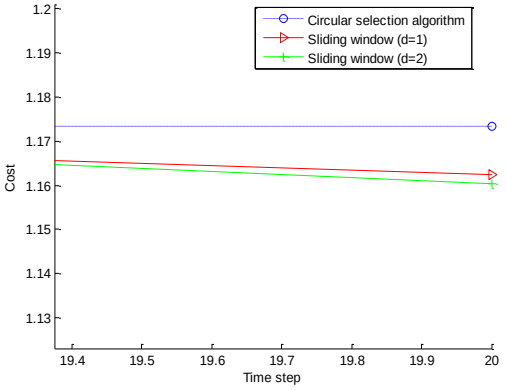

Figure 5: Comparison between circular selection algorithm, sliding window (d=1), and sliding window (d=2) at the final steps.

In Table I, performances of different algorithms are compared.

TABLE I: comparison of different algorithms.

	Sliding window $d=1$	Sliding window $d=2$	Threshold $f=1.001$	Randomly chosen sensors	Circular selection algorithm
Final cost function value	1.1624	1.1604	1.1614	1.3010	1.1735
elapsed time	0.005938	0.018012	0.009537	0.007952	0.005344

3.2 Simulation 2

Six sensors have been considered in this simulation.

$y_i[k] = C_i X[k] + v_i[k]$

In this simulation the matrix C_i will be constant as below

$$C_i = \begin{bmatrix} 1 & 0 & 0 & 0 \\ 0 & 1 & 0 & 0 \end{bmatrix}$$

The previous model parameters have been used despite of the sensor noise covariance which is different in this case:

$$R_1 = \begin{bmatrix} 1.75 & 0 \\ 0 & 0.55 \end{bmatrix}, R_2 = \begin{bmatrix} 0.75 & 0 \\ 0 & 1.36 \end{bmatrix}, R_3 = \begin{bmatrix} 1.74 & 0 \\ 0 & 0.7 \end{bmatrix}$$

$$R_4 = \begin{bmatrix} 1.7 & 0 \\ 0 & 0.6 \end{bmatrix}, R_5 = \begin{bmatrix} 1.95 & 0 \\ 0 & 0.43 \end{bmatrix}, R_6 = \begin{bmatrix} 1.6 & 0 \\ 0 & 0.8 \end{bmatrix}$$

We compare the results of the mentioned algorithms:

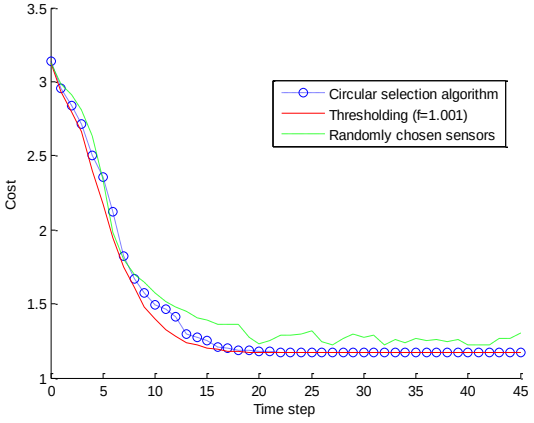

Figure. 6: Comparison between circular selection, thresholding, and randomly chosen algorithms.

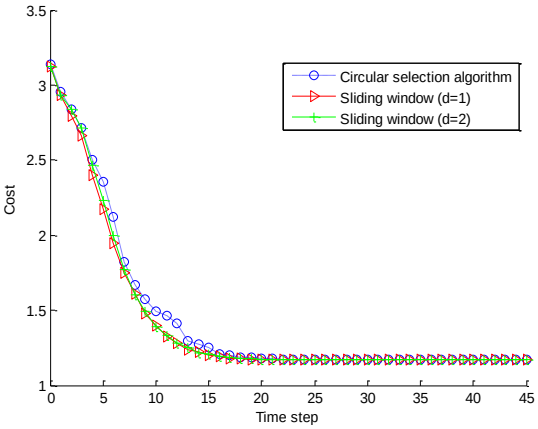

Figure. 7: Comparison between circular selection algorithm, sliding window (d=1), and sliding window (d=2).

In table II, the results of these algorithms can be viewed.

TABLE II: comparison of different algorithms

	Sliding window $d=1$	Sliding window $d=2$	Threshold $f=1$	Randomly chosen sensors	Proposed algorithm
Final cost function value	1.1686	1.1682	1.1686	1. 2323	1.1708
elapsed time	0.01455	0.1591	0.0293	0.0091	0.0085

From Tables I and II, it is clear that the circular selection algorithm has a good performance in terms of cost function reduction. Cost function graphs and the final cost function values of the sliding window, thresholding, and the circular selection algorithms are almost identical. However, in randomly chosen algorithm, the cost function value is higher than the other algorithms.

But in terms of reducing the computational burden, the circular selection algorithm has the best performance, even better than the randomly chosen algorithm. From Tables I and II, we can see that increasing number of sensors results in a better performance for the circular selection algorithm in terms of reduction of computation.

3.3 Simulation 3

In the following, the new algorithm is used for selecting multiple sensors assuming that there are four sensors in the network.

In this simulation, the matrix C_i will be as below

$$C_1=\begin{bmatrix}0&0&0&0\\0&1&0&0\end{bmatrix}, C_2=\begin{bmatrix}0&0&0&0\\0&1&0&0\end{bmatrix}$$

$$C_3=\begin{bmatrix}1&0&0&0\\0&1&0&0\end{bmatrix}, C_4=\begin{bmatrix}1&0&0&0\\0&0&0&0\end{bmatrix}$$

Measurement noise covariance's are as follows:

$$R_1=\begin{bmatrix}1.63&0\\0&0.55\end{bmatrix}, R_2=\begin{bmatrix}0.75&0\\0&1.37\end{bmatrix}$$

$$R_3=\begin{bmatrix}1.44&0\\0&0.6\end{bmatrix}, R_4=\begin{bmatrix}1.7&0\\0&0.57\end{bmatrix}$$

It is assumed that at each time step, two sensors are selected. Results are shown in Figure 8.

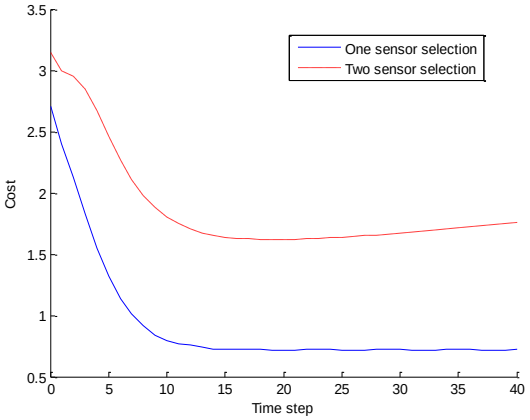

Figure 8: Comparison between proposed algorithm with two sensor selection in each time step and sliding window (d=1).

It is clear from Figure 8 that the proposed algorithm has better performance but it should be noted that using the proposed algorithm needs a more complex hardware.

3.4 Simulation 4

In this part, the matrix C is assumed to be constant and there are twelve sensors with the following covariance matrices

$$R_1=\begin{bmatrix}1.63&0\\0&1.55\end{bmatrix}, R_2=\begin{bmatrix}1.59&0\\0&1.69\end{bmatrix}, R_3=\begin{bmatrix}1.61&0\\0&1.59\end{bmatrix}$$

$$R_4=\begin{bmatrix}1.61&0\\0&1.57\end{bmatrix}, R_5=\begin{bmatrix}1.69&0\\0&1.53\end{bmatrix}, R_6=\begin{bmatrix}1.63&0\\0&1.51\end{bmatrix}$$

$$R_7=\begin{bmatrix}1.64&0\\0&1.55\end{bmatrix}, R_8=\begin{bmatrix}0.59&0\\0&2.75\end{bmatrix}, R_9=\begin{bmatrix}1.68&0\\0&1.58\end{bmatrix}$$

$$R_{10}=\begin{bmatrix}1.44&0\\0&1.6\end{bmatrix}, R_{11}=\begin{bmatrix}1.65&0\\0&1.55\end{bmatrix}, R_{12}=\begin{bmatrix}1.65&0\\0&1.53\end{bmatrix}$$

Using the proposed method for multi-sensor selection, one, two, three, and four optimal sensors are selected between twelve sensors.

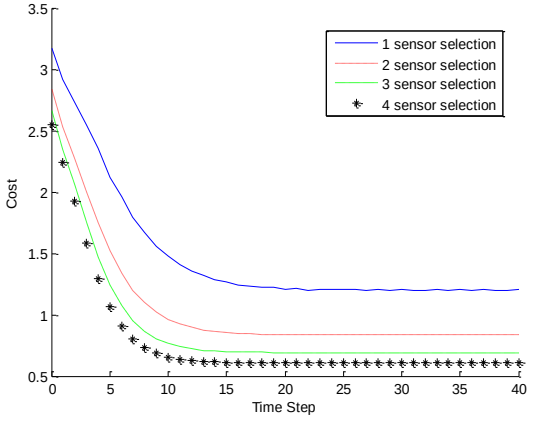

Figure 9: comparison between selection of one, two, three, and four sensors from twelve sensors.

4. Conclusions

It has been clarified that the circular selection algorithm was faster than the other algorithms such as sliding window and thresholding and it had a suitable performance in terms of finding optimum sensors. In other words, this algorithm reduces the computations while its performance in finding the optimal sensors is as good as other scheduling algorithms. According to the obtained results, it is possible to use the proposed algorithm instead of sliding window and thresholding algorithms.

In the case of selecting multiple sensors at each time step, it can be seen that the performance of the system has been improved but hardware problems will be greater. Number of selected sensors at each time step is related to system's expected accuracy and cost of the system.

References

[1] S. Roumeliotis and G. Bekey, "Distributed multi-robot localization," *IEEE Transactions on* Robotics and Automation, vol. 18, no. 5, pp. 781–795,Oct 2002.

[2] H. Karl, "Making sensor networks useful: Distributed services - the eyes project," *ESF Workshop*, La Spezia, Italy, 2002.

[3] D. Estrin, R. Govindan, J. Heidemann, and S. Kumar, "Next CenturyChallenges: Scalable Coordination in Sensor Networks," *in Proceeding of the Fifth Annual International Conference on Mobile Computing and Networking*, Seattle, WA, USA, August 15-19, 1999.

[4] J. Kahn, R. Katz, and K. Pister, "Next Century Challenges: Mobile Networking for 'Smart Dust'," *in Proceeding of the fifth annual ACM/IEEE international conference on Mobile computing and networking*, Seattle, WA, USA, August 15-19, 1999.

[5] V. Gupta, T. H. Chung, B. Hassibi, and R. M. Murray, "On a Stochastic Sensor Selection Algorithm with Applications in Sensor Scheduling and Sensor Coverage," *Automatica*, vol. 42, no. 2, pp. 251-260, 2006.

[6] V. Gupta, T. Chung, B. Hassibi, and R. M. Murray. "Sensor scheduling algorithms requiring limited computation," *In Proceedings of the International Conference on Acoustics, Speech and Signal Processing*, volume 3, 825-828, May 2004.

[7] J. Haartsen. "Bluetooth-the universal radio interface for ad hoc, wireless connectivity," *Ericsson Review*, vol. 3, pp. 110-117, 1998.

[8] T. Kailath, A. Sayed, and B. Hassibi, "*Linear Estimation*". Prentice-Hall,2000.

[9] V. Gupta, T. Chung, B. Hassibi and R. M. Murray, "Sensor scheduling algorithms requiring limited computation," *International Conference on Acoustics, Speech, and Signal Processing (ICASSP)*, Pasadena, CA, USA,2004.

[10] B. Safarinejadian, A. Rahimi, M. Mozaffari, "A new sensor scheduling method for distributed sensor network," *The 21st Iranian Conference on Electrical Engineering (ICEE)*, Mashhad, Iran, 2013.

[11] M. R. R. Khan and V. Tuzlukov, "Multisensor data fusion algorithms for estimation of a walking person position," *International Conference on Control Automation and Systems (ICCAS)*, pp. 863-867, 2010.

[12] D. Hall, "The Implementation of Data Fusion Systems," *Multisensor Fusion, Springer*, Vol. 70, pp. 419-433, 2002.

[13] J. G. D. Forney, "The Viterbi algorithm," *Proceedings of the IEEE*, Volume.61 , pp. 268–278, January 1973.

[14] B. Lincoln and B. Bernhardsson, "LQR optimization of linear system switching," *IEEE Transaction on Automatic Control*, vol. 47, pp. 1701-1705, 2002.

Behrooz Safarinejadian received his BS and MS degrees from the Electrical Engineering Department, Shiraz University, Shiraz, Iran, in 2002 and 2005, respectively. He received his Ph.D. degree from the Electrical Engineering Department, Amirkabir University of Technology, Tehran, Iran, in 2009. Since 2009, he has been with the Faculty of Electrical and Electronic Engineering, Shiraz University of Technology, Shiraz, Iran. His research interests include distributed sensor networks, estimation theory, statistical signal processing, computational intelligence, control systems theory and fault detection.

Abdolah Rahimi received his B.Sc. degree in telecommunication engineering from Azad University, Tehran, Iran, in 2006, and the M.Sc. degree in control engineering from Shiraz University of Technology, Shiraz, Iran, in 2013. His research interests include sensor scheduling, system identification and chaotic systems.

Theory and Experiment of Parasitic Element Effects on Spherical Probe-Fed Antenna

Javad Soleiman Meiguni*
Faculty of Electrical and Computer Engineering, Assistant Professor Semnan University, Semnan, Iran
javad.meiguni@ieee.org
Manouchehr Kamyab
Faculty of Electrical and Computer Engineering, Professor K. N. Toosi University of Technology, Tehran, Iran
kamyab@eetd.kntu.ac.ir
Ahmad Hosseinbeig
Faculty of Electrical and Computer Engineering, K. N. Toosi University of Technology, Tehran, Iran
hosseinbeig@ieee.org

Received: 22/Aug/2013 Accepted: 22/Oct/2013

Abstract
Theory and experiment of a spherical probe-fed conformal antenna with a parasitic element mounted on a spherical multilayer structure are presented in this paper. Rigorous mathematical Method of Moments (MoMs) for analyzing various radiating spherical structures is presented in this paper by using Dyadic Green's Functions (DGFs) in conjunction with Mixed Potential Integral Equation (MPIE) formulation. Linear Rao-Wilton-Glisson (RWG) triangular basis functions are applied in MPIE formulation. Current distributions on coaxial probe and conformal radiating elements are computed by using spatial domain Dyadic Green's Function (DGF) and its asymptotic approximation. A prototype of such an antenna is fabricated and tested. The effect of the parasitic element on the input impedance and radiation patterns of the antenna is investigated. It is shown that the antenna characteristics are improved significantly with the presence of the conducting parasitic element. Good agreement is achieved between the results obtained from the proposed methods and the measurement results.

Keywords: Asymptotic Approximation; Dyadic Green's Function; Spherical Probe-Fed Antennas.

1. Introduction

Probe-fed microstrip antennas embedded in layered spherical media have been studied theoretically and experimentally in recent years. Linear or circular polarizations can be achieved by proper design of these antennas making them applicable in base station satellite communication systems. There is an increasing interest of using microstrip antennas in aerodynamic applications due to their low profile, ease of fabrication and conformability.

Full-wave analysis of these antennas can be advantageous in design procedure. Full-wave numerical techniques based on Green's functions of the structures are too efficient and fast [1]-[3]. In [4]-[5], full-wave analysis of an arbitrary shape aperture coupled antenna placed on a layered sphere has been investigated by using spherical DGFs in combination with electromagnetic fields integral equation formulations. Radiation properties of a hemispherical dielectric resonator antenna, consisting of a monopole antenna placed in a dielectric hemisphere have been theoretically examined in [6]. The effect of a dielectric superstrate on the radiation pattern of a rectangular microstrip patch antenna has been investigated based on the spectral-domain MoMs in conjunction with the stationary phase method [6]-[7]. In [8], a numerical method has been presented to analyze stacked microstrip antennas considering the shape of the radiating elements, the junction of the probe, and the feed current. A strip model in the volume-surface integral equation (VSIE) formulation has been used to simplify the analysis of the probe-fed conformal microstrip antennas with arbitrary shapes [9]. An approach based on hybrid volume-surface integral equation formulation in combination with spherical dyadic Green's function (DGF) is presented in [10] to analyze aperture-coupled multilayer hemispherical dielectric resonator antennas (DRA) with conformal conducting patches.

In this paper, in order to model probe and patches with arbitrary shapes, RWG method [11] is used to analyze spherical probe-fed antennas with parasitic elements. Spherical DGF is applied in the moment's method formulation. As conformal radiating elements are considered in this paper, asymptotic approximation approach is

* Corresponding Author

also expressed. To validate the proposed method, a prototype of this antenna is implemented and tested. Comparison of the measured and calculated input impedance and radiation patterns shows good agreement between the results.

2. Theory

Figure 1 shows a conformal microstrip antenna and a conducting parasitic stack embedded in a four-layer sphere. A PEC sphere is located in the core of the structure and can be assumed as the antenna ground plane. The parasitic patch improves impedance characteristic and directivity of the antenna. In order to compute current distributions on the patches, MoM in conjunction with DGF of a four-layer sphere is used [12].

2.1 Mixed Potential Integral Equation Formulation

One of the efficient numerical methods with high pre-processing gain for analyzing electromagnetic structures is the method of moment where the source region must be divided into small cells. In this method, the unknown source currents are obtained via an integral equation formulation with appropriate Green's function. Such integral equations can be in space domain, spectral domain, or both of these two domains. In general, due to meshing the finite area source, methods based on integral equation formulations are more accurate and require less memory and time. For any class of integral equations namely Electric Field Integral Equation (EFIE), Magnetic Field Integral Equation (MFIE) or Mixed Potential Integral Equation (MPIE), appropriate type of Green's function should be used [11-12]. A set of formulation which uses auxiliary potentials and leads to MPIE formulation is weakly singular and can be easily applied in MoM.

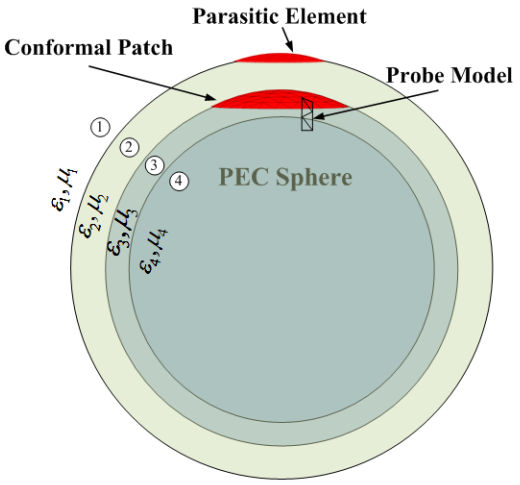

Fig. 1 Conformal patch and parasitic element with probe-fed modeling on a layered sphere.

To apply MoM, conducting surfaces are meshed with linear triangles and Rao-Wilton-Glisson (RWG) triangular basis functions are used to compute current distributions on common edges between two adjacent cells [11]. Hence, the surface current and electric flux densities are expanded in terms of their corresponding basis functions as follow:

$$\mathbf{J}_s(\mathbf{r}) = \sum_{n=1}^{N_M} I_n \mathbf{f}_n^S(\mathbf{r}), \tag{1}$$

In order to derive MPIE formulation in dyadic space, magnetic potential DGF ($\bar{G}_A$) and electric scalar Green's function (G_ψ) are required. $\bar{G}_A$ can be formulated by equating EFIE (2a) with MPIE (2b) and using integral and vector equivalence theorems:

$$\mathbf{E} = -j\,\omega\mu_f \iint_{s'} \overline{\mathbf{G}}_E^{(fs)} .\mathbf{J}(\mathbf{r}')ds', \tag{2a}$$

$$\mathbf{E} = -j\,\omega\mathbf{A} - \nabla\psi = -j\omega\mu_f \iint_{s'} \overline{\mathbf{G}}_A^{(fs)} .\mathbf{J}(\mathbf{r}')\,ds' - \nabla\iint_{s'} \nabla' G_\psi^{(fs)} .\mathbf{J}(\mathbf{r}')ds', \tag{2b}$$

$$\overline{\mathbf{G}}_A^{(fs)} = \overline{\mathbf{G}}_E^{(fs)} - \frac{1}{j\,\omega\mu_f}\nabla\nabla' G_\psi^{(fs)}, \tag{3}$$

where $\bar{G}_E^{(fs)}$ is the electric field dyadic Green's function of a multilayer sphere presented in [12]. The primed and unprimed coordinates and subscripts s and f refer to source and field quantities, respectively.

If the source region is segmented by linear triangles, unknown current coefficients in the antenna can be determined by applying RWG basis functions and satisfying the boundary conditions. Since tangential component of electric field vanishes on perfect conducting metal, impedance matrix is formulated as follows:

$$Z_{pq} = -\int_{s}\int_{s'}\left[\begin{array}{l} j\omega\, f_p(\mathbf{r}).\bar{\mathbf{G}}_A.f_q(\mathbf{r}') \\ +\left(\nabla.f_p(\mathbf{r})\right) G_\psi\left(\nabla'.f_q(\mathbf{r}')\right)\end{array}\right] ds'\,ds, \quad (4)$$

Where $\bar{G}_A$ and G_ψ are magnetic potential DGF and electric scalar Green's function, respectively. Galerkin's method is applied for test functions and the integration over the testing triangles can be avoided by using the centers of field triangles and approximate Galerkin's method [11]. Typically, in solving integral equations by MoM, integrating over segmented cells takes about 90% of computation volume. The Gaussian quadrature method can be used for integration over source triangles in RWG method. Applying 3-point Gauss quadrature is sufficient for this integration. Regarding Fig. 1, in order to obtain the impedance matrix of MoM, all interactions between source triangles (s=1,2) and field triangles (f=1,2) should be considered.

2.2 Asymptotic Method for Spherical DGFs

By using wave transformations, some solutions of the wave equation in various coordinates can be approximated by specific functions. Associated Legendre and Hankel transforms are used widely in spherical coordinates as mentioned in details in [15]. In a multilayer sphere, asymptotic approximations of the electric DGFs between layers can be used instead of using conventional forms of DGFs. As all interactions between current elements should be considered in computation of the MoM impedance matrix, asymptotic DGFs between layers as well as those on layers f=s=i are required. In this paper, i can be 1 or 2 regarding microstrip patch and parasitic element positions shown in Fig. 1. Asymptotic formulation related to a four-layer sphere is presented as follows:

$$\bar{\mathbf{G}}_A^{(fs)}\Big|_a = \begin{cases} g^{(f)}\bar{\mathbf{I}} & ;\ f=s \\ 0 & ;\ f\neq s \end{cases}, \quad (5a)$$

$$G_\psi^{(11)}\Big|_a = \frac{-j\omega\mu}{4\pi k_1^{\,2}}\left(\frac{e^{-jk_1R}}{R} - \left(g_1+g_2+g_3\right)\right), \quad (5b)$$

$$G_\psi^{(12)}\Big|_a = \frac{j\omega\mu}{4\pi k_1 k_2} t_1\left(\frac{e^{-jk_2R}}{R} - g_2 - g_3\right), \quad (5c)$$

$$G_\psi^{(21)}\Big|_a = \frac{j\omega\mu}{4\pi k_1 k_2}\frac{1}{t_1}\left(\left(1-w_1^{\,2}\right)\frac{e^{-jk_1R}}{R} - g_2 - g_3\right), \quad (5d)$$

$$G_\psi^{(22)}\Big|_a = \frac{-j\omega\mu}{4\pi k_2^{\,2}}\left(\frac{e^{-jk_2R}}{R} + \left(g_1-g_2-g_3\right)\right), \quad (5e)$$

$$g^{(f)} = \frac{e^{-jk_fR}}{R}, \quad (5f)$$

$$g_i = w_i\frac{a_i}{r}\frac{e^{-jk_iR_i}}{R_i}, \quad (5g)$$

$$w_i = \frac{\varepsilon_i - \varepsilon_{i+1}}{\varepsilon_i + \varepsilon_{i+1}}, \quad (5h)$$

$$t_i = \frac{2\sqrt{\varepsilon_i\,\varepsilon_{i+1}}}{\varepsilon_i + \varepsilon_{i+1}}, \quad (5i)$$

$$R = |r-r'|\ ;R_i = \sqrt{r'^2 + d_i^{\,2} - 2r'd_i\cos\gamma}, \quad (5j)$$

$$\cos\gamma = \cos\theta\cos\theta' + \sin\theta\sin\theta'\cos(\varphi-\varphi'), \quad (5k)$$

Where $d_t = a_t^2/r$ and $\bar{I}$ is the unit dyad.

Therefore, the input impedance of an antenna located on a multilayer sphere can be obtained using DGF or asymptotic approximation methods. Although asymptotic approximation method yields a higher convergence speed in antenna input impedance calculation, it cannot be utilized for radiation pattern determination since field and source points are not at the same distance from the sphere center. It should be mentioned that the proposed antenna can also be simulated with commercial softwares. However, simulator packages are highly dependent on meshing the structure, modeling the probe and size of radiation box. Therefore, more time and memory is required to obtain precise and stable results from simulator packages. Due to fast computation speed of the presented method, it is very efficient for the analysis of various spherical antennas.

2.3 Spherical to Cartesian Transformation of DGF

In order to obtain electromagnetic field components, we require multiplying DGFs and current element vector components for the case of interest. In order to perform multiplication, both DGFs and current vectors should be in the same coordinates. For the case that conformal antenna area is divided into curvilinear triangles as shown in Fig. 2 (a), current components to be considered are J_φ and J_θ which are in harmony with spherical components of DGFs [12]. However curvilinear meshing is complicated as compared with linear triangular meshing considered in this paper.

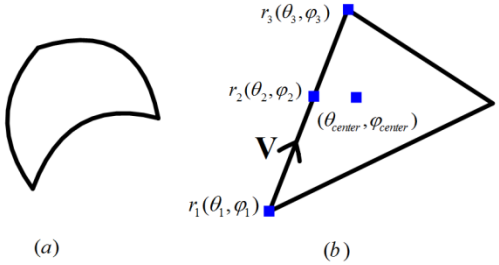

Fig.2. (a) Curvilinear triangle, (b) Linear triangle.

As current elements on common edges of linear meshes have Cartesian components, a new approach for dyad and vector multiplication is presented in this subsection. In order to multiply current vectors and DGFs, either Cartesian current vectors should be converted to spherical vectors or spherical DGFs should be converted to Cartesian ones. Converting a current vector $\mathbf{V}$; which connects two vertices of a triangle; from Cartesian to spherical coordinates results in a non-unique vector because J_φ and J_θ are different in each point on the edge such as $\mathbf{V}$ shown in Fig. 2(b). Since there are unique transformations of vectors from spherical to Cartesian coordinates, conversion of a spherical dyad to a Cartesian dyad can be exactly implemented. Therefore, by employing the centers of the field and source triangles in the calculation of DGFs in Cartesian coordinates, the electric field vector can be expressed as:

$$\mathbf{E}^{(Cartesian)} = -j\omega\mu_f \iint_{s'} \overline{\mathbf{G}}^{(Cartesian)} . \mathbf{J}^{(Cartesian)}(\mathbf{r}')\, ds' \quad (6)$$

Thus by using triangular linear meshes in Cartesian coordinates only $\overline{\mathbf{G}}$ needs to be converted from spherical to Cartesian coordinates. For this purpose, each unit vector should be transformed from spherical to Cartesian coordinates. As DGFs represent interactions between field and source points, the first and second vectors of each dyad correspond to field and source points, respectively. All spherical dyad components can be converted to Cartesian dyads. As an example the conversion equation of $\hat{r}\hat{\theta}$ component of a dyad is extracted as follows:

$$\hat{r}\hat{\theta} = (\sin\theta_f \cos\varphi_f\, \hat{x} + \sin\theta_f \sin\varphi_f\, \hat{y} + \cos\theta_f\, \hat{z}) \\ (\cos\theta_s \cos\varphi_s\, \hat{x} + \cos\theta_s \sin\varphi_s\, \hat{y} - \sin\theta_s\, \hat{z}), \quad (7)$$

which subscripts f and s refer to field and source points, respectively. Therefore, the Cartesian DGFs compatible with vector currents components can be obtained by using the aforementioned conversion method. Using this approach is efficient when a vector is requested as the output of an antenna problem solution. For example to determine the near and far field radiation patterns of an antenna all E_x, E_y, E_z components of electric field can be calculated. It should be noted that the proposed antenna can be simulated with commercial softwares. However, simulator packages are highly dependent on meshing the structure, probe modeling and the size of radiation box. Therefore, more time and memory is required in order to obtain precise and stable results from simulator packages.

3. Results

In order to validate the proposed method, a prototype of a spherical probe-fed microstrip patch antenna is implemented and tested. The antenna dimensions are given in Table I. The PEC spherical shell consists of two hemispheres constructed by a CNC instrument. Two holes are cut on two sides of the sphere to pass the coaxial cable through the sphere and connect the inner conductor of the cable to the microstrip patch. The structure can also be tested with only one hemisphere above a planar perfect ground structure. The antenna is excited by a 20cm RG-58U coaxial cable of 50Ω characteristic impedance. The cable is connected to the microstrip patch at 1cm distance from the center of the patch. The circular patch antenna has been made from a RT/duroid 5870 substrate of 0.8mm thickness and dielectric constant of 2.33. A circular parasitic element is located above the patch by using a spacer material of unit relative permittivity. Figure 3 illustrates the fabricated antenna.

Table 1: Dimensions of the Probe-Fed Spherical Antenna

PEC sphere radius	5 cm
Layer 2 (εr=1) thickness	20 mm
Layer 3 (εr=2.33) thickness	0.8 mm
Conformal Patch Antenna	$0^\circ < \theta_{Patch} < 20.3^\circ$
Parasitic Element	$0^\circ < \theta_{Parasitic} < 7^\circ$

The parasitic element has been divided to 36 triangles yielding 48 common edges between plus and minus triangles and the conformal patch has been segmented into 104 triangles leading to 145 common edges. The probe is meshed into 4 triangles. Hence, there are 198 basis functions used in the MoM. In the computation of input impedance, as source triangles are near field triangles, at least 70 terms of spherical harmonics series should be considered in electric scalar Green's function to obtain a good solution. On the other hand, considering the first 20 terms of spherical harmonics is sufficient to obtain radiation patterns of about 2% error. Figure 3 illustrates the return loss of the antenna with and without the parasitic stack. The input impedance/admittance of antenna depends on current distribution of source elements in the antenna and this fact comes from the integration method in conjunction with MPIE formulation.

As it can be noticed, using the parasitic element yields a better return loss and increases the return loss bandwidth. As illustrated in Fig. 4, there is good agreement between the results obtained from measurement, asymptotic approach and DGF method.

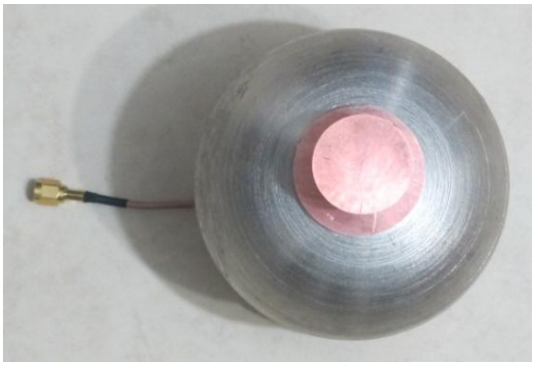

Fig. 3 Prototype of the spherical probe-fed microstrip antenna

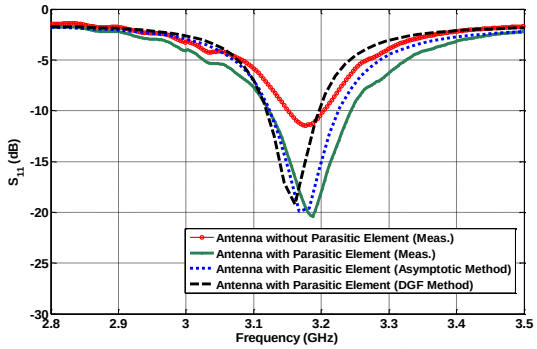

Fig. 4. Computed and measured return loss of the spherical multilayer probe-fed antenna.

Fig. 5 demonstrates the radiation patterns of the spherical probe-fed antenna at 3.15 GHz with parasitic element obtained from analytical solution and the measurement of the antenna. As it can be noticed, good agreement between the results is achieved. The difference is due to the probe inductive reactance, partial dielectric over the PEC sphere and fabrication tolerance. Typically, a matching circuit should be designed for a spherical aperture-coupled antenna to match the input impedance of the antenna to a 50Ω load. In the presented method, it takes about 8 minutes to compute E- or H-planes radiation patterns (with 60 divisions of θ) with a Core 2 Quad @ 2.86 GHz processor. The fast computation time of this method is considerable in comparison with CAD simulator packages and is very efficient for analysis of spherical antennas.

Figure 6 illustrates the measured radiation patterns with and without the parasitic element. It is observed that the stack increases the antenna directivity and decreases side lobes levels in the radiation patterns.

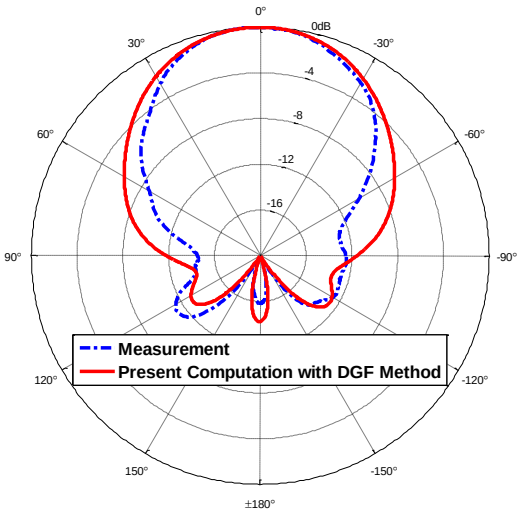

(a)

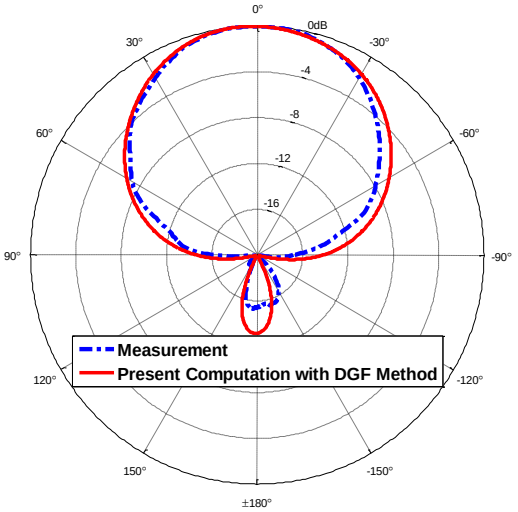

(b)

Fig. 5 Radiation patterns of the spherical probe-fed antenna at 3.15 GHz with parasitic element; (a) E-Plane, (b) H-Plane.

As shown in Fig. 6, parasitic element makes antenna radiation patterns more directive but it increases cross polarization radiations. The latter is because of electromagnetic fields perturbation due to the existence of parasitic element.

The antenna efficiency is measured by a Bluetest reverberation chamber setup and is about 86% and 83% at 3.1GHz and 3.2GHz, respectively. A standard antenna is used to measure the gain of the antenna with and without the parasitic element. Table II shows the antenna gain at different frequencies. It is noticed that the gain of the antenna is increased with the presence of the parasitic element.

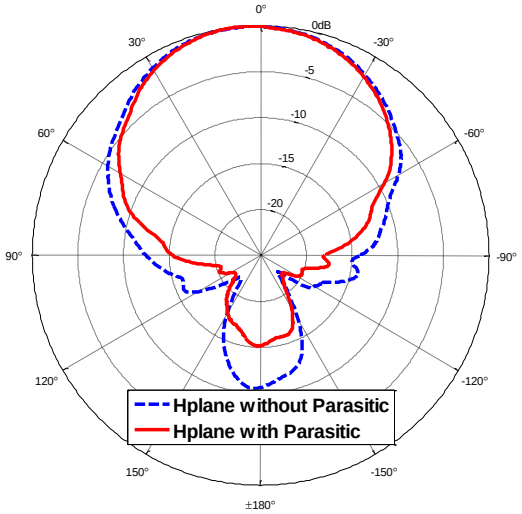

Fig. 6 H-Plane radiation patterns of the spherical probe-fed antenna with and without parasitic elements at f=3.2GHz.

Table 2:
Measured Gain of the Spherical Probe-Fed Antenna

Frequency (GHz)	Gain Without Parasitic Element (dB)	Gain With Parasitic Element (dB)
2.95	3.45	4.31
3.05	5.3	5.9
3.15	6.05	6.9
3.25	1.15	2.32

4. Conclusion

Full-wave analysis of a probe-fed microstrip antenna with a conformal parasitic element mounted on a three-layer spherical structure has been presented in this paper. Green's functions required in MPIE formulation have been extracted. The antenna has been analyzed by using linear triangular cells and by modeling the coaxial probe. Near and far fields of the antenna have been calculated resulting in computation of the input impedance and radiation patterns of the antenna, respectively. To validate the present computation, a spherical probe-fed microstrip antenna has been implemented and tested. Robustness and accuracy of the proposed method have been verified by comparing the results of our method with those of the measurement. The parasitic element improves the antenna characteristics such as input impedance, gain and radiation patterns.

Acknowledgements

The authors would like to thank the K. N. Toosi University Wireless Test Lab. for the measurement of the antenna efficiency.

References

[1] C. T. Tai, *Dyadic Green's Functions in Electromagnetics Theory*, New York: IEEE Press, 1994.

[2] W. C. Chew, *Waves and Fields in Inhomogeneous Media*, New York: IEEE Press, 1995.

[3] A. Fallahi and B. Oswald, "On the computation of electromagnetic dyadic Green's function in spherically multilayered media," *IEEE Trans. Microwave Theory Tech*., vol. MTT-59, no. 6, pp. 1433–1440, Jun. 2011.

[4] Javad. S. Meiguni, M. Kamyab, and A. Hosseinbeig, "Theory and experiment of spherical aperture-coupled antennas," *IEEE Trans. Antennas Propagat*., vol. 61, no. 05, pp. 2397-2403, May 2013.

[5] Javad. S. Meiguni, M. Kamyab, and A. Hosseinbeig, "Spherical Aperture-Coupled Antennas with Parasitic Element," *Applied Computational Electromagnetics Society (ACES) Journal*, vol. 27, no. 12, pp. 999-1006, Dec. 2012.

[6] Z. Sipus, N. Burum, and J. Bartolic1, "Analysis of rectangular microstrip patch antennas on spherical structures," *Microw. Opt. Technol. Lett*., vol. 36, issue 4, pp. 276–280, Feb. 2003.

[7] T. Fortakia, L. Djouaneb, F. Chebarab & A. Benghalia, "Radiation of a rectangular microstrip patch antenna covered with a dielectric layer," *International Journal of Electronics*, vol.95, issue 9, pp. 989-998, 2008.

[8] J.P. Damiano and A. Papiernik, "Survey of analytical and numerical models for probe-fed microstrip antennas," *IEE Proc.-Microw. Antennas Propag*., Vol. 141, no. I, pp. 15–21, February 1994.

[9] M. He, Q. Chen, Q. Yuan, K. Sawaya , X. Xu, "A Simple Strip Model in the Volume-Surface Integral Equation for Analysis of Arbitrary Probe-Fed Conformal Microstrip Antennas," *IEEE Antennas and wireless propag Letter*, vol. 8, pp. 530–533, Feb. 2009.

[10] A. Hosseinbeig, M. Kamyab, and Javad. S. Meiguni, "Theory of aperture-coupled hemispherical dielectric resonator antennas with radiating elements," *International Journal of Electronics and Communications (AEU)*, Available online 31 May 2013.

[11] S. M. Rao, D. R. Wilton, and A. W. Glisson, "Electromagnetic scattering by surfaces of arbitrary shape," *IEEE Trans. Antennas Propag*., vol. 30, pp. 409–418, May 1982.

[12] L.W. Li, P. S. Kooi, M. S. Leong, and T. S. Yeo, "Electromagnetic dyadic Green's function in spherically multilayered media," *IEEE Trans. Microwave Theory Tech*., vol. 42, pp. 2302-2310, Dec. 1994.

[13] R. F.Harrington, *Field Computation by Moment Methods*, IEEE press series in Electromagnetic Waves, 1991.

[14] W. C. Gibson, *The Method of Moments in Electromagnetics*, Chapman & Hall/CRC, Taylor & Francis Group, 2008.
[15] R. F. Harrington, *Time-Harmonic Electromagnetic Fields*, IEEE press, John Wiley & Sons inc., 2001.
[16] S. K. Khamas, "Asymptotic extraction approach for antennas in a multilayered spherical media," *IEEE Trans. Antennas Propag*., vol. 58, no. 3, pp. 1003–1008, Mar. 2010.

Javad Soleiman Meiguni was born in 1982 in Tehran, Iran. He received his B.S. from Semnan University, Semnan, Iran and M.S. from K. N. Toosi University of Technology, Tehran, Iran in 2005 and 2008, respectively all in Electrical Engineering. He received his Ph.D. in telecommunications at K. N. Toosi University of Technology, Tehran, Iran. Currently, he is an assistant professor at the faculty of electrical and computer engineering in Semnan University. He has participated in many projects inside and outside the university. His research is mainly focused on the areas of antennas and EM modeling, numerical techniques in electromagnetics by using dyadic Green's functions, antenna design and measurement, active and passive microwave and millimeter-wave circuit design. During his PhD. studies he has published 6 ISI papers (including IEEE Transactions on Antenna and Propagation journal, Applied Computational Electromagnetic Society (ACES) journal, Electromagnetics journal, International Journal of Electronics and Communications (AEU) and ELEX journal), 3 scientific research papers and 3 papers in conference proceeding.

Manouchehr Kamyab received the B.S. and M.S. from the University of Tehran, Tehran, Iran, and the PhD degree from Michigan State University, in 1982, in electrical engineering. His research interest includes the metamaterials and their applications in antenna engineering, electrically small antennas, microwave and millimeter-wave circuits, and mobile communication systems. He was a professor in the Department of Electrical Engineering, K.N. Toosi University of Technology, Tehran, Iran. Dr. Kamyab has been leading a group of graduate students in the areas of negative-refraction metamaterials and their microwave applications, integrated antennas and components for broad-band wireless telecommunications, novel antenna beam-steering techniques, millimeter and sub-millimeter-wave circuits, as well as scattering and inverse scattering problems.

Ahmad Hosseinbeig was born in 1983 in Tehran, Iran. He received the B.S. in electrical engineering from Shahid Bahonar University, Kerman, Iran and M.S. in telecommunications engineering from K. N. Toosi University of Technology, Tehran, Iran in 2006 and 2008, respectively. He received his Ph.D. in telecommunications engineering at K. N. Toosi University of Technology, Tehran, Iran. His main area of interest is numerical techniques in electromagnetic theory, analysis and design of spherical aperture-coupled Dielectric Resonator Antennas (DRA) using DGFs, antenna design and measurement, microwave and high frequency circuit design.

Ten Steps for Software Quality Rating Considering ISO/IEC

Hassan Alizadeh*
Information Technology and Digital Media Developments Centre, Ministry of Culture, Tehran, Iran.
alizadeh@farhang.gov.ir
Bahram Sadeghi Bigham
Department of Computer Science and Information Technology, Assistant Professor Institute for Advanced Studies in Basic Sciences, Zanjan, Iran.
b_sadeghi_b@iasbs.ac.ir
Hossein Afsari
Information Technology and Digital Media Developments Centre, Ministry of Culture, Tehran, Iran.
h.afsari@outlook.com

Received: 08/Oct/2012 Accepted: 31/Aug/2013

Abstract
In software rating area, it is necessary to apply a measurement reference model to evaluate the quality of software. The standard 25030 is an example of an evaluation system which is based on stakeholders' requirements. In this study, an attempt has been made to establish a model in which all implicit and explicit requirements of stakeholders, users and policy makers have been taken into account. In addition, AHP method has been followed to weigh the indicators used in the model. The results show applicability of the model to meet the requirements of Iranian users.

Keywords: Software Quality Evaluation, Software Rating, Content Based Software Packages, Software Evaluation Standard.

1. Introduction

In the area of software rating, those methods which are based on user's requirements are considered as the valuable methods by which better interaction between supply and sale sections is achievable. In order to rate the quality of the produced software, a quality evaluation method must be applied. Taking into account the inclusive view about the ability of software's functions it is impossible to evaluate the contents of software by using it, because the model is not able to evaluate the content. There are some other methods of software evaluation which is not based on user's opinion. Indeed, these methods are more scientific and they study and focus on standard features of a software function. Mentioned features are defined and demonstrated by acceptable references. In this issue, ISO can be mentioned as an example. Alizadeh et al. [1] offer different groups after extraction and localization of features of software evaluation. Beata et al. [3] and Kasunie [5] have worked on different kinds of measurements on this topic. It is to say, result of each production can be demonstrated in different ways. This can be accepted or rejected, can be calibrated, ranked or rated (that is done in this survey). Also, production and results can be grouped (without priority) or can be ranked. Output of mentioned studies is ranking of software that is used by result of former studies.

Software according to primary aim of categories in four groups of educational, Encyclopedic, general and child and adolescent separately are used for evaluation.

In every category, separate general criteria like user interface (UI) and installation etc. are considered. Specific weight is defined for every feature in each software groups which are the results of AHP model on experts.

It can be mentioned that if the method of evaluation has been designed based on 25030 set [1-4], it would be accepted. Considering the standards mentioned above, this study attempts to extract a general model which is applicable for measuring the quality of software in ten steps.

In Section 2, we focus on identification of system requirements and stakeholder. Also these types of needs can be founded in two distinct formats. Models and criteria are included in Section 3. In this section, ISO and features of ISO is discussed. In mentioned parts, result of weighting and ways of computation of marks for each software are defined that the mark will be between Zero to one hundred (0-100). The last section is included the conclusion and tasks that can be done in the future.

* Corresponding Author

2. Requirements

In the **first stage**, the requirements of system are determined. This step is performed in five phases. The first and the second phases are dedicated to clarification of evaluation purposes and investigation of stakeholders respectively. The second phase also involves the assessment of users' requirements as the main stakeholders [5, 6]. Fig.1 shows the relation between stakeholders' requirements in the system.

Software quality evaluation with qualitative requirement has been defined as the evaluation purpose in the first step.

Through the **second step** the type of product for evaluation which is related to evaluation purpose is determined. The main part of evaluation process is to identify the products. This model considers media software as the product for evaluation purposes. Media software enhances the scientific and cultural awareness of users and entertains them simultaneously. They also have direct and indirect effects on psychological and cultural aspects of users.

2.1 Stakeholders

The **third step** is to identify the system's stakeholders. A stakeholder is a person who has the right to claim the system or to be shared in the system to fulfill their requirements and expectations. The requirements and expectation of stakeholders are different and can be classified in three general categories:

Software producers: This category either provides the contents which are used to influence the cultural, mental and psychological aspects of users or tries to entertain the audiences by providing some interesting contents and functions. To do so, some required tools or functions are designed.

End users: This category contains software's audiences whose requirements about the software contents or functions are fulfilled through using the software.

Policy makers and supervisors: This category contains governments and supervising institutes whose duty is to inspect the published digital contents or assessment of the digital publication sphere to investigate the situation of people, society and digital publishers. The obtained result will be applied in cultural, social, political or security areas.

It should be noted that in this study the scope of software qualitative requirements involves the requirements defined by the users and the policy makers. Once the stake holders has been determined in the **fourth step**, their requirements including society needs and expectations, known limitation on the clients and final users requirements are taken into account. The user's requirements are classified into two classes: Implicit and explicit requirements.

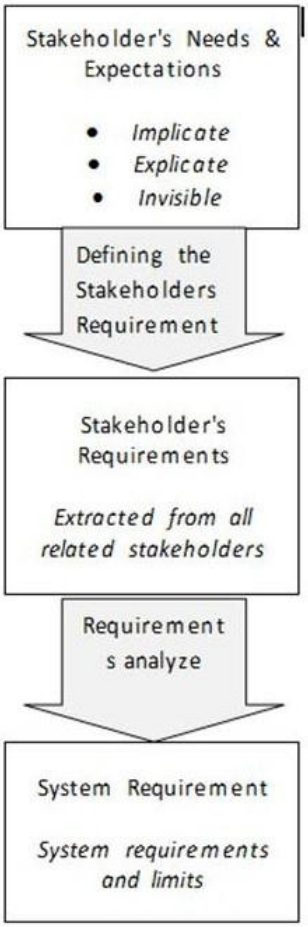

Figure1: Analysis of stakeholders' requirements

2.2 Explicit requirements

The explicit requirements are determined by the users. The fulfillment of this type of requirement leads to the better understanding of the users about the capability of the software that are applied by users. An end user follows two purposes and two basic elements when using software. In the other words, two basic requirements lead them to purchase software which is called explicit requirements. This type of requirement is related to the software **content** and operating certain **functions**. Some of available functions in media software are: media distribution function, training function, research function (offering research content, sound and video processing function, computational function).

2.3 Implicit requirements

They are expressed but are the real needs. Regarding to the research field of the media software producers and the judgment experts, the following implicit needs were determined for any software:

1. Packaging appearance: The user receives the media software product as an in sale package, so the appearance of the software packaging is considered as one of the user requirements. In fact, any media software can be considered as a "commercial off the shelf software product".

2. Internal consistency and installation: Media software in its nature is software, therefore two basic factors must be considered when using it. It must fulfill the internal efficiency and consistency. In the other words, it has the characteristics of reliability, efficiency, maintainability and security without any failure and fault. These characteristics are necessary in order to install, perform, activate and delete a program as well as having appropriate software type and agreement to addresses.

3. User interface: It is observable and touchable part of software that user is dealt with directly and includes information channels that provide communication between user and computer. The user interface in media software is generally one of the two following types: choice interface and user graphical interface. Another implicit user need is user interface.

4. Support: Since the majority of the media software users are ordinary people, receiving supportive services is one of the requirements of the users. After determination of stake-holder's needs, at the **fifth step** the system requirements are determined. A system often includes different elements with certain specifications and responds to the different purposes of the system. To operate, the system requirements must be transformed to the requirements of different elements in the system. The obtained result from the requirement definition process is called stakeholders requirement. In this step, for each of the elements defined in previous step (extracted from the user needs), the quality requirements are defined.

3. Model and Criteria

In this stage, the reference model and its criteria are designed and determined. Two characteristics have been determined based on clarified requirements: content and function. Regarding to the implied needs, the other four characteristics including software packaging, internal consistency, user interface and supportive services will be determined.

Software quality model is completed by determining criteria (attributes) for each of the six previous characteristics (in three layers). In the **sixth step**, the criteria (attributes) were determined. Attribute is inherent characteristic of a species or object that can be determined quantitatively and qualitatively by human or automatic tools.

Attribute is divided in two groups: permanent attribute that exists in nature of things and acquired attribute of a system, process or product (such as product price, product owner). The acquired attribute is not the inherent qualitative attribute of a system, process or product.

Quantity determination and quality evaluation of a software product is performed by setting some criteria which are related to the quality attributes. In the **seventh step**, for each of the attributes, the quality characteristics and the criteria are determined in three layers. Using the criteria which were designed in previous step, the quality model is designed at the second step. Quality of a system is result of the constituent quality and the quality of software depends on its ability to meet implicit and explicit requirements under certain conditions.

Quality of the model is a set of defined attributes along with their relationship that provides a framework to determine quality requirements for evaluation purposes. Quality model is used as a framework to grantee the conformity of all the quality aspects with internal aspect and also the user view point. In regard to the extracted requirements at the pervious step, the following quality model has been extracted and in every basic quality attribute, the secondary attributes have been defined. In this model, two aspects of quality are defined:

- Internal software quality: it contains software package, internal consistency, user interface, content, function and support.
- Quality in use: the user's ideas are obtained about software components.

Defined quality attributes cover all the quality aspects for majority of the media software products, so it can be used to assure the complete coverage of quality. The next step is to design quality model, for determination of the weight for each characteristic and criterion. One of the basic problems arises during the weighing process is how to determine some major differences between different media software based on their importance. For example, in children software because of the necessity of attractiveness in software appearance, the experts consider user interface as the most important aspect while in an encyclopedia software, the main characteristic is content of the software.

Therefore, at the next step (the **eighth step**), all of software packages have been determined. Thus considering the field under study as well as

expert's opinion, the following general types related to content based software were defined: Encyclopedia software, Training software, Children software, General software and Functional software.

4. Weighting and Rating

The last stage in designing the model is to weigh and rate the levels. AHP method was followed in weighing process to determine the weights of characteristics and criteria (applicable for any software). Finally to determine rating levels based on the designed quality measurement, the quality of the software measured based on a population sample and the rating level was determined. In the **ninth step**, the weights of criteria were determined following AHP method. This process is one of the famous multi criteria decision making methods. This method can be used to make decision considering some competitive options and decision criteria. The criteria can be qualitative and quantitative. The problem is solved by forming a hierarchical form. So, the first step is to form a decision tree composed of three levels. The first level of the tree represents the purpose of decision maker and the last level represents competitive alternatives which are compared to each other. The objective is to obtain the weights based on the relative importance of available alternatives. The intermediate level of the tree is the most important level representing some criteria by which competitive alternatives are compared to each other. Table 1, shows the main six criteria and the related weights for four types of software.

Table 1: The weighting factors for characteristics of different software using AHP method

	Encyclopedic	Training	Children	General
Packaging	%3.5	%4.5	%13.5	%11.6
Internal Consistency	%9.5	%7.5	%7.8	%15.9
User Interface	%14.3	%18.7	%31.6	%11.1
Function	%14.1	%32.5	%18.9	%22.5
Content	%53.1	%28.2	%25.3	%34.8
Supportive service	%5.5	%8.6	%5.6	%9.4
Total	%100	%100	%100	%100

This level includes several layers. AHP process requires pair wise comparisons based on a tilde. In this regard, "Expert Choice" software was applied during the following steps:

Tenth step Determine rating level through following three processes (Table 2):

1: Software quality evaluation based on the quality model was used for 190 software and the results obtained.

2: The results transferred to some people who were familiar with evaluation of software process completely without any past knowledge about the software. They were asked to classify the transferred results.

3: Finally the list of the classification in the second step was compared to the values obtained at the first step. The maximum and minimum values were determined and all the values were normalized.

The rating shown in Table 2 was based on the user requirements. There are other two stars named “exportable” and “certain innovation and intelligence” which are complementary stars (not mentioned in Table 2) with the purpose of improvement in the quality level of products.

Table 2: Range of scores corresponding to each star

Number of stars	Scores obtained
No star	$0 \le \alpha < 30$
One Star	$30 \le \alpha < 50$
Two star	$50 \le \alpha < 70$
Three star	$70 \le \alpha \le 100$

5. Conclusion and future works

In this paper, a quality evaluation model was offered considering the standard 25030 and based on the internal quality of software and quality in use. A standard method was derived from standard 25030 to design the model. Also, this model is derived from media software constituents regarding the cultural requirements of users from media software. Moreover, a scientific method is offered to measure the quality of content in measurement reference model and define quality characteristics by which all quality aspects for most of the media software are covered. Therefore the application of the model can highly assure the complete coverage of quality. In future researches, the weighting of third and fourth functions can also be taken into account in order to decrease the effect of personal judgments and to consider more quantitative criteria.

Acknowledgement

The authors wish to acknowledge Mrs Najmeh Madadi, Mr. Meisam Abdoli, Meisam ZargarVafa, Ali Javedani and Madjid Paksima, whose help aided in the completion of this study.

References

[1] Hassan Alizadeh, Hossein Afsari and Bahram Sadeghi Bigham, Rating System for Software based on International Standard Set (Square) 25000 ISO/IEC, Third International Conference on Contemporary Issues in Computer and Information Sciences. (CICIS 2012) , (2012) pp. 584-588.

[2] Beata Czarnacka-Chrobot, The ISO/IEC Standards for the Software Processes and Products Measurement, SoMeT (2009), 187-200.

[3] Beata CzarnackaChrobot, Analysis of the Functional Size Measurement Methods Usage by Polish Business Software Systems Providers, IWSM/Mensura (2009), 17-34.

[4] A. Abran L. Buglione, The Software Measurement Body of Knowledge, Proceedings of 1st Software Measurement European Forum (SMEF), Rome (2004).

[5] M. Kasunic, The State of Software Measurement Practice: Results of 2006 Survey, Software Engineering Institute, Carnegie Mellon University, Pittsburgh (2006).

[6] CMMI Product Team, CMMI for Development, Version 1.2, Software Engineering Institute, Carnegie Mellon University, Pittsburgh (2006).

[7] ISO/IEC 90003:2004 Software Engineering, Guidelines for the application of ISO 9001:2000 to computer software, ISO, Geneva (2004).

Dr. Hassan Alizadeh is the Advisor to Ministry of Culture and Islamic Guidance and director of Information Technology and Digital Media Developments Centre. His research interests are quality and management in the IT related fields.

Dr. Bahram Sadeghi Bigham is an Assistant Professor in Computer Sciences and IT in the Institute for Advanced Studies in Basic Sciences (IASBS), where He is recognized as the founder and director of the RoboScience lab. Dr. Sadeghi has the founder and the general chairman of the International Conference on Contemporary Issues in Computer and Information Sciences (WWW.CICIS.IR). Prior to arriving at IASBS, Dr. Sadeghi worked as a Postdoctoral Fellow at the University of Cardiff in the School of Computer Science. In June 2008, He completed his Ph.D. at Amirkabir University of Technology (Tehran Polytechnic), where he also completed a M.Sc. in 2000. His B.Sc. is from University of Birjand in Mathematics.

Hossein Afsari Born in 1979, Tabriz, Iran, studied Electrical Engineering, Tabriz University, graduated in theology in Qom University, Bachelor of Information Technology and Digital Media Development Center of the Ministry of Culture and Islamic Guidance, Secretary of the "The 6th Int'l Digital Media Festival", (IDMF 2012).

A New Method for Detecting the Number of Coherent Sources in the Presence of Colored Noise

Shahriar Shirvani Moghaddam*
Faculty of Electrical and Computer Engineering, Associate Professor Shahid Rajaee Teacher Training University, Tehran, Iran
sh_shirvani@srttu.edu
Somaye Jalaei
Faculty of Electrical and Computer Engineering, M.Sc. Shahid Rajaee Teacher Training University, Tehran, Iran
somayejalaei2@gmail.com

Received: 29/Nov/2012 Accepted: 31/Aug/2013

Abstract
In this paper, a new method for determining the number of coherent/correlated signals in the presence of colored noise is proposed which is based on the Eigen Increment Threshold (EIT) method. First, we present a new approach which combines EIT criterion and eigenvalue correction. The simulation results show that the new method estimates the number of noncoherent signals in the presence of colored noise with higher detection probability respect to MDL, AIC, EGM and conventional EIT. In addition, to apply the proposed EIT algorithm to detect the number of sources in the case of coherent and/or correlated sources, a spatial smoothing preprocessing is added. In this case, simulation results show 100% detection probability for signal to noise ratios greater than -5dB. Final version of the proposed EIT-based method is a simple and efficient way to increase the detection probability of EIT method in the presence of colored noise considering either coherent/correlated or noncoherent sources.

Keywords: Eigen Increment Threshold, Colored Noise, Coherent Signal, Eigenvalue Correction, EIT, EGM.

1. Introduction

Array signal processing can be applied to many applications, such as radar, sonar, remote sensing, astronomy, seismology and mobile communications. In this field, estimating direction of arrival (DOA) of signals in an array of sensors, has received a considerable amount of attention during the last two decades [1]. Most of the existing estimation techniques, assume that the number of sources is known a priori and may give misleading results if the wrong number of sources is considered. Therefore, to achieve good results in DOA estimation, it is a key problem to determine the number of signals correctly [2, 3].

There are a number of different methods to detect the number of sources. Akaike's information criterion (AIC) and minimum description length (MDL) are the two most popular methods that detect the number of signals based on information theoretic criteria [4]. According to these algorithms, the number of signals is determined as the value for which the AIC or MDL criteria, is minimized [5]. Recently, these methods have been studied in [6] for source enumeration and most of these research devoted to modify this approach. For example, their methods cannot resolve coherent sources. In [7], a new approach has been proposed that can resolve coherent sources. The method uses the MDL principle, and decomposes data into signal and noise components. The MDL descriptor is then computed for signal and noise components separately, and the results are added to obtain the total MDL cost.

In addition to MDL and AIC methods, some other algorithms that consider a bound or threshold for eigenvalues are proposed. Chen et al. [8] proposed a method for determining the number of sources by setting an upper bound on the values of the eigenvalues. This bound is determined by an adjustable parameter, so its performance is better than MDL at low SNRs (signal to noise ratios), and better than AIC at high SNRs. Zhang et al. [9] offered a set of eigenvalue Gradient methods (EGMs), which like AIC and MDL methods, it also enumerate the number of non-coherent sources according to the eigenvalues of auto-correlation matrix.

In [10], the performance of three popular methods, AIC, MDL and EGM is evaluated. Simulation results for determining the number of noncoherent sources show that EGM offers higher performance with respect to MDL and AIC, in low SNRs. Moreover, simulation results for smoothed algorithms, in the case of coherent/ correlated sources, show higher detection probability for EGM compared to AIC and MDL.

Due to higher performance of Eigen Increment Threshold (EIT) method with respect

* Corresponding Author

to the AIC and MDL methods, it is widely adopted. In contrast, the energy will be shifted to the biggest eigenvaule and it directly leads to increase EIT threshold and the occurrence of under-estimation when unequal power sources exist. To overcome this phenomenon, the modified EIT suggested in [11] is appropriate which uses a recursive method to avoid the influence of the bigger eigenvalue. Considering this modification, the detection probability can be evidently increased in the case of unequal power sources.

All of the above mentioned algorithms, such as: MDL, AIC, EGM and EIT have been derived based on the assumption that the noise of the sensors is white. In practice, signals experience colored noise which causes a rapid decrease in the performance of the conventional methods.

Jing and Rong [12] addressed a novel effective accurate detection algorithm in spatial color noise by using the canonical correlation coefficients of the joint covariance matrix. Compared with the other algorithms, this algorithm has a better performance and lower complexity. Recently, Zhen et al. [13] established a new method to eliminate the inequality of the noise eigenvalues caused by colored noise for coherent signals. It combines the information theoretic criteria and eigenvalue correction to estimate the number of coherent signals.

In this paper, a novel algorithm to detect the number of sources in the presence of colored noise is proposed. The approach is based on a combination of EIT and eigenvalue correction. Since conventional EIT can detect only the number of noncoherent sources, we use forward/backward spatial smoothing (FBSS) technique [14,15] to determine the number of coherent signals. The simulation results demonstrate the effectiveness of the proposed algorithm and show that the presented method offers higher performance and lower complexity in a joint state. It means that the proposed algorithm can be used to detect the number of coherent/correlated sources in the presence of colored noise.

This paper is organized as follows. After the statement and formulation of the problem in Section 2, Section 3 describes the details of the EIT method for non-coherent sources in the presence of white noise. Section 4 presents a new algorithm as a combination of eigenvalue correction technique and EIT for determining the number of sources in colored noise. Section 5 presents FBSS technique as a preprocessing step for determining the number of coherent/correlated sources. Section 6 demonstrates the simulation results. Finally, Section 7 concludes this research.

2. Signal Model

Suppose that P narrowband signals, emitted from the far field impinging on array of M sensors $(M > P)$. The observed data from M sensor array, can be described as follows

$$x(t) = As(t) + n(t) \qquad t = 1,2,\dots,N \tag{1}$$

where $A = [a(\theta_1)a(\theta_2)\dots a(\theta_P)]$ is the matrix of array manifold, $s(t) = [s_1(t)\, s_2(t) \dots s_P(t)]^T$ is the vector of signal, and $n(t) = [n_1(t)n_2(t) \dots n_M(t)]^T$ is the vector of noise. Noise sequence $n_1(t), n_2(t), \dots, n_M(t)$ is colored Gaussian noise which is zero mean and uncorrelated with the signals [12]. The covariance matrix for array output is

$$R = E[x(t)x^H(t)] = AR_sA^H + R_n \tag{2}$$

where $R_s = E\{s(t)s^H(t)\}$ and $R_n = E\{n(t)n^H(t)\}$ are the correlation matrix of signal and noise, respectively. In practice, considering ergodic processes, correlation matrix is acquired from limited data, that is

$$\widehat{R} = \frac{1}{N}\sum_{t=1}^{N} x(t)x^H(t) \tag{3}$$

where N is the number of snapshots.

To simplify the presentation and also determining the number of sources from $\widehat{R}$, we consider the following assumptions [11].

- The array manifold, defined as the set of steering vectors is known.
- Any subset of M steering vectors from the array manifold is linearly independent.
- Arriving signals $s_i(t)$ are stationary narrowband signals with similar center frequencies.
- The number of sensors is greater than the number of sources, namely $M > P$.

3. Detecting the Number of Sources using EIT

Just like EGM method, EIT also determines the number of noncoherent sources according to the eigenvalues of auto-correlation matrix. Therefore, after calculating the spatial auto-correlation matrix of the output data $x(t)$ of the sensor array by Eq. 3, we arrange the eigenvalues in descending order.

$$\lambda_1 \geq \cdots \geq \lambda_P \geq \lambda_{P+1} \geq \cdots \geq \lambda_M \tag{4}$$

There is a significant difference between λ_P and λ_{P+1}. Hence, by checking the difference

between neighbor eigenvalues and setting an upper bound on the values of the eigenvalues, the number of P signals can be detected. This threshold is given as [11]:

$$\lambda_i - \lambda_{i+1} \le \text{threshold} \equiv \eta(M,N)\frac{P_s}{\left(1+\sqrt{P_s/\lambda_M}\right)^2} \quad (5)$$

$$i = M-1, M-2, \dots, 1$$

where P_s is the power of source, and $\eta(M,N)$ is a coefficient function with following features:

- $\eta(M,N) = 1$ when $N \to \infty$
- $\eta(M,N)$ increases when N reduces
- $\eta(M,N)$ decreases when M increases

By finding out all i that satisfy $\Delta\lambda_i \le$ threshold to construct the set $\{i_k\} = \{i|\Delta\lambda_i \le \text{threshold}\}$ and taking $i_0 = \min\{i_k\}$, the estimated number of signals is $\hat{p} = i_0 - 1$.

4. New Eigenvalue corrected EIT-based Technique

EIT has a good performance in the presence of white noise, but capability of this algorithm will be sharply declined when signals experience colored noise. Therefore, for smoothing the spatial colored noise, we can use eigenvalue correction method which generates best correction values to getting properly results. "Colored noise cannot be effectively smoothed if the correction eigenvalue is too small. In other hand, not only noise eigenvalue but also signal eigenvalue can be affected if the correction eigenvalue is too large". The eigenvalues of $\widehat{R}$ given by Eq. 4, and e_i is correction value of $\lambda_i (i = 1,2,\dots,M)$. In order to smooth colored noise effectively, e_i is defined as [13]:

$$e_i = \sqrt{\sum_{j=1}^{i}\lambda_j} \qquad i = 1,2,\dots M \quad (6)$$

Consequently, the corrected eigenvalue named $c_i (i = 1,2,\dots,M)$, can be obtained by:

$$c_i = \lambda_i + e_i \quad (7)$$

For each eigenvalue, related new corrected eigenvalue will be calculated. Suppose that there are k signals, we can get M eigenvalues after decomposing covariance matrix, that is

$$\lambda_1 \ge \cdots \ge \lambda_P \ge \lambda_{P+1} \ge \cdots \ge \lambda_M \quad (8)$$

Using Eq. 6, they become corrected as $\tilde{\lambda}_1 \ge \cdots \ge \tilde{\lambda}_P \ge \tilde{\lambda}_{P+1} \ge \cdots \ge \tilde{\lambda}_M$. where

$$\tilde{\lambda}_i = \lambda_i + \sqrt{\sum_{j=1}^{i}\lambda_j} \qquad i = 1,2,\dots,M \quad (9)$$

Substituting Eq. 9 into Eq. 5, threshold function becomes:

$$\tilde{\lambda}_i - \tilde{\lambda}_{i+1} \le \text{threshold} \equiv \eta(M,N)\frac{P_S}{\left(1+\sqrt{P_S/\tilde{\lambda}_M}\right)^2} \quad (10)$$

$$i = M-1, M-2, \dots, 1$$

By finding out all i that satisfy $\Delta\tilde{\lambda}_i \le$ threshold and taking out $i_0 = \min(i_k)$, someone can get the number of signals as $\hat{p} = i_0 - 1$.

5. Forward/ Backward Spatial Smoothing Technique

Spatial smoothing is based on a preprocessing scheme that divides the total array of M sensors, into overlapped sub-arrays of size M_0 (see Fig. 1) and then, generates the average of the sub-array output covariance matrices. Let $x_l^f(t)$ stands for the output of the lth sub-array for $l = 1,2,\dots L \equiv M - M_0 + 1$ where L denotes the total number of these forward sub-arrays [14].

$$x_l^f(t) = [x_l(t), x_{l+1}(t), \dots, x_{l+M_0-1}(t)]^T \quad (11)$$

Then, the covariance matrix of the lth sub-array is

$$R_l^f = E\left[x_l^f(t)(x_l^f(t))^H\right] \quad (12)$$

Forward spatially smoothed covariance matrix R^f as the mean of the forward sub-array covariance matrices is

$$R^f = \frac{1}{L}\sum_{l=1}^{L} R_l^f \quad (13)$$

The covariance matrix of the lth backward sub-array is given by

$$R_l^b = E\left[x_l^b(t)(x_l^b(t))^H\right] \quad (14)$$

In the same way as Eq. 13, the spatially smoothed backward sub-array covariance matrix R^b is

$$R^b = \frac{1}{L}\sum_{l=1}^{L} R_l^b \quad (15)$$

Finally, the forward/backward smoothed covariance matrix $\widetilde{R}$ as the mean of R^f and R^b is given by

$$\widetilde{\mathbf{R}} = \frac{\mathbf{R^f}+\mathbf{R^b}}{2} \quad (16)$$

The smoothed covariance matrix $\widetilde{R}$ in Eq. 16 has exactly the same form as the covariance matrix for some non-coherent situations. It means that $\widetilde{R}$ can be used instead of $\widehat{R}$. The eigenstructure-based techniques can be applied to this smoothed covariance matrix, to successfully estimate the number of coherent sources [14].

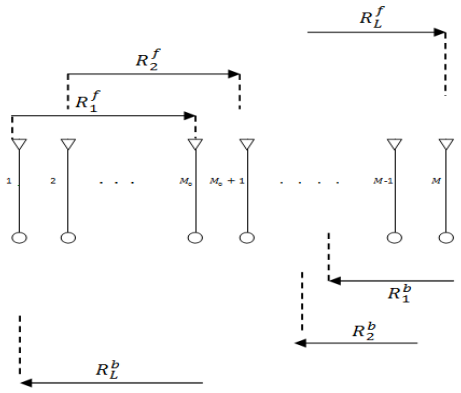

Fig 1. The forward/backward sub-arrays in FBSS scheme [14].

Finally, the Proposed EIT-based algorithm which determines the number of coherent sources in the presence of colored noise is summarized as follows:

Table 1: Summary of the proposed FBSS-based EIT algorithm

Step1.	Compute the smoothed covariance matrix $\widetilde{R}$ by: $\widetilde{R} = \frac{R^f + R^b}{2}$ Then, get *M* eigenvalues after decomposing it.
Step2.	Use Eq. 6 to correct *M* eigenvalues. Corrected eigenvalues become $\tilde{\lambda}_1 \geq \cdots \geq \tilde{\lambda}_P \geq \tilde{\lambda}_{P+1} \geq \cdots \geq \tilde{\lambda}_M$
Step3.	Substitute corrected eigenvalues into Eq. 5. The revised threshold function can be derived and threshold inequality as 10 should be checked:
Step4.	$\hat{p} = i_0 - 1$

6. Conclusions

In this research, the effectiveness of conventional and the proposed EIT algorithm is compared with MDL, AIC and EGM in different cases, numerically. All simulations are run in MATLAB software and associated figures are extracted from simulation results of this investigation. In Figure 2, the performance of the proposed EIT equipped with eigenvalue correction method is compared with EGM and conventional EIT methods. Both methods of Figure 3 are the new proposed ones. Finally, the simulation results of Figure 4 are reported for the first time in this research.

Consider a linear array of 8 sensors, exposed to the two non-coherent signals arriving from 0° and 10°. The inter-element spacing is half of the wavelength.

In the first experiment, the performance of the proposed EIT-based algorithm is compared with conventional EIT and EGM in the case of colored noise. Spatial colored noise is obtained by filtering white noise through a first order auto-recursive (AR1) filter, given by

$$y(i) = \alpha y(i-1) + x(i) \qquad (17)$$

where $\alpha \in [0,1]$ is the noise correlation coefficient of adjacent sensors.

In this experiment, $\alpha = 0.6$, $\eta(M,N) = 2$ and the number of snapshots is 200. The simulation results as depicted Fig. 2 show that despite the conventional EIT fails to detect the correct number of sources in the presence of colored noise, the proposed eigenvalue corrected EIT-based algorithm offers 100% success for SNRs greater than $-1dB$. In addition, for SNRs lower than $2dB$, the proposed method has a much better detection performance than the EGM algorithm.

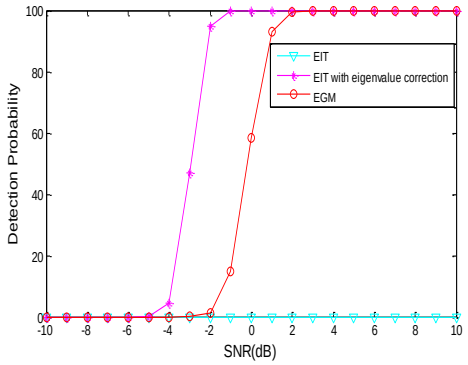

Fig 2. The detection probability versus SNR for experiment 1.

In the second experiment, noncherent signals with equal power impinge on array at 0° and 10°, *SNR*=10*dB*, the number of snapshots is 200 and noise correlation coefficient changes from 0 to 1 with step size 0.1. As shown in Fig. 3, for all correlation coefficients of noise, the conventional EIT method is completely ineffective. In contrast, the proposed EIT-based algorithm can offer 100% detection probability for $\alpha \in [0.1,0.8]$.

In this part, spatial smoothing method is applied to solve the coherency and the number of coherent sources is estimated considering the smoothed output signal of array antenna. As the experiment 3, the performance of the proposed FBSS-based EIT and EGM algorithms under different SNRs, for coherent sources and colored noise is investigated. Three coherent signals with equal powers impinge on array at 0°, $5^\circ$and 10°. Path coefficients for coherent signals are (0.7+0.7j), (0.6+0.5j) and (0.2+0.4j). ULA has 9

elements, $\alpha = 0.6$ and SNR changes from -10dB to 10dB with step size 2dB. Also, $M_0 = 7$ and the number of snapshots is 200.

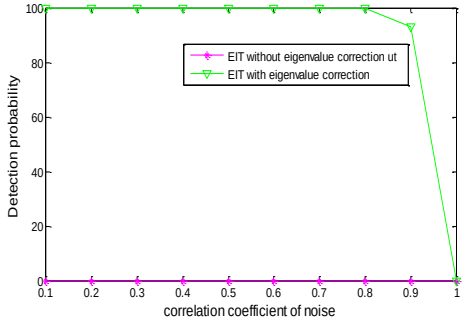

Fig 3. The detection probability versus noise correlation coefficient for experiment 2.

As illustrated in Fig. 4, the proposed FBSS-based EIT algorithm can determine the number of sources exactly when the SNR is greater than -3dB. In other word, using FBSS-based proposed EIT algorithm, SNR will be improved 9dB with respect to FBSS-based EGM.

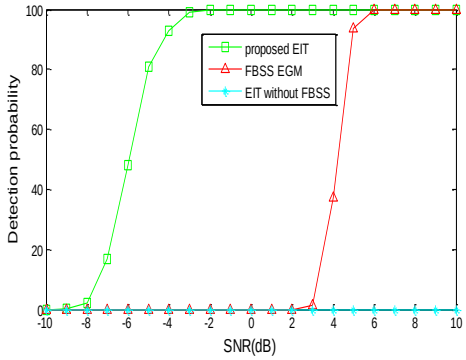

Fig 4. The detection probability versus SNR for experiment 3.

In order to show that the proposed method is computationally efficient, Table 2 lists the computational costs of two algorithms in terms of the number of multiplications/divisions, additions/subtractions, comparisons with a threshold, minimizations and logarithmic operators. It shows that the proposed method needs lower computational complexity with respect to the Zhen et al. [13] method. Here, M is the number of sensors and K is the number of signals.

Table 2: Comparison of computational complexity

Algorithm	Proposed EIT	Zhen et al. [13]
The number of Multiplications/ divisions	4	$M - K + 8$
The number of Additions/ subtractions	$3M + 1$	$3M - K + 4$
The number of Comparisons with a threshold	$M - 1$	None
Minimizations	None	M
The number of Logarithmic operators	None	1

7. Conclusions

In this paper, a new EIT-based algorithm that combines the EIT criterion and eigenvalue correction is proposed which is able to determine the number of both noncoherent and coherent signals in colored noise. When the signal sources are coherent, conventional threshold-based methods, EGM and EIT, cannot separate signal and noise eigenvalues and are not able to detect the number of signal sources. In this research, to overcome the effect of coherency, forward-backward spatial smoothing method is used. Hence, in the first step, the smoothed covariance matrix is fed to eigenstructure-based techniques to successfully estimate the number of coherent sources. In the second step, the noise eigenvalues of the smoothed covariance matrix are corrected using the eigenvalue correction technique. Finally, in the case of colored noise, corrected eigenvalues are used to find the threshold.

The effectiveness of the proposed EIT-based algorithm was verified through numerical examples. Simulation results showed that the proposed method estimates well the number of coherent or noncoherent signals in the presence of colored noise. Moreover, it was shown that the proposed method needs lower computational complexity compared to the previous method.

Acknowledgments

This work has been supported by Research Institute for ICT (ITRC) under contract number 19248/500 (28.12.1390).

References

[1] S. Shirvan Moghaddam, and S. Almasi Monfared, "A Comprehensive Performance Study of Narrowband DOA Estimation Algorithms," International Journal on Communications Antenna and Propagation (IRECAP), Vol. 1, No. 4, Aug. 2011, pp. 396-405.

[2] J. Liu, J. Xin, N. Zheng, and A. Sano, "Detection of the Number of Coherent Narrowband Signals with L-Shaped Sensor Array," in IEEE 10th International Conference on Signal Processing (ICSP), Oct. 2010, pp. 323-326.

[3] D.B. Williams, Detection: Determining the Number of Sources, Digital Signal Processing Handbook, CRC Press, 1999.

[4] S. Valaee, and P. Kabal, "An Information Theoretic Approach to Source Enumeration in Array Signal Processing," IEEE Transactions on Signal Processing, Vol. 52, No. 5, May 2004, pp. 1171–1178.

[5] M. Wax, and T. Kailath, "Detection of Signals by Information Theoretic Criteria," IEEE Transactions on Acoustics, Speech, and Signal Processing, Vol. 33, No. 2, April 1985, pp. 387–392.

[6] J. Jiang, M. Ann Ingram, "Robust Detection of Number of Sources Using the Transformed Rotational Matrix," in IEEE Wireless Communications and Networking Conference (WCNC'04), March 2004, Vol. 1, pp. 501-506.

[7] M. Wax, and I. Ziskind, "Detection of the Number of Coherent Signals by the MDL Principle," IEEE Transactions on Acoustics, Speech, and Signal Processing, Vol. 37, No. 8, Aug. 1989, pp. 1190-1196.

[8] W. Chen, K.M. Wong, and J.P. Reilly, "Detection of the Number of Signals: A Predicted Eigen-Threshold Approach," IEEE Transactions on Signal Processing, Vol. 39, May 1991, pp. 1088-1991.

[9] Q. Zhang, Y. Yin, and J. Huang, "Detecting the Number of Sources Using Modified EGM," in IEEE Region 10 Conference (TENCON), Nov. 2006, pp. 1-4.

[10] S. Shirvani Moghaddam, S. Jalaei, "Determining the Number of Coherent Sources Using FBSS-based Methods," Frontiers in Science, Vol. 2, No. 6, Dec. 2012, pp. 203-208.

[11] F. Chu, J. Huang, M. Jiang, Q. Zhang, and T. Ma, "Detecting the Number of Sources Using Modified EIT," in 4th IEEE Conference on Industrial Electronics and Applications (ICIEA), May 2009, pp. 563-566.

[12] L. Jing-hua, and L. Rong, "Source Number Detection in Spatial Correlated Color Noise Using the Canonical Correlation Coefficients," in 4th IEEE Conference on Industrial Electronics and Applications (ICIEA), May 2009, pp. 1597-1601.

[13] J. Zhen, X. Si, and L. Liu, "Method for Determining Number of Coherent Signals in the Presence of Colored Noise," Journal of Systems Engineering and Electronics, Vol. 21, No. 1, 2010, pp. 27–30.

[14] S.U. Pillai, and B.H. Kwon, "Forward/Backward Spatial Smoothing Techniques for Coherent Signals Identification," IEEE Transactions on Acoustics, Speech, and Signal Processing, Vol. 37, No. 1, 1989, pp. 8-15.

[15] T.J. Shan, M. Wax, and T. Kailath, "On Spatial Smoothing of Estimation of Coherent Signals," IEEE Transactions on Acoustics, Speech, and Signal Processing, Vol. 33, No. 4, 1985, pp. 806-811.

Shahriar Shirvani Moghaddam received the B.Sc. degree from Iran University of Science and Technology (IUST), Tehran, Iran and M.Sc. degree from Higher Education Faculty of Tehran, Iran, both in Electrical Engineering, in 1992 and 1995, respectively. Also, he received the Ph.D. degree in Electrical Engineering from Iran University of Science and Technology (IUST), Tehran, Iran, in 2001. He has more than 70 refereed international scientific journal and conference papers, 2 text books on digital communications and one book chapter on MIMO systems. Since 2003, he has been with the Faculty of Electrical and Computer Engineering, Shahid Rajaee Teacher Training University (SRTTU), Tehran, Iran. He was nominated as the best researcher and the best teacher in the SRTTU University in 2010 and 2011, respectively. Currently, he is an associate professor in Digital Communications Signal Processing (DCSP) research laboratory of SRTTU. His research interests include adaptive antenna array beamforming, direction of arrival estimation, and power control and beamforming in cellular relay networks.

Somaye Jalaei received the B.Sc. degree from Shahed University, Tehran, Iran and M.Sc. degree from Shahid Rajaee Teacher Training University (SRTTU), Tehran, Iran, both in Electrical Engineering, in 2009 and 2013, respectively.